BEM SOLUTION OF UNSTEADY CONVECTION-DIFFUSION TYPE FLUID FLOW PROBLEMS

A THESIS SUBMITTED TO
THE GRADUATE SCHOOL OF NATURAL AND APPLIED SCIENCES
OF
MIDDLE EAST TECHNICAL UNIVERSITY

BY

HANDE FENDOĞLU

IN PARTIAL FULFILLMENT OF THE REQUIREMENTS
FOR
THE DEGREE OF DOCTOR OF PHILOSOPHY
IN
MATHEMATICS

MAY 2020

Approval of the thesis:

BEM SOLUTION OF UNSTEADY CONVECTION-DIFFUSION TYPE FLUID FLOW PROBLEMS

submitted by **HANDE FENDOĞLU** in partial fulfillment of the requirements for the degree of **Doctor of Philosophy in Mathematics Department, Middle East Technical University** by,

Prof. Dr. Halil Kalıpçılar
Dean, Graduate School of **Natural and Applied Sciences** ______________

Prof. Dr. Yıldıray Ozan
Head of Department, **Mathematics** ______________

Prof. Dr. Canan Bozkaya
Supervisor, **Mathematics, METU** ______________

Prof. Dr. Münevver Tezer-Sezgin
Co-supervisor, **Mathematics, METU** ______________

Examining Committee Members:

Prof. Dr. Nevzat Güneri Gençer
Electrical and Electronics Engineering, METU ______________

Prof. Dr. Canan Bozkaya
Mathematics, METU ______________

Prof. Dr. Ayhan Aydın
Mathematics, Atılım University ______________

Prof. Dr. Niyazi Şahin
Mathematics, Ankara Yıldırım Beyazıt University ______________

Prof. Dr. Ömür Uğur
Institute of Applied Mathematics, METU ______________

Date:

I hereby declare that all information in this document has been obtained and presented in accordance with academic rules and ethical conduct. I also declare that, as required by these rules and conduct, I have fully cited and referenced all material and results that are not original to this work.

Name, Surname: Hande Fendoğlu

Signature :

ABSTRACT

BEM SOLUTION OF UNSTEADY CONVECTION-DIFFUSION TYPE FLUID FLOW PROBLEMS

Fendoğlu, Hande
Ph.D., Department of Mathematics
Supervisor: Prof. Dr. Canan Bozkaya
Co-Supervisor: Prof. Dr. Münevver Tezer-Sezgin

May 2020, 131 pages

The time-dependent convection-diffusion-reaction (CDR) type equations with constant and variable convective coefficients are solved by using two different boundary element methods (BEM), namely dual reciprocity BEM (DRBEM) and domain BEM (DBEM), in the spatial discretization while an implicit backward finite difference scheme is used in time. In the applications of DRBEM and DBEM, the fundamental solutions of both CDR equation and the modified Helmholtz (mH) equation are made use of. This results in some leftover terms (e.g. time derivative of the unknown) in the equations; and consequently some leftover domain integrals after the weighting process of the differential equations with each aforementioned fundamental solutions. The treatment of these leftover domain integrals generates different BEM formulations. That is, the DRBEM arises following the transformation of these domain integrals into equivalent boundary integrals by using radial basis functions, while keeping these domain integrals and computing them numerically, produce the DBEM. The physical applications of the present techniques are mainly on the solutions of some fluid dynamics problems which are governed by time-dependent CDR

type equations.

In this respect, first the time-dependent magnetohydrodynamic (MHD) flow equations which are actually convection-diffusion type equations with constant convective coefficients, are solved in ducts with straight and perturbed walls of variable electrical conductivities in the presence of an inclined magnetic field. It is found that for MHD duct flow problems, the DBEM results are almost invariant to the use of the fundamental solutions of either convection-diffusion (CD) or mH equations, while DRBEM with the fundamental solution of CD equation gives reasonably good results. Both methods capture good the well-known MHD flow characteristics for increasing values of Hartmann number. Secondly, the problems governed by Navier-Stokes and/or energy equations are considered in order to extend the application of the present method to the non-linear CD type equations with variable convective coefficients. Thus, the DBEM with the fundamental solution of CD equation is employed for the solution of the benchmark problems of fluid dynamics and heat transfer such as lid-driven cavity, natural and MHD-natural convection flow in cavities and channels. It is observed that, the obtained numerical findings are quite compatible with the physics of the fluid flow and the temperature distribution for moderate values of Reynolds, Rayleigh and Hartmann numbers.

Keywords: Convection-diffusion-reaction equation, MHD flow, DRBEM, DBEM

ÖZ

ZAMANA BAĞLI KONVEKSİYON-DİFÜZYON TİPİNDEKİ AKIŞKAN AKIMI PROBLEMLERİNİN SINIR ELEMANLARI METODU İLE ÇÖZÜMÜ

Fendoğlu, Hande
Doktora, Matematik Bölümü
Tez Yöneticisi: Prof. Dr. Canan Bozkaya
Ortak Tez Yöneticisi: Prof. Dr. Münevver Tezer-Sezgin

Mayıs 2020 , 131 sayfa

Bu tezde, zamana bağlı konveksiyon-difüzyon-reaksiyon (CDR) tipinde olan, sabit veya değişken konvektif katsayilara sahip denklemler, iki farklı sınır elemanları metodu ile çözülmüştür. Bu metodlar sırasıyla, karşılıklı sınır elemanları yöntemi (DRBEM) ve bölge sınır elemanları yöntemidir (DBEM) ve bu metodlar uzaydaki ayrıklaştırma için kullanılmıştır. Zaman düzleminin ayrıklaştırılmasında ise kapalı olan geri yönde sonlu fark şeması kullanılmıştır. DRBEM ve DBEM uygulamalarında hem CDR hem de modifiye edilmiş Helmholtz (mH) denklemlerinin temel çözümlerinden faydalanılmıştır. Bahsedilen temel çözümler yardımıyla diferensiyel denklemlerin ağırlıklandırılma işlemi sırasında denklemdeki bazı terimler (bilinmeyenin zamana bağlı türevi gibi) sürece dahil edilmemektedir ve bunun sonucunda bu terimlerden oluşan bölge integralleri artakalmaktadır. Birbirinden farklı sınır elemanları yöntemlerinin doğuşu, artakalan bu bölge integrallerini ele alış biçimlerinin farklılığından kaynaklanmaktadır. Öyle ki, DRBEM bu bölge integrallerinin radyal baz fonksiyonları yardımıyla eşdeğer sınır integrallerine dönüştürülmesi sonucunda or-

taya çıkarken, DBEM ise bu bölge integrallerinin mevcut integral denklemi içerisinde tutularak nümerik şekilde hesaplanması ile doğmuştur. Kullanılan tekniklerin başlıca uygulama alanları bazı akışkanlar mekaniği problemlerinin çözümleri üzerine olup bu problemler zamana bağlı CDR tipindeki denklemlerle ifade edilmektedir.

Bu bağlamda, ilk olarak konveksiyon-difüzyon tipindeki denklemlerin sabit konvektif katsayılara sahip bir örneği olan zamana bağlı magnetohidrodinamik (MHD) akış problemlerinin nümerik çözümleri araştırılmıştır. MHD akış problemleri, değişken elektrik iletkenliği olan düz yüzeye yada engebeli yüzeye sahip kanallarda, eğimli bir manyetik alanın etkisi altında nümerik olarak çözülmüştür. DBEM, CD ve mH denklemlerinin temel çözümlerinin her ikisinin kullanımında da oldukça iyi sonuçlar verirken DRBEM, CD denkleminin temel çözümünün kullanılmasıyla makul sonuçlar vermektedir. Metodların her ikisi de Hartmann sayısının büyüyen değerlerinde, literatürde bilinen MHD akış karakteristiğiyle örtüşen sonuçlar vermiştir. Tezin ikinci kısmında, kullandığımız nümerik metodlar, lineer olmayan CD tipindeki değişken konvektif katsayılı denklemlerin nümerik çözümlerinin bulunması için uygulanmıştır. Bu sebeple, akışkanlar mekaniği ve ısı transferi problemlerine örnek olarak, üst kapağı hareketli kanal akış problemi, doğal konveksiyon ve MHD-doğal konveksiyon kanal akış problemleri, DBEM ile CD denkleminin temel çözümü kullanılarak çözülmüştür. Elde edilen nümerik sonuçlar belirli değerlerdeki Reynolds, Rayleigh ve Hartmann sayıları için akışkanlar mekaniği ve ısı dağılım problemlerinin genel fizik yapısıyla uyum içerisindedir.

Anahtar Kelimeler: Konveksiyon-difüzyon-reaksiyon denklemi, Magnetohidrodinamik akış, Karşılıklı sınır elemanları yöntemi, Bölge sınır elemanları yöntemi

To my husband, Salih,
and my lovely son, Ali

ACKNOWLEDGMENTS

First and foremost, I am deeply indebted to my advisor Prof. Dr. Canan Bozkaya, for her relentless support, immense knowledge, patiently guiding me through this whole journey and being a tremendous mentor to me, and Prof. Dr. Münevver Tezer, my co-advisor, for her invaluable guidance and astute advice all along. Words cannot express how privileged I feel to have the opportunity to work with them, and fortunate I feel to have them as my role models.

I also would like to thank my thesis committee members Prof. Dr. Nevzat Güneri Gençer and Prof. Dr. Ömür Uğur for their many valuable suggestions during my thesis progress presentations. I would also like to thank other members of my thesis defense committee, Prof. Dr. Ayhan Aydın and Prof Dr. Niyazi Şahin, for their helpful suggestions and reviewing my study. Many thanks to my friends Merve and Cemre for their companionship.

I gratefully acknowledge the financial support of The Scientific and Technological Research Council of Turkey (TÜBİTAK).

I offer my special thanks to my mother, Asiye, and my father, Metin, for their unconditional love, support and all the benevolence they have showered upon me all throughout my life. I also thank my sisters and brother for their friendships. My sister Beyza has always been there for me to help when I needed, which I will always treasure. My gratitude is extended to my mother- and father-in-law, Rabia and Hasan Tahsin, for their kind support.

I owe heartfelt thanks to my husband Salih for his love, encouragement and support throughout the Ph.D. and beyond. He always believed in me and I feel very lucky to have him in my life.

I thank my lovely son, Ali, for being the joy of my life and my little dearest friend.

TABLE OF CONTENTS

LIST OF TABLES

TABLES

LIST OF FIGURES

FIGURES

LIST OF ABBREVIATIONS

ABBREVIATIONS

$\vec{a} = (a_1, a_2)$	convection coefficient
B	induced magnetic field
B_0	strength of the magnetic field
c_p	specific heat at constant pressure
F	coordinate matrix
f_j	radial basis functions
g	gravitational acceleration vector
H, G	BEM matrices
h	potential source term
K	permeability of porous media
K_0	modified Bessel function of the second kind and of order zero
K_1	modified Bessel function of the second kind and of order one
k	thermal conductivity
L	number of interior nodes
L_0	characteristic length
l	element length
M	Hartmann number
M_1, M_2	domain integrals
N	number of boundary nodes
$\vec{n}$	unit outward normal to the boundary
P	pressure
Pr	Prandtl number
Ra	Rayleigh number

Re	Reynolds number
r	magnitude of the position vector $\vec{r} = (r_x, r_y)$ between the source point (x_i, y_i) and the field point (x, y)
T	temperature
T_c	cold wall temperature
T_h	heated wall temperature
t	time
U_0	characteristic velocity
u, v	velocity components
$\hat{u}$	particular solution
u^*	fundamental solution
q^*	normal derivative of u^*
$\mathbf{V}$	velocity
w	vorticity
α	thermal diffusivity
$\alpha_j(t), \varphi_j(t), \lambda_j(t)$	set of time-dependent undetermined coefficients
β	inclination angle of the externally applied magnetic field
$\bar{\beta}$	thermal expansion coefficient
Γ	boundary of the domain
γ	Euler constant
Δ	Dirac delta
ΔT	temperature difference between surfaces on the fluid
δ	Kronecker delta function
ε	diffusion coefficient
$\varepsilon_\Omega, \varepsilon_{\Gamma_1}, \varepsilon_{\Gamma_2}$	Residuals
λ	variable wall conductivity parameter
μ	dynamic viscosity

μ_0	permeability of free space ($= 4\pi \times 10^{-7}$)
ν	kinematic viscosity ($= \frac{\mu}{\rho}$)
ξ	perturbation parameter
ρ	fluid density
σ	electrical conductivity
$\sigma(t, x)$	reaction coefficient
ψ	stream function
Ω	spatial domain
CDR	convection-diffusion-reaction
CD	convection-diffusion
mH	modified Helmholtz
FDM	finite difference method
FEM	finite element method
FVM	finite volume method
BEM	boundary element method
DBEM	domain boundary element method
DRBEM	dual reciprocity boundary element method
MHD	Magnetohydrodynamics
NS	Navier-Stokes

CHAPTER 1

INTRODUCTION

Fluid dynamics, as a discipline, studies the behavior of fluid in motion (e.g. moving liquids or gases), where the fluid flow may be steady or unsteady, uniform or nonuniform, laminar or turbulant; one, two or three dimensional. Fluid dynamics has a wide range of scientific applications, ranging from designing canal, dam or piping systems, to modelling aerodynamics of supersonic airplanes. As such, it also relates to our daily lives. For instance, fluid dynamics principles can explain [2]:
• why airplanes must have streamlined smooth surface to have an efficient flight while golf balls need to have rough surfaces (dimpled) to have efficient throw;
• why we observe the surface of the water sometimes smoothly and sometimes roughly when it flows from the faucet;
• why it is impossible for the human ear to hear the supersonic airplane until it has gone past;
• how aerodynamic designs of cars effect the running of gasoline.
The list of applications can be continued. The main point is; fluid dynamics is a very important and practical subject. The principles of fluid dynamics; conservation of mass, conservation of momentum and conservation of energy, can provide a sound foundation of the fundamental aspects of fluid dynamics.

To solve a fluid dynamics problem, we need to take into account various properties of the fluid, such as flow velocity, pressure, density and temperature, each as a function of space and time. The governing equations of fluid dynamics problem are nonlinear partial differential equations. In general, this type of equations does not have a tractable analytical solution and requires the use of some numerical techniques. The numerical techniques which are conventionally used, are based on domain discretization, i.e. the finite difference method (FDM), the finite volume method (FVM) and the finite element method (FEM) [3, 4, 5]. These methods discretize the whole domain of the problem with elements or cells. However, these methods have difficulties in handling the curved geometries and the boundary conditions. Such applications are either not possible (for FDM) or practically infeasible or computationally enormously costly since discretizing the whole domain requires processing very large quantities of data. Moreover, modelling infinite regions or moving boundary problems are other difficulties the FEM faces with.

The boundary element method (BEM) provides a remedy to such difficulties [1]. It is an efficient alternative to domain discretization techniques (FDM, FVM or FEM), by requiring a smaller system of equations due to the discretization of the boundary of the computational domain; and thus being computationally much less costly. It is a boundary-only nature scheme and needs only the boundary values to provide a solution to the problem under consideration. The BEM has a wide range applications in engineering, such as torsion of noncircular bars, deflection of elastic membranes, bending of simply supported plates, heat transfer and fluid flow problems. Formally, BEM transforms a given set of differential equations defined in the domain into equivalent integral equations on the boundary by using the fundamental solution of the whole governing equation. In most of the cases, the fundamental solution for the whole governing equation is not available. In this case, some alternative BEM techniques are developed, namely the dual reciprocity BEM (DRBEM) and the domain BEM (DBEM), which use the fundamental solution corresponding not all but some of the terms of the governing equations. Thus, the basic integral equations of the DRBEM and DBEM involve domain integrals due to the leftover terms not used in the fundamental solutions. In DRBEM, these domain integrals are approximated and also transformed by radial basis functions, while in DBEM they are kept in the integral equation and then computed numerically.

This chapter proceeds as follows: First, the definition of the problem and motivation are explained and then governing equations of the considered problems are given; namely magnetohydrodynamic (MHD) flow equations, Navier-Stokes (NS) and natural convection flow equations. Before we conclude, the literature survey is given, and the chapter is concluded with the originality and the plan of the thesis.

1.1 Motivation and Problem Definition

Convection-diffusion-reaction (CDR) type equations have attracted considerable interest from many researchers due to their various applications in biology, ecology, engineering and medicine. Convection represents the movement of a substance within a medium (e.g. water or air). Diffusion refers to the movement of the substance from a medium of high concentration to the low concentration, providing the uniform distribution of the substance. A chemical reaction represents the process that gives the interconversion of chemical substances. These type of equations represent quantities such as population size or concentration of nutrients, pollutants and other chemicals in the atmosphere, groundwater and surface water (subject to given constraints). For example, self-purification of a river can be formulated in terms of biological demand for oxygen and the dissolved oxygen concentration by using CDR equations [6]. Models concerning tumour invasion, tumour angiogenesis and bacterial pattern formation are also described by CDR type equations [7].

Solving CDR type equation is a difficult task due to the nature of the equation which includes first and second order partial derivatives with respect to space. According to the value of the diffusion coefficient, the CDR equation becomes parabolic (diffusion-dominated) or hyperbolic (convection-dominated). Traditional FDM and FEM generally give accurate results for the former but not the latter, in which case oscillations and smoothing of the wave front are introduced [1]. When BEM is applied to these equations it can be seen that BEM seems to be relatively free from these problems. Thus, DRBEM and DBEM will be employed in this thesis to solve the convection-dominated CDR equations with different fundamental solutions namely: the fundamental solution of Laplace, convection-diffusion-reaction (CDR) and modified Helmholtz (mH) equations. As a consequence, the importance of analysis of numerical methods for the accurate solution of CDR equation has motivated this thesis.

Time-dependent CDR equations with constant convective coefficients are used to express not only concentration of nutrients problem but also MHD duct flow problems. Further, time-dependent CDR equations with variable convective coefficients are used to explain the fluid flow and the fluid dynamics problems which include Navier-

Stokes equations in channels, lid-driven cavity flow and natural convection flow, etc. Both type of CDR equations have a significant spot in the literature. Therefore, in this thesis, the emphasis is given not only to the time-dependent CDR type equations with constant convective coefficients, but also the convection-diffusion (CD) type equations with variable convective coefficients.

1.2 Governing Equations for the Considered Problems

This section focuses on the mathematical models of the problems which will be solved in the present thesis. As mentioned before, the aim is to numerically solve the problems which are governed by time-dependent CDR equations using two boundary element methods with different fundamental solutions. In this respect, some fluid dynamics problems with or without the effect of an externally applied magnetic field are considered since the governing equations of these problems are actually time-dependent or steady CD/CDR type equations with either constant or variable convective coefficients.

1.2.1 Magnetohydrodynamic Flow Equations

Magnetohydrodynamics is a branch of science which studies the motion of electrically conducting fluids under magnetic fields. The main idea of the MHD is based on the mutual interaction of fluid flow and magnetic fields; the fluid motion generates the magnetic field (through Ohm's Law) and the effect of magnetic fields creates a force on the fluid which causes a change on the magnetic field [8]. As CDR problems, the MHD flow problem in channels has also a wide range of engineering applications such as power generation, acceleration, geothermal energy extraction, conducting plasma in physics, producing liquid metals, nuclear fusion, etc. [9]. The MHD flow is a challenging area due to its simultaneous consideration of the fluid mechanics equations and electromagnetic equations which results in interaction of velocity and magnetic field. The other difficulty of the MHD flow problem is the satisfaction of the divergence-free conditions on the velocity and induced magnetic field.

The governing MHD equations consist of Navier-Stokes equations and Maxwell's equations of electromagnetism through Ohm's law. The velocity can be expressed as $\mathbf{V} = (0, 0, V'(x', y', t'))$ indicating the action only in the z-direction and the induced magnetic field takes the form $\mathbf{B} = (B_0 \sin\beta, B_0 \cos\beta, B'(x', y', t'))$ under the effect of a constant and uniform oblique magnetic field of strength B_0 making an angle β with the positive y-axis. The z-axis is chosen as the axis of the duct. The transient, laminar, fully developed flow of an incompressible, viscous and electrically conducting fluid in a rectangular duct subject to oblique magnetic field can be expressed in the following dimensional form [10]:

$$\begin{aligned} \mu\nabla^2 V' + \frac{B_0}{\mu_0}\sin\beta\frac{\partial B'}{\partial x'} + \frac{B_0}{\mu_0}\cos\beta\frac{\partial B'}{\partial y'} &= \frac{\partial P}{\partial z'} + \rho\frac{\partial V'}{\partial t'} \\ \frac{1}{\sigma\mu_0}\nabla^2 B' + B_0\sin\beta\frac{\partial V'}{\partial x'} + B_0\cos\beta\frac{\partial V'}{\partial y'} &= \frac{\partial B'}{\partial t'} \end{aligned} \quad \text{in} \quad \Omega \tag{1.1}$$

where μ_0 is the permeability of free space ($= 4\pi \times 10^{-7} H/m$), σ is the electrical conductivity of the fluid, ρ is the fluid density, P is the pressure in the fluid and $\frac{1}{\sigma\mu_0}$ represents magnetic diffusivity. Introducing dimensionless variables [8],

$$x = \frac{x'}{L_0}, \quad y = \frac{y'}{L_0}, \quad t = \frac{t'U_0}{L_0}, \quad V = \frac{V'}{U_0}, \quad B = \frac{B'}{U_0\mu_0\sqrt{\sigma\mu}} \tag{1.2}$$

where L_0 is characteristic length, μ is the viscosity and

$$U_0 = -L_0^2(\frac{\partial P}{\partial z'})/\mu \tag{1.3}$$

is the characteristic velocity, and substituting in Equation (1.1), the non-dimensional form of the MHD equations (1.1) are obtained as

$$\begin{aligned} \nabla^2 V + M\sin\beta\frac{\partial B}{\partial x} + M\cos\beta\frac{\partial B}{\partial y} &= -1 + \frac{\partial V}{\partial t} \\ \nabla^2 B + M\sin\beta\frac{\partial V}{\partial x} + M\cos\beta\frac{\partial V}{\partial y} &= \frac{\partial B}{\partial t} \end{aligned} \quad \text{in} \quad \Omega \tag{1.4}$$

for $t > 0$. Here, M is Hartmann number which is defined by

$$M = \frac{B_0 L_0 \sqrt{\sigma}}{\sqrt{\mu}} \tag{1.5}$$

and it is the magnitude of the vector $\overrightarrow{M} = (M_x, M_y)$ with components given as

$$M_x = M\sin\beta, \quad M_y = M\cos\beta. \tag{1.6}$$

Thus, Equations (1.4) are reduced to

$$\begin{aligned} \nabla^2 V + M_x \frac{\partial B}{\partial x} + M_y \frac{\partial B}{\partial y} &= -1 + \frac{\partial V}{\partial t} \\ \nabla^2 B + M_x \frac{\partial V}{\partial x} + M_y \frac{\partial V}{\partial y} &= \frac{\partial B}{\partial t} \end{aligned} \qquad \text{in} \quad \Omega \tag{1.7}$$

for $t > 0$.

1.2.2 Fluid Dynamics Equations

Fluid dynamics is a discipline of fluid mechanics that describes the flow of fluids. An important application area for numerical simulation is the investigation of the behavior of fluid flow. The behavior of fluids (liquids or gases) can be observed in almost all areas of life ranging from complex technical applications to the more ordinary situations of daily life. To understand the interesting phenomena associated with fluid dynamics, one must consider the fundamental principles that govern the motion of fluid particles. The main physical principles of fluid dynamics are the continuity, momentum and energy equations. In this section, these principles are presented for the two-dimensional flow.

1.2.2.1 Conservation of Mass

The fundamental rule of conservation of mass is that mass can neither be created nor destroyed. Conservation of mass requires that the mass of a system remain constant as the system moves through the flow field which means time rate of change of the system mass is equal to zero. If one consider the mass flux through differential control volume it can be stated that, rate of mass flux out of control volume must be equal to the rate of accumulation of mass within control volume which is expressed as [11, 12],

$$\frac{\partial \rho}{\partial t'} + u' \frac{\partial \rho}{\partial x'} + v' \frac{\partial \rho}{\partial y'} + \rho\left(\frac{\partial u'}{\partial x'} + \frac{\partial v'}{\partial y'}\right) = 0 \tag{1.8}$$

where **V** $= (u', v')$ is the fluid velocity field. In general, $\frac{D}{Dt'}$ denotes the rate of change which is

$$\frac{D}{Dt'} = \frac{\partial}{\partial t'} + u' \frac{\partial}{\partial x'} + v' \frac{\partial}{\partial y'} \tag{1.9}$$

in cartesian coordinates. Thus, Equation (1.8) can be written as

$$\frac{D\rho}{Dt'} + \rho\nabla \cdot \mathbf{V} = 0. \tag{1.10}$$

This is known as the most general form of the continuity equation. For incompressible fluids, the fluid density ρ is a constant throughout the flow field which is the case considered in this thesis. Thus, Equation (1.10) becomes

$$\nabla \cdot \mathbf{V} = 0 \tag{1.11}$$

or

$$\frac{\partial u'}{\partial x'} + \frac{\partial v'}{\partial y'} = 0 \tag{1.12}$$

1.2.2.2 Conservation of Momentum (Newton's Second Law)

Newton's second law of motion states that, time rate of change of the linear momentum of the system is equal to the sum of the external forces acting on the system. By conservation of momentum law, the momentum equations are given by [2, 12]

$$\rho\frac{Du'}{Dt'} = \rho g_x - \frac{\partial P'}{\partial x'} + \mu(\frac{\partial^2 u'}{\partial x'^2} + \frac{\partial^2 u'}{\partial y'^2}) \tag{1.13}$$

$$\rho\frac{Dv'}{Dt'} = \rho g_y - \frac{\partial P'}{\partial y'} + \mu(\frac{\partial^2 v'}{\partial x'^2} + \frac{\partial^2 v'}{\partial y'^2}) \tag{1.14}$$

where $\mathbf{g} = (g_x, g_y)$ is gravitational acceleration vector. When these two equations above are combined with the continuity equation (1.12), the problem becomes well-posed. Equations (1.13) and (1.14) can be expressed in a compact form as [11]

$$\rho\frac{D\mathbf{V}}{Dt'} = \rho\mathbf{g} - \nabla P' + \mu\nabla^2\mathbf{V}. \tag{1.15}$$

1.2.2.3 Energy Equation

A statement of this principle is the first law of thermodynamics: Rate of change of energy inside the fluid element is equal to the summation of net heat flux into the element and rate of work done on the element due to the body and surface forces. By the principle of conservation of energy and Fourier laws in a control volume the energy equation is given by [13],

$$\frac{\partial T'}{\partial t'} + \mathbf{V} \cdot \nabla T' = \frac{k}{\rho c_p}\nabla^2 T' \tag{1.16}$$

in which c_p and k represent the specific heat and the thermal conductivity, respectively. When the temperature of the fluid is under the influence of external forces these additional force terms are involved in the energy equation. The non-dimensional form of energy equation is derived as follows

$$\frac{\partial T}{\partial t} + u\frac{\partial T}{\partial x} + v\frac{\partial T}{\partial y} = \frac{1}{PrRe}\nabla^2 T \tag{1.17}$$

by using the dimensionless variable $T = \frac{T' - T_c}{T_h - T_c}$ in which T_c and T_h represent cold and heated wall temperatures, respectively.

1.2.3 Navier-Stokes Equations

The Navier-Stokes (NS) equations are at the heart of the fluid flow modeling and are named by mathematicians L. M. H. Navier (1785-1836) and Sir G. G. Stokes (1819-1903) who derived the mathematical formulations. NS equations have a wide range of engineering applications such as motion of stars, blood flow, ocean current, modeling the weather, fluid flow in channels, air flow around a wing, pollution dispersion, the design of power stations, aircrafts and cars etc. They provide a mathematical model of physical conservation law of mass, momentum, energy and species concentration which results in continuity and momentum equations. These equations consist of non-linear partial differential equations which can be written in terms of primitive physical variables or dependent ones. The nonlinearity causes certain difficulties to solve these equations analytically. Analytical solutions are obtained for only some cases with simplified physical assumptions. Thus, NS equations are needed to be solved using numerical techniques for most of the real life physical problems.

The continuity equation (1.11) and the momentum equation (1.15) can be written as a pair of simultaneous partial differential equations in velocity-pressure form which are nonlinear and second-order by neglecting body forces as follows

$$\begin{aligned} \nabla \cdot \mathbf{V} &= 0 && (1.18)\\ \rho\frac{D\mathbf{V}}{Dt'} &= \mu\nabla^2\mathbf{V} - \nabla P'. && (1.19) \end{aligned}$$

The non-dimensional form of NS equations can be expressed as [14]

$$\frac{\partial u}{\partial x} + \frac{\partial v}{\partial y} = 0 \tag{1.20}$$

$$\frac{\partial u}{\partial t} + u\frac{\partial u}{\partial x} + v\frac{\partial u}{\partial y} = \frac{1}{Re}\nabla^2 u - \frac{\partial P}{\partial x} \tag{1.21}$$

$$\frac{\partial v}{\partial t} + u\frac{\partial v}{\partial x} + v\frac{\partial v}{\partial y} = \frac{1}{Re}\nabla^2 v - \frac{\partial P}{\partial y} \tag{1.22}$$

by using the non-dimensional variables given below

$$u = \frac{u'}{U_0}, \quad v = \frac{v'}{U_0}, \quad P = \frac{P'}{\rho U_0^2}, \quad t = \frac{t'U_0}{L_0}, \quad x = \frac{x'}{L_0}, \quad y = \frac{y'}{L_0} \tag{1.23}$$

where U_0, $Re = \frac{\rho U_0 L_0}{\mu}$ and μ denote characteristic velocity, Reynolds number and dynamic viscosity, respectively. The velocity-pressure form of NS equations has some disadvantages due to the fact that the boundary condition of pressure field does not exist. Therefore, we define the Navier-Stokes equations in new variables to avoid the pressure term. The stream function-vorticity formulation can be defined as an efficient form of NS equations due to the elimination of pressure term and automatic satisfaction of continuity equation. However, some difficulties associated with the solution of these equations arise from the nonlinearity of vorticity transport equation and the unknown boundary conditions of vorticity. In order to obtain the stream function-vorticity form of NS equations (1.20)-(1.22) the stream function ψ is defined as

$$u = \frac{\partial \psi}{\partial y}, \qquad v = -\frac{\partial \psi}{\partial x} \tag{1.24}$$

which satisfies the continuity equation (1.12) automatically. To be able to derive the stream function equation, we use the definition of vorticity as $\mathbf{w} = \nabla \times \mathbf{u}$

$$w = \frac{\partial v}{\partial x} - \frac{\partial u}{\partial y} = \frac{\partial}{\partial x}(-\frac{\partial \psi}{\partial x}) - \frac{\partial}{\partial y}(\frac{\partial \psi}{\partial y}) = -\nabla^2 \psi. \tag{1.25}$$

Equations (1.21) and (1.22) are differentiated with respect to y and x, respectively and the Equation (1.21) is subtracted from the Equation (1.22). Then, one can obtain the vorticity transport equation as follows

$$\frac{\partial w}{\partial t} + u\frac{\partial w}{\partial x} + v\frac{\partial w}{\partial y} = \frac{1}{Re}\nabla^2 w. \tag{1.26}$$

Thus, the time-dependent Navier-Stokes equations in stream function-vorticity form become

$$\nabla^2 \psi = -w \tag{1.27}$$

$$\frac{\partial w}{\partial t} + u\frac{\partial w}{\partial x} + v\frac{\partial w}{\partial y} = \frac{1}{Re}\nabla^2 w. \tag{1.28}$$

1.2.4 Natural Convection Flow

Heat transfer due to convection includes the energy exchange between a surface and an adjacent fluid. This heat transfer can be classified as forced convection, natural convection and mixed convection. In the forced convection, the fluid motion is generated by an external force (lid, fan or pump). For instance, lid-driven cavity problems are the most famous examples for the forced convection. On the other hand, the natural convection is a type of flow, of motion of a liquid or a gas, in which the fluid motion is not generated by any external source (like a pump, fan, suction device, etc.) but by some parts of the fluid being heavier than other parts. Changes in temperature cause variations in the fluid density which arises the Buoyancy forces. Buoyancy forces induce the motion (e.g. hot fluid tends to rise, cold to fall) and it produces the convection naturally. In nature, convection cells formed from air raising above sunlight-warmed land or water are a major feature of all weather systems. Convection is also seen in the rising plume of hot air from fire, plate tectonics, oceanic currents and sea-wind formation. A very common industrial application of natural convection is free air cooling without the aid of fans: this can happen on small scales (computer chips) to large scale process equipment, energy storage, meteorology and climatology. The ventilation between indoors and outdoors and the design of double glazing are some applications of natural convection that we see in daily life.

Natural convection flow arises from the addition of energy equation to NS equations. The non-dimensional stream function-vorticity-temperature formulation are given as [15]

$$\begin{aligned}
\nabla^2\psi &= -w && (1.29)\\
\frac{\partial w}{\partial t} + u\frac{\partial w}{\partial x} + v\frac{\partial w}{\partial y} &= Pr\nabla^2 w + RaPr\frac{\partial T}{\partial x} && (1.30)\\
\frac{\partial T}{\partial t} + u\frac{\partial T}{\partial x} + v\frac{\partial T}{\partial y} &= \nabla^2 T. && (1.31)
\end{aligned}$$

where T, Pr and Ra are the temperature, Prandtl number and Rayleigh number, respectively. Equations (1.29), (1.30) and (1.31) must be considered simultaneously. Thus, it is difficult to solve these equations analytically. The addition of energy equation to the NS equations necessities the inclusion of the force term $RaPr\frac{\partial T}{\partial x}$ to the vorticity transport equation with the new dimensionless quantities [14],

$$\text{Prandtl number :} \qquad Pr = \frac{\nu}{\alpha} \tag{1.32}$$

$$\text{Rayleigh number :} \qquad Ra = \frac{g\bar{\beta}\Delta T L_0^3}{\alpha\nu} \tag{1.33}$$

where $\nu = \frac{\mu}{\rho}$ is the kinematic viscosity, α is the thermal diffusivity, $\bar{\beta}$ is thermal expansion coefficient, ΔT is the temperature difference between surface and the fluid. The Prandtl number describes the relative strength of the diffusion of momentum to that of heat. Typical values are taken as 0.71 for air, around 7 for water and around 0.015 for mercury [16].

1.3 Literature Survey

The convection–diffusion-reaction equation describes physical phenomena where energy, particles or other physical quantities are moving inside a physical system. The domain discretization techniques such as finite difference method and finite element method have been widely used for the solution of both steady and transient convection or diffusion-dominated problems.

There have been many studies on the steady case, however, the works carried only on the transient problems will be mentioned here, since this thesis focuses on the solution of transient equations. Clavero and Gracia [17] have solved the transient convection-diffusion problem by using FDM while a combined FDM-FEM has been employed by Douglas and Russell [18]. They indicate that these schemes have much smaller time-truncation errors than those of standard methods.

On the other hand, FEM has been used for the discretization of time-dependent convection-diffusion-reaction equations by Tezduyar $et\ al.$ [19]. They observe accurate results with minimal oscillations while John and Schmeyer [20] use FEM with small diffusion parameter. Burman and Fernández [21] are interested in CDR problems in which the advection dominates, and they obtain stable results using a symmetric, weakly consistent stabilization while Codina and Blasco [22] use FEM to solve CDR equation based on the decomposition of the unknowns into resolvable and subgrid scales. Furthermore, a discontinuous Galerkin FEM has been proposed for the space-time discretization of a CDR equation in the work [23]. In [24], a comparison of some FEM approaches, such as streamline-upwind Petrov-Galerkin and least-squares, has been presented to solve the CDR problems.

On the other hand, the boundary element method (BEM) which is an efficient alternative to domain discretization techniques due to its boundary-only nature, has been recently employed for the solution of convection-diffusion type equations in the works [25, 26, 27] by Grigoriev and Dargush. They present the high-order BEM solutions for CD problems and obtain good accuracy even for predominantly convective flows. The transient CD problem has been studied by Cunha et al. [28] using both DBEM and time domain BEM (TDBEM) and obtained results are compared with FEM solutions; and good agreement is observed between BEM and FEM results. Singh and Tanaka [29] provide DRBEM results with two kinds of fundamental solutions of CD equations and they obtain accurate results. AL-Bayati and Wrobel [30] present a novel formulation of the DRBEM for solving two-dimensional transient CDR problems with spatial variable velocity field. This new formulation is devoted to handle the time derivation and the variable velocity field; and hence an excellent agreement with the analytical solution is observed. Moreover, an Eulerian-Lagrangian BEM technique has been proposed in the work [31].

In the first part of the thesis, the numerical solutions of the convection-diffusion type equations with constant convective coefficients are obtained by DBEM and DRBEM with the fundamental solutions of convection-diffusion and modified Helmholtz equations. The application of DBEM with the fundamental solution of CD equation to CDR equation is a new contribution to the field which is not previously explored in the literature. In this respect, the unsteady CDR equation in a square cavity for which the analytical solution is available, is considered as a first application of our numerical methods.

Another important application area of the convection-diffusion type equations with constant convective coefficients is the MHD duct flow problems which is considered as a second physical application of the thesis. Steady MHD flows have been studied widely compared to the transient MHD flows in regular domains like rectangular/triangular ducts with straight boundaries (e.g. [32, 33, 34]) and in complex geometries like annular-like domains in [35].

However, an extensive literature survey on the time-dependent MHD flow problems will be given here since the thesis focuses on the time-dependent CDR type equations. The unsteady MHD flow equations have been studied using the finite element method (FEM) in two-dimensional rectangular, circular and triangular pipes by Singh and Lal [36]. They observed that when the wall conductivity and Hartmann number increase, the flux through a section is reduced and the steady-state is approached at a faster rate. Salah $et\ al.$ [37] developed a solution algorithm for the three-dimensional coupled MHD flow. This method is valid for both high and low magnetic Reynolds numbers.

Seungsoo and Dulikravich [38] have given a finite difference method (FDM) for three-dimensional unsteady MHD flow in a rectangular channel along with a temperature variation. Additionally, Sheu and Lin [39] proposed CDR model for solving unsteady MHD flow with a FDM on non-staggered grids using a transport scheme in each ADI spatial sweep. Their results are in good agreement with the analytical solutions and show high rate of convergence. Some meshless methods have also been proposed for solving MHD flow equations in channels of different cross-sections and for arbitrary wall conductivities.

Dehghan and Mirzaei [40, 41], and Loukopoulos $et\ al.$ [42], presented meshless local boundary integral equation method, meshless Local Petrov Galerkin method and localized meshless point collocation method, respectively, for solving unsteady MHD flow equations.

A numerical scheme which is a combination of the dual reciprocity BEM for space and the differential quadrature method (DQM) for the time discretization, is proposed by Bozkaya and Tezer-Sezgin [43] for the solution of unsteady MHD flow problem in a regular rectangular duct with insulated walls. Thus, the solution is obtained at any required time level without the need of step-by-step computation with respect to time. For the unsteady MHD flow in a duct with arbitrary wall conductivity, the BEM formulation with time-dependent fundamental solution is presented by Bozkaya and Tezer-Sezgin [44], and the numerical solutions are obtained for higher values of Hartmann numbers compared to some previous studies.

On the other hand, the time-dependent MHD flow in a rectangular duct with a perturbed boundary subject to an external magnetic field is considered as a physically challenging problem but studied rarely. The effect of the boundary perturbation on the fluid flow has been given in the work of Mahabaleshwar $et\ al.$ [45] and for the steady MHD flow, in the study of Marušić-Paloka and Pažanin [46] for the Darcy-Brinkman flow and for incompressible viscous flow by Jäger [47]. In the work of Aydın and Tezer-Sezgin [48], the MHD flow direct and Cauchy problems in a rectangular duct with a perturbed slipping upper boundary are solved asymptotically with the use of DRBEM to recover the slip length on the perturbed boundary through the slip boundary conditions for relatively small values of Hartmann number.

When MHD equations are solved with DRBEM, fundamental solution of Laplace equation is widely used in the literature [43, 44, 48]. However, in the present thesis, the DRBEM with the fundamental solutions of CD and mH equations are used, for the first time to solve the unsteady MHD flow in both regular and irregular ducts with variable wall conductivities. Moreover, the use of domain BEM technique is also a further contribution to the solution of the same problem for the purpose of comparison of the results obtained by both techniques.

In the second part of the thesis, we deal with the convection-diffusion type equations with variable convective coefficients. Specifically, some fluid dynamics problems which are governed by the time-dependent NS equations are considered. Some studies about these problems are summarized below. Since in this thesis we consider NS equations in stream function-vorticity formulation, only the studies which solve the NS equations in this formulation are mentioned here.

Starting with earlier studies, 2-D incompressible NS equations are solved by Ghia $et\ al.$ [49] to discuss the effectiveness of the coupled strongly implicit multigrid method (CSI-MG) in the determination of high-Re fine-mesh flow solutions while Onishi $et\ al.$ [50] present a new type of boundary conditions on vorticity which are convenient for boundary elements. The direct BEM technique is employed for solving nonlinear flow equations by simple iterations. In computational scheme, they use the boundary element upwind technique to increase the order of stability.

Ghadi $et\ al.$ [51] has given solution incompressible Navier-Stokes problem by the use of continuous Lagrange finite elements technique. This technique splits the vorticity into two components. Semi-discretization is used for time and classical characteristic method in the discretization of advective terms. Later, they improve this technique by linearizing the advective term and uncoupling both variables in [52], and so they overcome the difficulty which arises from the lack of the boundary conditions for the vorticity. The lid-driven cavity flow problem is considered with classical piecewise linear FEM, and numerical results give better accuracy than their previous work. Tezduyar $et\ al.$ [19] presented the streamline upwind/Petrov-Galerkin method to solve the NS equations in stream function-vorticity formulation. Both viscous and inviscid cases are considered. They use the implicit-explicit and grouped element-by-element iteration techniques to increase the accuracy. The obtained results show good agreement with the published ones until that time.

Sousa and Sobey [53] developed global iteration matrix formulation to examine the effect on numerical stability of different numerical schemes for vorticity boundary conditions. Luo and Jiang [54] established reduced-order extrapolated Crank–Nicolson finite spectral element method to solve the NS equations by using the proper orthogonal decomposition for reducing the order of the coefficient vector of the classical Crank–Nicolson finite spectral element method. This new method is tested by employing some numerical examples; and results reveal that the effectiveness and feasibility of the reduced-order extrapolated Crank–Nicolson finite spectral element method is quite well.

A messless method which is based on least squares techniques is applied by Lashckarbolok and Jabbari [55] to the 2-D incompressible NS equations. As an example, lid-driven cavity flow is considered for different Reynolds number. Kim $et\ al.$ [56] employed meshfree collocation method to solve the NS equations in stream function-vorticity form. To obtain the vorticity boundary conditions, meshfree approximation is used. Effectiveness and accuracy of the method are examined by some examples which includes lid-driven cavity flow.

Considering the number of the studies which investigate the solution of 2-D incompressible NS equations in stream function-vorticity form, boundary element techniques have limited number of studies when compared the other techniques. Ramsak

$et\ al.$ [57] developed the subdomain based BEM technique for modelling of 2-D unsteady laminar flow using stream function–vorticity formulation of the Navier–Stokes equations. The subdomain technique aims to combine the known BEM accuracy with the computational efficiency of other numerical techniques like FEM or FVM. Ghadimi and Dashtimanesh [58] developed coupled numerical algorithm which combines FDM and DRBEM. In this algorithm, vorticity transport equation is solved by FDM while Poisson equation is solved by the DRBEM. One-sided lid-driven cavity flow problem is investigated and they obtained reasonable results for higher values of Reynolds number ($Re = 10.000$).

Another attractive research field is natural convection heat flow in fluid flow modelling. The natural convection flow in a square cavity is investigated by Shu and Xue [15]. The generalized differential quadrature method is employed to obtain the solution. Neumann and Dirichlet type boundary conditions are employed on the cavity walls and different approaches are used to handle them.

The meshless local Petrov–Galerkin method (MLPG) is expressed by Sheikhi $et\ al.$ [59] to solve natural convection heat transfer in turbulent regimes which is governed by NS and energy equations and they are incorporated with the Spalart–Allmaras model which governs the turbulent viscosity. Moving least-squares interpolation has been used to approximate the fluid variables. This study includes three different cavity of natural heat transfer as in a square cavity, between two concentric cylinders of square outer and circular inner walls and through a fluid bounded by two concentric circular cylinders. Results are obtained for higher values of Rayleigh numbers. MLPG is also employed by Arefmanesh $et.\ al.$ [60] to simulate the buoyancy-driven fluid flow and heat transfer in a differentially-heated square cavity having a wavy baffle attached to its higher temperature side wall.

Liang and Zhang [61] used two-grid finite element method to solve the natural convection problem while Šarler $et\ al.$ [62] used DRBEM with fundamental solution of Laplace equation to solve the steady natural convection problem in a porous medium.

As it can be seen, the fluid dynamics problems governed by the NS equation in stream function-vorticity form and/or energy equation are extensively studied in different computational domains by several numerical techniques including DRBEM with the fundamental solution of Laplace equation. However, since these equations can be considered with variable convective coefficients, we employ both DBEM and DRBEM for the solutions of NS equations as an extension of the first part of the thesis. It is observed that the use of DBEM and DRBEM with the fundamental solution of CD is an alternative scheme for the solution of these kind of problems.

1.4 Originality of the Thesis

In this thesis, we solve the time-dependent convection-diffusion-reaction type equations with constant and variable convective coefficients by using the numerical techniques, namely, DRBEM and DBEM. In particular, we study the DRBEM and DBEM with two distinct fundamental solutions of CDR and mH equations. To the best of authors' knowledge, we are the first to use the DBEM with the fundamental solution based on CDR equation. Moreover, we obtain solutions for the convection-dominated cases as well, which is a challenging task given that, other widely-celebrated numerical techniques generally fall short of providing a solution for such cases.

An additional novelty of the thesis is that the DBEM and DRBEM with the fundamental solutions of CDR and mH equations are applied for the first time to the transient MHD flow problems in ducts not only with flat but also with perturbed walls. The rectangular duct with straight boundaries are subject to inclined magnetic field, but in the case of the perturbed boundary ducts the external magnetic field is applied vertically. Further, the no-slip walls are considered to be either insulated or conducting with variable conductivity, thus, it can be said that the general type of boundary conditions are employed for the induced magnetic field.

In the second part of the thesis, the applications of the DBEM and DRBEM are extended to the solution of CD type equations with variable convective coefficients. As physical applications, some basic fluid dynamics problems governed by NS equations, namely lid-driven cavity, natural convection, MHD natural convection and channel flow are solved since these equations are of the form of CD equations with variable coefficients involving the unknown velocity components. Then, DBEM with the fundamental solution of CD equation is employed in the thesis as a new contribution for the solution of these nonlinear equations.

1.5 The Outline of the Thesis

In Chapter 2, DRBEM and DBEM formulations are provided with different fundamental solutions. At first, DRBEM with fundamental solutions of Laplace, convection-diffusion-reaction and modified Helmholtz equations are expressed. Then, DBEM with fundamental solutions of convection-diffusion-reaction and modified Helmholtz equations are explained elaborately.

In Chapter 3, the time-dependent CDR type equations with constant convective coefficients are investigated numerically. That is, both DRBEM and DBEM are employed to solve these equations with fundamental solutions of either convection-diffusion or modified Helmholtz equations. Basically, two types of problems are considered. First, the CDR equation, for which the exact solution is available, is considered in order to validate our numerical simulations and computer codes. Then, the analysis is carried for the main interest of this chapter, which are the time-dependent MHD flow problems in either regular or irregular ducts with perturbed walls under various types of boundary conditions. Specifically, we consider MHD duct flow problem with insulated and/or variable conductivity wall conditions under the effect of either horizontal, vertical or oblique magnetic field. The obtained numerical results are analyzed and compared with respect to efficiency of the numerical methods, suitability of the used fundamental solutions and the type of computational domain.

In Chapter 4, solutions of time-dependent CD type equations with variable convective coefficients are obtained by using both DRBEM and DBEM with fundamental solution of convection-diffusion equation. As in Chapter 3, the application of the methods are explained through the CD equation with variable coefficients and the codes are validated by the exact solution of the heat conduction problem which is governed by the CD equation with varying coefficients in a square computational domain. Then, the techniques are implemented for some fluid dynamics problems, namely, lid-driven flow, natural convection flow, channel flow and MHD natural convection flow in a porous medium. All these problems are governed by the NS equations and energy equation in the presence of a heat source, in which the momentum and energy equations can be treated as CD type equations involving variable convective coefficients which are functions of the unknown.

In Chapter 5, the important numerical findings of the considered problems are summarized.

CHAPTER 2

THE DRBEM AND THE DBEM FORMULATIONS

The boundary element method is a well-established numerical technique which gives the solution for wide-range of the engineering problems such as torsion of noncircular bars, deflection of elastic membranes, bending of simply supported plates, heat transfer and fluid flow problems, etc. Also, it provides an efficient alternative to the other numerical techniques such as finite difference method and finite element method. The main advantage of the BEM is the much smaller system of equations compared to domain discretization techniques, i.e. FDM, FEM. Moreover, there is a considerable reduction in the data required to run a problem by BEM since it is a boundary-only nature scheme and needs only the boundary values to provide the solution to the problem under consideration. Thus, the dimensionality of the problem is reduced by one which results in less computational and data preparation effort than the other domain discretization techniques.

The aim of the BEM is to transform the given differential equations defined in the domain into equivalent integral equations defined only on the boundary of the problem. The weighted residual formulations are employed to produce these direct integral equations. BEM procedure requires inherent use of the fundamental solutions for the whole governing equations. Such fundamental solutions are not generally available and this is the initial restriction of the BEM. Moreover, the nonhomogeneous terms in the governing equations of the problem result in domain integrals in the formulation of BEM and BEM suffers to eliminate them. Thus, some alternative techniques, namely dual reciprocity BEM and domain BEM, in which the fundamental solutions apply only to a piece of the governing equations, have been developed. The application of these alternative BEM techniques deals with a leftover domain integral in the integral equation. In DRBEM, the leftover domain integral is transformed into an equivalent boundary integral by means of radial basis functions while it is preserved and evaluated by the use of numerical integration in DBEM.

The formulations of these boundary element methods will be explained by using the time-dependent convection-diffusion-reaction equation which is given by

$$\frac{\partial u}{\partial t} - \varepsilon \nabla^2 u + \vec{a} \cdot \nabla u + \sigma u = h \quad \text{in} \quad (0, T] \times \Omega \tag{2.1}$$

where $u(x,t)$ is the solution, $\vec{a} = (a_1, a_2)$ denotes the convection coefficient with constant terms, $\sigma(t,x)$ is the reaction coefficient, h is a potential source term in a considered finite time interval $(0,T]$. To be able to have a well-defined problem, the boundary conditions can be taken as Dirichlet type ($u = \bar{u}$), Neumann type ($\frac{\partial u}{\partial n} = \bar{q}$) or mixed type ($\alpha u + \mu \frac{\partial u}{\partial n} = g$) on the boundary Γ of the spatial domain Ω. Here, α and μ are constants and $\bar{u} = \bar{u}(x,y,t)$, $\bar{q} = \bar{q}(x,y,t)$ and $g = g(x,y,t)$ are given functions. On the other hand, the initial condition is given as

$$u = u_0 \ \text{ in } \ \Omega \times \{t = 0\}. \tag{2.2}$$

Section 2.1 is devoted to the DRBEM formulation of Equation (2.1) using three different fundamental solutions, namely, fundamental solution of Laplace equation (Section 2.1.1), fundamental solution of convection-diffusion-reaction equation (Section 2.1.2) and fundamental solution of modified Helmholtz equation (Section 2.1.3). Section 2.2 deals with the DBEM formulations of Equation (2.1). The DBEM with the fundamental solution of convection-diffusion-reaction equation (Section 2.2.1) and the DBEM with the fundamental solution of modified Helmholtz equation (Section 2.2.2) are presented elaborately.

2.1 The Dual Reciprocity Boundary Element Method

Dual reciprocity BEM is one of the alternative boundary element technique which aims to overcome the difficulties that BEM confronts. DRBEM transforms the domain integrals into equivalent boundary integrals by using a suitable fundamental solution which corresponds to the steady-state problem. The terms except the ones that we use for the fundamental solution are considered as nonhomogeneous terms, and these are approximated by means of radial basis functions.

2.1.1 DRBEM with the fundamental solution of Laplace equation

This section is devoted to the application of DRBEM with the fundamental solution of Laplace equation [1] for the time-dependent convection-diffusion-reaction Equation (2.1). All the terms except the Laplacian are considered as the inhomogeneity, which is denoted by b, and they are approximated by means of radial basis functions in order to transform the differential equation into an equivalent boundary integral equation. In order to show the application in a compact form, Equation (2.1) is rewritten in a form of Poisson's equation as follows

$$\nabla^2 u = b(x, y, t, u, u_x, u_y, u_t) \quad \text{in} \quad \Omega. \tag{2.3}$$

The general boundary conditions are taken as

$$\begin{aligned} u &= \bar{u} && \text{on} \quad \Gamma_1 && (2.4)\\ q &= \frac{\partial u}{\partial n} = \bar{q} && \text{on} \quad \Gamma_2 && (2.5) \end{aligned}$$

where $\bar{u}$ and $\bar{q}$ are given functions, $\vec{n}$ is the outward normal vector and $\Gamma = \Gamma_1 \cup \Gamma_2$.

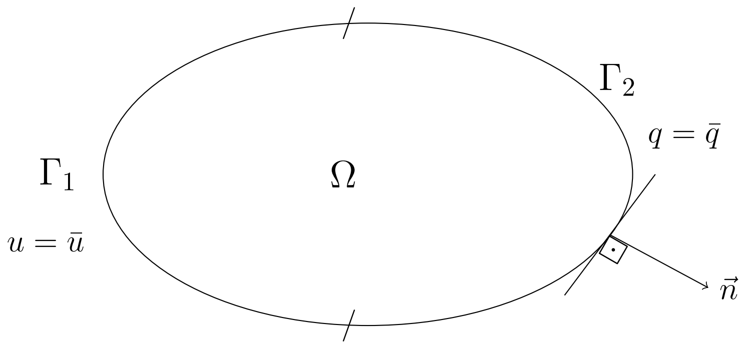

Figure 2.1: The computational domain and boundary conditions

Following the method of weighted residuals as in the application of BEM [1], the errors between the exact and approximate solutions (u and $\tilde{u}$) and their normal derivatives (q and $\tilde{q}$) can be minimized by orthogonalizing the errors with respect to weight functions [1].

The residuals are defined as

$$\begin{aligned} \varepsilon_\Omega &= \nabla^2\tilde{u} - b \neq 0 \qquad \text{in} \quad \Omega, && (2.6)\\ \varepsilon_{\Gamma_1} &= \tilde{u} - \bar{u} \neq 0 \qquad \text{on} \quad \Gamma_1, && (2.7)\\ \varepsilon_{\Gamma_2} &= \tilde{q} - \bar{q} \neq 0 \qquad \text{on} \quad \Gamma_2. && (2.8) \end{aligned}$$

These residuals can be weighted by weight functions u^*, $\bar{u}^*$ and $\bar{\bar{u}}^*$ as

$$\int_\Omega \varepsilon_\Omega u^* d\Omega + \int_{\Gamma_1} \varepsilon_{\Gamma_1}\bar{u}^* d\Gamma + \int_{\Gamma_2} \varepsilon_{\Gamma_2}\bar{\bar{u}}^* d\Gamma = 0 \tag{2.9}$$

or

$$\int_\Omega (\nabla^2\tilde{u} - b)u^* d\Omega + \int_{\Gamma_1} (\tilde{u} - \bar{u})\bar{u}^* d\Gamma + \int_{\Gamma_2} (\tilde{q} - \bar{q})\bar{\bar{u}}^* d\Gamma = 0. \tag{2.10}$$

The purpose of this procedure is to force the residuals to be zero in an average sense. Applying the Green's second identity successively two times to the domain integral in (2.10); and by choosing $\bar{u}^* = \frac{\partial u^*}{\partial n}$ and $\bar{\bar{u}}^* = -u^*$, we get the following equation

$$\int_\Omega \tilde{u}\nabla^2 u^* d\Omega + \int_{\Gamma_1} u^* \frac{\partial \tilde{u}}{\partial n} d\Gamma_1 - \int_{\Gamma_2} q^* \tilde{u} d\Gamma_2 - \int_{\Gamma_1} q^* \bar{u} d\Gamma_1 + \int_{\Gamma_2} u^* \frac{\partial \bar{u}}{\partial n} d\Gamma_2 = \int_\Omega b u^* d\Omega. \tag{2.11}$$

The weight function u^* is chosen as the fundamental solution of Laplace equation to eliminate the domain integral on the left hand side of Equation (2.11). That is, u^* is chosen as the function satisfying the equation

$$\nabla^2 u^* = -\Delta(r - r_i) \tag{2.12}$$

where Δ is the Dirac delta[1] function and r and r_i are the positions vectors of the field point (x, y) and the source point (x_i, y_i), respectively. Hence, u^* and its normal derivative q^* are [1]

$$u^* = \frac{1}{2\pi} \ln \frac{1}{|r - r_i|}, \qquad q^* = -\frac{1}{2\pi} \frac{(r - r_i).\vec{n}}{|r - r_i|^2}. \tag{2.13}$$

[1] For any continuous function $f(x)$ at x_i, Dirac delta function is defined with the properties

$$\Delta(x - x_i) = \begin{cases} \infty, & x = x_i \\ 0, & x \neq x_i \end{cases}, \quad \int_\Omega \Delta(x - x_i) d\Omega = 1 \quad \text{and} \quad \int_\Omega f(x)\Delta(x - x_i) d\Omega = \begin{cases} f(x_i), & x_i \in \Omega \\ 0, & x_i \notin \Omega. \end{cases}$$

To be able to rewrite the Equation (2.11) in a more compact form, we define the boundary conditions as

$$u = \begin{cases} \bar{u} & \text{on} \quad \Gamma_1 \\ \tilde{u} & \text{on} \quad \Gamma_2 \end{cases} \qquad\qquad q = \begin{cases} \bar{q} & \text{on} \quad \Gamma_1 \\ \tilde{q} & \text{on} \quad \Gamma_2 \end{cases}$$

where $\tilde{u}$ and $\tilde{q}$ are the unknown approximate values.

Then, Equation (2.11) becomes

$$-c_i u_i - \int_\Gamma q^* u d\Gamma + \int_\Gamma u^* q d\Gamma = \int_\Omega b u^* d\Omega \tag{2.14}$$

where $u_i = u(x_i, y_i)$ and the source point (x_i, y_i) may be either an interior or a boundary node. Here, $\int_\Omega u\nabla^2 u^* d\Omega = \int_\Omega u\Delta(r - r_i) d\Omega = -c_i u_i$ and c_i is the constant defined by

$$c_i = \begin{cases} \frac{\theta_i}{2\pi}, & i \in \Gamma \\ 1, & i \in \Omega \setminus \Gamma \end{cases}$$

with the internal angle θ_i at the point $i = (x_i, y_i)$ in radians (see Figure 2.2)

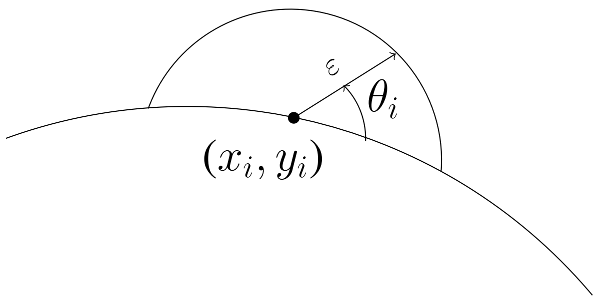

Figure 2.2: Configuration of the constant c_i

The leftover domain integral on the right hand side of Equation (2.14) will be transformed into an equivalent boundary integral by means of radial basis functions. That is, the solution of Equation (2.3) can be expressed as the sum of the homogeneous solution (since the fundamental solution of Laplace equation is used) and a particular solution $\hat{u}$ such that

$$\nabla^2 \hat{u} = b. \tag{2.15}$$

Generally, it is difficult to find a particular solution $\hat{u}$ especially for the time-dependent or non-linear equations. In this case, DRBEM aims to use series of particular solutions $\hat{u}_j$ instead of a single function $\hat{u}$. The number of the particular solutions $\hat{u}_j$ composes of the sum of boundary and interior nodes, i.e. there are totally $N + L$ particular solutions, where N and L represent the number of boundary and interior nodes, respectively. Then, the inhomogeneity b is approximated as

$$b \approx \sum_{j=1}^{N+L} \alpha_j(t) f_j(x, y) \tag{2.16}$$

where $\alpha_j(t)$ is a set of time-dependent undetermined coefficients and f_j are the radial basis functions which are linked to the particular solutions $\hat{u}_j$ as

$$\nabla^2 \hat{u}_j = f_j. \tag{2.17}$$

The f_j functions are defined as geometry-dependent and there is no restriction on these functions. That is, there are different types of radial basis functions and each of which results in a different particular solution $\hat{u}_j$ for the Poisson equation (2.17). In Equation (2.16), b is expressed by an approximation of radial basis functions; and DRBEM idea will be constructed by pursuing this approximation. Although the approximation is still valid, in practice, the equality sign ($=$) will be used instead of approximation sign ($\approx$) starting from Equation (2.18) in order to be compatible with the literature [1].

Substituting Equation (2.17) into Equation (2.16) yields

$$b = \sum_{j=1}^{N+L} \alpha_j(t)(\nabla^2 \hat{u}_j) \tag{2.18}$$

which can be substituted into the Equation (2.14) to give the following expression

$$c_i u_i + \int_\Gamma q^* u d\Gamma - \int_\Gamma u^* q d\Gamma = -\sum_{j=1}^{N+L} \alpha_j(t) \int_\Omega (\nabla^2 \hat{u}_j) u^* d\Omega. \tag{2.19}$$

When the Green's second identity is also applied to the right hand side of Equation (2.19), we obtain the following integral equation defined only on the boundary of the domain Ω for each source node i,

$$c_i u_i + \int_\Gamma q^* u d\Gamma - \int_\Gamma u^* q d\Gamma = \sum_{j=1}^{N+L} \alpha_j(t)(c_i \hat{u}_{ji} + \int_\Gamma q^* \hat{u}_j d\Gamma - \int_\Gamma u^* \hat{q}_j d\Gamma) \quad (2.20)$$

where the normal derivative $\hat{q}_j$ of $\hat{u}_j$ is defined as

$$\hat{q}_j = \frac{\partial \hat{u}_j}{\partial n} = \frac{\partial \hat{u}_j}{\partial x}\frac{\partial x}{\partial n} + \frac{\partial \hat{u}_j}{\partial y}\frac{\partial y}{\partial n}. \quad (2.21)$$

In order to solve the integral Equation (2.20), the boundary is discretized by dividing it into N segments or elements. Constant, linear, or higher order elements can be used to discretize the boundary. For easiness, we use constant boundary element to explain the formulations. The points where the unknown values are considered are called "nodes" and if they are taken in the middle of the elements, the formulation is called the BEM with constant elements (see Figure 2.3).

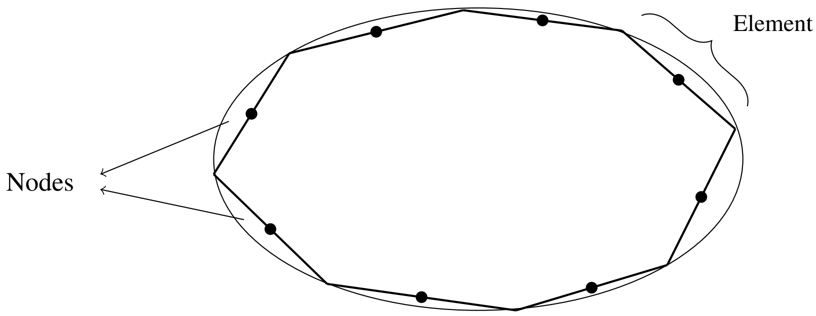

Figure 2.3: Discretization of boundary with constant elements

The values u and q are assumed to be constant over each element and equal to the value at the mid-element node. Hence, the values of u and q can be taken out of the integrals as constant u_k and q_k for each element k. Then, Equation (2.20) can be discretized with summation over the constant boundary elements and expressed as follows

$$\begin{aligned} c_i u_i + \sum_{k=1}^{N} u_k \int_{\Gamma_k} q^* d\Gamma \quad &- \quad \sum_{k=1}^{N} q_k \int_{\Gamma_k} u^* d\Gamma \qquad (2.22) \\ &= \quad \sum_{j=1}^{N+L} \alpha_j(t)(c_i \hat{u}_{ji} + \sum_{k=1}^{N} \int_{\Gamma_k} q^* \hat{u}_j d\Gamma - \sum_{k=1}^{N} \int_{\Gamma_k} u^* \hat{q}_j d\Gamma). \end{aligned}$$

Since $\hat{u}$ and $\hat{q}$ are known functions when f is defined, there is no need to approximate them within each boundary element as done for u and q. Integrating over each boundary element, Equation (2.22) can be written as

$$c_i u_i + \sum_{k=1}^{N} H_{ik} u_k - \sum_{k=1}^{N} G_{ik} q_k = \sum_{j=1}^{N+L} \alpha_j(t)(c_i \hat{u}_{ji} + \sum_{k=1}^{N} H_{ik} \hat{u}_{kj} - \sum_{k=1}^{N} G_{ik} \hat{q}_{kj}). \quad (2.23)$$

The index k is used for the nodes which are the field points. By the use of the collocation technique, Equation (2.23) is expressed as

$$Hu - Gq = \sum_{j=1}^{N+L} \alpha_j(t)(H\hat{u}_j - G\hat{q}_j). \quad (2.24)$$

The components of the matrices H and G are

$$\begin{aligned} H_{ij} &= c_i \delta_{ij} - \frac{1}{2\pi} \int_{\Gamma_j} \frac{(r - r_i).\vec{n}}{|r - r_i|^2} d\Gamma_j, & (2.25) \\ G_{ij} &= \frac{1}{2\pi} \int_{\Gamma_j} \ln \frac{1}{|r - r_i|} d\Gamma_j, & (2.26) \\ H_{ii} &= c_i, & (2.27) \\ G_{ii} &\approx \frac{l}{2\pi}(\ln \frac{2}{l} + 1) & (2.28) \end{aligned}$$

where $i, j = 1, ..., N$, l is the length of each boundary element and δ_{ij} is the Kronecker delta function defined by

$$\delta_{ij} = \begin{cases} 1, & \text{if} \quad i = j \\ 0, & \text{if} \quad i \neq j. \end{cases}$$

The diagonal entries of the matrix H are directly equal to c_i, since $\frac{\partial r}{\partial n} = 0$ along a constant element in the integral (2.25), while G_{ii} are evaluated analytically taking care of the singularity [1].

Finally, after consideration of the vectors $\hat{u}_j$ and $\hat{q}_j$ to be one column of the matrices $\hat{U}$ and $\hat{Q}$, respectively, Equation (2.24) can be rewritten without summation to produce

$$Hu - Gq = (H\hat{U} - G\hat{Q})\alpha \quad (2.29)$$

where α is the vector containing $\alpha_j(t)$.

In the formulations of DRBEM, several types of f_j can be chosen. The only restriction is that the matrix F of size $(N+L) \times (N+L)$, which is obtained by taking f_j as columns, must be nonsingular. Throughout the thesis, the polynomial type radial basis functions are employed in the application of DRBEM. The polynomial type radial basis functions are [1]

$$f_j = p_1 + p_2 r_j + p_3 r_j^2 + \ldots + p_{m+1} r_j^m \tag{2.30}$$

and corresponding particular solutions $\hat{u}$ and their normal derivatives $\hat{q}$ are (from Equation (2.17) and (2.21))

$$\hat{u} = p_1 \frac{r_j^2}{4} + p_2 \frac{r_j^3}{9} + \ldots + p_{m+1} \frac{r_j^{m+2}}{(m+2)^2}, \tag{2.31}$$

$$\hat{q} = (p_1 \frac{r_j}{2} + p_2 \frac{r_j^2}{3} + \ldots + p_{m+1} \frac{r_j^{m+1}}{m+2}) \frac{\partial r}{\partial n} \tag{2.32}$$

where p_i are arbitrarily chosen constant coefficients (mostly they are taken as $p_i = 1$). Alternatively, logaritmic type radial basis function and corresponding particular solution $\hat{u}$ and its normal derivative $\hat{q}$ are given as [63]

$$f_j = r_j^2 \ln r_j, \qquad \hat{u} = \ln r_j \frac{r_j^4}{16} - \frac{r_j^4}{32}, \qquad \hat{q} = (\ln r_j \frac{r_j^3}{4} + \frac{r_j^3}{16}) \frac{\partial r}{\partial n}. \tag{2.33}$$

Equation (2.29) is the basis for the application of the dual reciprocity boundary element method and involves discretization of the boundary only. Defining the interior nodes is not necessary to obtain the boundary solution. However, arbitrary number of interior points are taken to obtain the solution both on the boundary and in the interior.

As it was expressed in Equation (2.16), b is approximated by radial basis functions f_j. If the value of b is computed at $N+L$ different points, a set of equations can be obtained in matrix form as [1]

$$b = F\alpha \tag{2.34}$$

which can be inverted as

$$\alpha = F^{-1} b(x, y, t, u, u_x, u_y, u_t) \tag{2.35}$$

where b is the function involving u and its partial derivatives, therefore α cannot be calculated explicitly.

By Equation (2.1) and (2.3), b can be written as

$$b = \frac{1}{\varepsilon}\frac{\partial u}{\partial t} + \frac{a_1}{\varepsilon}\frac{\partial u}{\partial x} + \frac{a_2}{\varepsilon}\frac{\partial u}{\partial y} + \frac{1}{\varepsilon}\sigma u - \frac{1}{\varepsilon}h. \tag{2.36}$$

Then, by substituting it into Equation (2.35) we obtain

$$\alpha = F^{-1}b = F^{-1}(\frac{1}{\varepsilon}\frac{\partial u}{\partial t} + \frac{a_1}{\varepsilon}\frac{\partial u}{\partial x} + \frac{a_2}{\varepsilon}\frac{\partial u}{\partial y} + \frac{1}{\varepsilon}\sigma u - \frac{1}{\varepsilon}h). \tag{2.37}$$

To relate the nodal values of u to nodal values of its derivatives $\frac{\partial u}{\partial x}$ and $\frac{\partial u}{\partial y}$, a mechanism needs to be constructed. Considering the approximation given in Equation (2.16), u is also approximated by the same coordinate functions $f_j(x, y)$ as follows

$$u \approx \sum_{j=1}^{N+L} \beta_j(t) f_j(x, y) \tag{2.38}$$

where $\beta_j \neq \alpha_j$ and it can also be expressed in matrix form

$$u = F\beta. \tag{2.39}$$

Differentiating (2.39) with respect to x and y, respectively, produces the space derivatives of the solution u

$$\frac{\partial u}{\partial x} = \frac{\partial F}{\partial x}F^{-1}u, \qquad \frac{\partial u}{\partial y} = \frac{\partial F}{\partial y}F^{-1}u \tag{2.40}$$

and Equation (2.37) results in

$$\alpha = F^{-1}(\frac{1}{\varepsilon}\frac{\partial u}{\partial t} + \frac{a_1}{\varepsilon}\frac{\partial F}{\partial x}F^{-1}u + \frac{a_2}{\varepsilon}\frac{\partial F}{\partial y}F^{-1}u + \frac{1}{\varepsilon}\sigma u - \frac{1}{\varepsilon}h). \tag{2.41}$$

Equation (2.29) can be written as follows for the solution at boundary nodes

$$H_{BS}u_{BS} - G_{BS}q_{BS} = (H_{BS}\hat{U}_{BS} - G_{BS}\hat{Q}_{BS})\alpha \tag{2.42}$$

and for the solution at interior nodes

$$Iu_{IS} = -H_{IS}u_{BS} + G_{IS}q_{BS} + (I\hat{U}_{IS} + H_{IS}\hat{U}_{BS} - G_{IS}\hat{Q}_{BS})\alpha \tag{2.43}$$

where BS and IS denote boundary and interior solutions, respectively. One global scheme is obtained by combining the Equation (2.42) and Equation (2.43) as an enlarged system

$$\underset{H}{\begin{bmatrix} \underset{(N\times N)}{H_{BS}} & \underset{N\times L}{0} \\ \underset{(L\times N)}{H_{IS}} & \underset{L\times L}{I} \end{bmatrix}} \underset{u}{\begin{bmatrix} \underset{N\times 1}{u_{BS}} \\ \underset{L\times 1}{u_{IS}} \end{bmatrix}} - \underset{G}{\begin{bmatrix} \underset{(N\times N)}{G_{BS}} & \underset{N\times L}{0} \\ \underset{(L\times N)}{G_{IS}} & \underset{L\times L}{0} \end{bmatrix}} \underset{q}{\begin{bmatrix} \underset{N\times 1}{q_{BS}} \\ \underset{L\times 1}{0} \end{bmatrix}} =$$

$$\left[\underset{H}{\begin{bmatrix} \underset{(N\times N)}{H_{BS}} & \underset{N\times L}{0} \\ \underset{(L\times N)}{H_{IS}} & \underset{L\times L}{I} \end{bmatrix}} \underset{\hat{U}}{\begin{bmatrix} \underset{N\times(N+L)}{\hat{U}_{BS}} \\ \underset{L\times(N+L)}{\hat{U}_{IS}} \end{bmatrix}} - \underset{G}{\begin{bmatrix} \underset{(N\times N)}{G_{BS}} & \underset{N\times L}{0} \\ \underset{(L\times N)}{G_{IS}} & \underset{L\times L}{0} \end{bmatrix}} \underset{\hat{Q}}{\begin{bmatrix} \underset{N\times(N+L)}{\hat{Q}_{BS}} \\ \underset{L\times(N+L)}{0} \end{bmatrix}} \right] \underset{\alpha}{\begin{bmatrix} BS \\ + \\ IS \end{bmatrix}}$$

Figure 2.4: Enlarged DRBEM system of equations

which can be expressed by the following $(N + L) \times (N + L)$ matrix-vector equation

$$Hu - Gq = (H\hat{U} - G\hat{Q})\alpha. \tag{2.44}$$

Substituting α vector from Equation (2.41) we obtain

$$\varepsilon(Hu - Gq) = (H\hat{U} - G\hat{Q})F^{-1}\left(\frac{\partial u}{\partial t} + a_1\frac{\partial F}{\partial x}F^{-1}u + a_2\frac{\partial F}{\partial y}F^{-1}u + \sigma u - h\right) \tag{2.45}$$

which can be expressed in terms of a first order system of a ordinary differential equations in time

$$C\dot{u} + \widetilde{H}u - \widetilde{G}\frac{\partial u}{\partial n} - Ch = 0. \tag{2.46}$$

Here, the matrices C, $\widetilde{H}$ and $\widetilde{G}$ are

$$C = -(H\hat{U} - G\hat{Q})F^{-1}, \tag{2.47}$$

$$\widetilde{H} = \varepsilon H + CR_1 + CR_2 + C\sigma, \tag{2.48}$$

$$\widetilde{G} = \varepsilon G \tag{2.49}$$

and

$$R_1 = a_1 \frac{\partial F}{\partial x} F^{-1}, \qquad R_2 = a_2 \frac{\partial F}{\partial y} F^{-1}. \tag{2.50}$$

The time derivative $\dot{u} = \frac{\partial u}{\partial t}$ in Equation (2.46) is discretized by using implicit backward finite difference approximation as

$$\frac{\partial u}{\partial t}^{(m+1)} = \frac{u^{(m+1)} - u^{(m)}}{\Delta t} \tag{2.51}$$

and the Equation (2.46) becomes

$$(\widetilde{H} + \frac{C}{\Delta t}) u^{(m+1)} - \widetilde{G} \frac{\partial u}{\partial n}^{(m+1)} = \frac{C}{\Delta t} u^{(m)} + C h^{(m)} \tag{2.52}$$

where m denotes the time iteration.

After the insertion of boundary conditions and the rearrangement, the system results in a linear system

$$Az = d \tag{2.53}$$

where A is a full matrix of size $(N + L) \times (N + L)$, d is a known vector and z is the solution vector which involves the unknown values of both u and $q = \frac{\partial u}{\partial n}$ on the boundary and interior of the problem domain according to the given boundary conditions.

2.1.2 DRBEM with the fundamental solution of convection-diffusion-reaction equation

In this section, DRBEM is employed to solve Equation (2.1) by using the fundamental solution of convection-diffusion-reaction equation. Therefore, the terms in Equation (2.1) except the convection, diffusion and reaction terms are treated as nonhomogeneity. Similar to the DRBEM application given in Section 2.1.1, we start with applying weighted residual formulations as

$$\begin{aligned} \int_\Omega \varepsilon \nabla^2 u u^* d\Omega \quad &- \quad \int_\Omega (a_1 \frac{\partial u}{\partial x} + a_2 \frac{\partial u}{\partial y}) u^* d\Omega - \int_\Omega \sigma u u^* d\Omega \\ &+ \quad \int_{\Gamma_1} \varepsilon (\tilde{u} - \bar{u}) q^* d\Gamma - \int_{\Gamma_2} \varepsilon (\tilde{q} - \bar{q}) u^* d\Gamma = \int_\Omega (\frac{\partial u}{\partial t} - h) u^* d\Omega. \end{aligned} \tag{2.54}$$

When the Green's second identity is applied to the first domain integral in (2.54) successively two times and to the second domain integral once, we obtain

$$\begin{aligned}\int_{\Omega}(\varepsilon\nabla^2 u^* + a_1\frac{\partial u^*}{\partial x} + a_2\frac{\partial u^*}{\partial y} - \sigma u^*)ud\Omega - \varepsilon\int_{\Gamma} q^* ud\Gamma \quad &+ \quad \varepsilon\int_{\Gamma} u^*\frac{\partial u}{\partial n}d\Gamma \\ -\int_{\Gamma}(a_1 u^* n_x u + a_2 u^* n_y u)d\Gamma \quad &= \quad \int_{\Omega}(\frac{\partial u}{\partial t} - h)u^* d\Omega.\end{aligned} \tag{2.55}$$

Then, to eliminate the domain integral on the right hand side of Equation (2.55) u^* is chosen as the fundamental solution of convection-diffusion-reaction equation [2]. That is [1],

$$u^* = \frac{1}{2\pi\varepsilon}\exp(-\frac{a_1 r_x + a_2 r_y}{2\varepsilon})K_0(sr) \tag{2.56}$$

where $K_0(sr)$ is the modified Bessel function of the second kind and of order zero. Its normal derivative is

$$q^* = \frac{1}{2\pi\varepsilon}\exp(-\frac{a_1 r_x + a_2 r_y}{2\varepsilon})[-sK_1(sr)\frac{\partial r}{\partial n} - \frac{1}{2\varepsilon}(a_1 n_x + a_2 n_y)K_0(sr)]. \tag{2.57}$$

where $K_1(sr)$ is the modified Bessel function of the second kind and of order one and $s = \sqrt{\frac{\sigma}{\varepsilon} + \frac{a_1^2 + a_2^2}{4\varepsilon^2}}$. Thus, Equation (2.55) is reduced to

$$c_i u_i + \varepsilon\int_{\Gamma} q^* ud\Gamma - \varepsilon\int_{\Gamma} u^*\frac{\partial u}{\partial n}d\Gamma + \int_{\Gamma}(a_1 u^* n_x u + a_2 u^* n_y u)d\Gamma = -\int_{\Omega}(\frac{\partial u}{\partial t} - h)u^* d\Omega \tag{2.58}$$

with i denoting the source point (x_i, y_i). The domain integral on the right hand side of Equation (2.58) is approximated by radial basis functions f_j as

$$\frac{\partial u}{\partial t} - h \approx \sum_{j=1}^{N+L}\psi_j(t)f_j(x,y) \tag{2.59}$$

where $\psi_j(t)$ is a set of time-dependent undetermined coefficients and the radial basis functions f_j are linked to the particular solutions $\hat{u}_j$ with

[2] u^* is the fundamental solution of convection-diffusion-reaction equation. That is, u^* satisfies

$$\varepsilon\nabla^2 u^* + a_1\frac{\partial u^*}{\partial x} + a_2\frac{\partial u^*}{\partial y} - \sigma u^* = -\Delta(r - r_i).$$

$$\varepsilon\nabla^2\hat{u}_j - a_1\frac{\partial \hat{u}_j}{\partial x} - a_2\frac{\partial \hat{u}_j}{\partial y} - \sigma\hat{u}_j = f_j. \tag{2.60}$$

Substitution of Equation (2.60) into Equation (2.59) and then into Equation (2.58), gives

$$\begin{aligned} c_iu_i + \varepsilon\int_\Gamma q^*ud\Gamma \;&-\; \varepsilon\int_\Gamma u^*\frac{\partial u}{\partial n}d\Gamma + \int_\Gamma (a_1u^*n_xu + a_2u^*n_yu)d\Gamma \\ &= \; -\int_\Omega \sum_{j=1}^{N+L}\psi_j(t)(\varepsilon\nabla^2\hat{u} - a_1\frac{\partial\hat{u}}{\partial x} - a_2\frac{\partial\hat{u}}{\partial y} - \sigma\hat{u})u^*d\Omega. \end{aligned} \tag{2.61}$$

Application of Green's second identity also to the domain integral on the right hand side of Equation (2.61) results in an integral equation defined only on the boundary

$$\begin{aligned} c_iu_i \;&+\; \varepsilon\int_\Gamma q^*ud\Gamma - \varepsilon\int_\Gamma u^*\frac{\partial u}{\partial n}d\Gamma + \int_\Gamma (a_1u^*n_xu + a_2u^*n_yu)d\Gamma \\ &= \; \sum_{j=1}^{N+L}\psi_j(t)(c_iu_{ji} + \varepsilon\int_\Gamma q^*\hat{u}d\Gamma - \varepsilon\int_\Gamma u^*\frac{\partial\hat{u}}{\partial n}d\Gamma + \int_\Gamma (a_1u^*n_x\hat{u} + a_2u^*n_y\hat{u})d\Gamma). \end{aligned} \tag{2.62}$$

Here, the particular solutions can be taken as [29]

$$\hat{u}_j = r_j^3, \tag{2.63}$$

$$\hat{u}_j = \frac{r_j^2}{4} + \frac{r_j^3}{9}, \tag{2.64}$$

$$\hat{u}_j = \frac{r_j^4}{32}(2\log r_j - 1) + \frac{r_j^2}{4} + \frac{r_j^3}{9} \tag{2.65}$$

with their normal derivatives

$$\hat{q}_j = (3r_j^2)\frac{\partial r}{\partial n}, \tag{2.66}$$

$$\hat{q}_j = (\frac{r_j}{2} + \frac{r_j^2}{3})\frac{\partial r}{\partial n}, \tag{2.67}$$

$$\hat{q}_j = (\frac{1}{4}r_j^3\log r_j - \frac{1}{16}r_j^3 + \frac{1}{3}r_j^2 + \frac{1}{2}r_j)\frac{\partial r}{\partial n}. \tag{2.68}$$

Then, the corresponding radial basis functions f_j are obtained as follows:

$$
\begin{aligned}
f_j &= 9\varepsilon r_j - (3r_j)(a_1 r_x + a_2 r_y) - \sigma r_j^3, && (2.69)\\
f_j &= \varepsilon(1+r_j) - (\frac{1}{2} + \frac{r_j}{3})(a_1 r_x + a_2 r_y) - \frac{\sigma}{36}(9r_j^2 + 4r_j^3), && (2.70)\\
f_j &= \varepsilon(1 + r_j + r_j^2 \log r_j) - (\frac{1}{4} r_j^2 \log r_j - \frac{1}{16} r_j^2 + \frac{1}{3} r_j + \frac{1}{2})(a_1 r_x + a_2 r_y) \\
&- \sigma(\frac{r_j^4}{32}(2\log r_j - 1) + \frac{r_j^2}{4} + \frac{r_j^3}{9}) && (2.71)
\end{aligned}
$$

through Equation (2.60). Discretizing the boundary using constant elements, we can write the Equation (2.62) in matrix-vector form as

$$
Hu - Gq = (H\hat{U} - G\hat{Q})\varphi \tag{2.72}
$$

where φ is the vector which includes $\varphi_j(t)$. Collocating $(\frac{\partial u}{\partial t} - h)$ at $(N+L)$ different points, a set of equations $(\frac{\partial u}{\partial t} - h) = F\varphi$ can be obtained where F is the coordinate matrix obtained by taking f_j as columns. Then, one arrives at

$$
\varphi = F^{-1}(\frac{\partial u}{\partial t} - h) \tag{2.73}
$$

and using Equation (2.72) the following system is obtained

$$
Hu - G\frac{\partial u}{\partial n} = (H\hat{U} - G\hat{Q})F^{-1}(\frac{\partial u}{\partial t} - h) \tag{2.74}
$$

where

$$
\begin{aligned}
H_{ij} &= c_i \delta_{ij} && (2.75)\\
&- \frac{1}{2\pi}\int_{\Gamma_j} \exp(-\frac{a_1 r_x + a_2 r_y}{2\varepsilon})[sK_1(sr)\frac{\partial r}{\partial n} - (\frac{a_1}{2\varepsilon}n_x + \frac{a_2}{2\varepsilon}n_y)K_0(sr)]d\Gamma_j, \\
G_{ij} &= \frac{1}{2\pi}\int_{\Gamma_j} \exp(-\frac{a_1 r_x + a_2 r_y}{2\varepsilon})K_0(sr)d\Gamma_j. && (2.76)
\end{aligned}
$$

H_{ii} and G_{ii} need special treatment which are calculated analytically by taking care of the singularity. Since $\frac{\partial r}{\partial n} = 0$ in Equation (2.75) due to the normal $\vec{n}$ and the distance r from the source point are always perpendicular to each other, K_1 vanishes in Equation (2.75) and in Equations (2.75) and (2.76) only the function K_0 is approximated as $K_0(sr) \approx -(\ln(\frac{1}{2}sr) + \gamma)$ in which γ is the Euler constant [64]. Then, the diagonal entries H_{ii} and G_{ii} become

$$H_{ii} = c_i + \frac{1}{2\pi}\int_{\Gamma_i}(\ln\frac{1}{r} - \ln\frac{s}{2} - \gamma)d\Gamma_i(\frac{a_1 n_x + a_2 n_y}{2\varepsilon}), \tag{2.77}$$

$$G_{ii} = \frac{1}{2\pi}\int_{\Gamma_i}(\ln\frac{1}{r} - \ln\frac{s}{2} - \gamma)d\Gamma_i. \tag{2.78}$$

To be able to integrate the above expressions, a change of coordinates (see Figure 2.5)

$$r = \left|\frac{l}{2}\xi\right|, \qquad d\Gamma = dr = \frac{l}{2}d\xi \tag{2.79}$$

is used where l is the length of the element Γ_i.

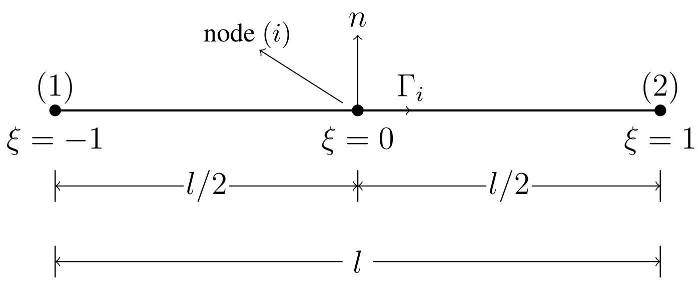

Figure 2.5: Constant element coordinate system [1]

Equation (2.78) can be expressed as

$$\begin{aligned}
G_{ii} &= \frac{1}{2\pi}\int_{Point(1)}^{Point(2)}(\ln\frac{1}{r} - \ln\frac{s}{2} - \gamma)d\Gamma_i \qquad \text{(by symmetry)} && (2.80)\\
&= \frac{1}{\pi}\int_{node(i)}^{Point(2)}(\ln\frac{1}{r} - \ln\frac{s}{2} - \gamma)dr && (2.81)\\
&= \frac{l}{2\pi}\int_{node(i)}^{Point(2)}(\ln\frac{2}{l\xi} - \ln\frac{s}{2} - \gamma)d\xi && (2.82)\\
&= \frac{l}{2\pi}(\ln\frac{2}{l} - \ln\frac{s}{2} - \gamma + \int_0^1 \ln\frac{1}{\xi}d\xi). && (2.83)
\end{aligned}$$

Since the last integral in Equation (2.83) is equal to 1
(that is, $\int_0^1 \ln\frac{1}{\xi}d\xi = \lim_{a\to 0^+}\int_a^1 \ln\frac{1}{\xi}d\xi = 1$ (using integration by parts)), we arrive at

$$H_{ii} \approx c_i + \frac{l}{2\pi}(\ln\frac{2}{l} - \ln\frac{s}{2} - \gamma + 1)(\frac{a_1 n_x + a_2 n_y}{2\varepsilon}), \tag{2.84}$$

$$G_{ii} \approx \frac{l}{2\pi}(\ln\frac{2}{l} - \ln\frac{s}{2} - \gamma + 1). \tag{2.85}$$

In Equation (2.74), the time derivative is again discretized by using implicit backward difference approximation (see Equation (2.51)) giving the following iterative matrix-vector equation

$$(H + \frac{C}{\Delta t})u^{(m+1)} - G\frac{\partial u}{\partial n}^{(m+1)} = \frac{C}{\Delta t}u^{(m)} + Ch^{(m)} \tag{2.86}$$

where m represents the time iteration and

$$C = -(H\hat{U} - G\hat{Q})F^{-1}. \tag{2.87}$$

Inserting the boundary conditions into Equation (2.86) gives the linear system of equations $Az = d$ where A is the coefficient matrix of size $(N + L) \times (N + L)$, d is a known vector and z is the solution vector, containing the unknown values of u and $\frac{\partial u}{\partial n}$ either on the boundary and/or interior of the domain depending on the given boundary conditions.

2.1.3 DRBEM with the fundamental solution of modified Helmholtz equation

In this section, our focus is on the numerical discretization of Equation (2.1) by the DRBEM which makes use of the fundamental solution of modified Helmholtz equation. For this, the convection-diffusion-reaction equation (2.1) with constant convection coefficient $\vec{a} = (a_1, a_2)$ is first transformed into the modified Helmholtz equation by using a time-dependent exponential type transformation [28]

$$u(x, y, t) = \exp(\frac{a_1 r_x + a_2 r_y}{2\varepsilon})\phi(x, y, t). \tag{2.88}$$

This reduces Equation (2.1) to an inhomogeneous modified Helmholtz equation

$$\nabla^2\phi - s^2\phi = \frac{1}{\varepsilon}(\frac{\partial \phi}{\partial t} - h_1) \tag{2.89}$$

where

$$h_1 = h\exp(-\frac{a_1 r_x + a_2 r_y}{2\varepsilon}), \qquad s = \sqrt{\frac{\sigma}{\varepsilon} + \frac{a_1^2 + a_2^2}{4\varepsilon^2}}. \tag{2.90}$$

Here, r is the magnitude of the position vector $\vec{r} = (r_x, r_y)$ between the source point (x_i, y_i) and the field point (x, y).

The method of weighted residual will be pursued as in the previous sections. By weighting Equation (2.89) with the fundamental solution u^* and applying the Green's second identity two times, one can obtain the following integral equation [1]

$$\int_\Omega (\nabla^2 u^* - s^2 u^*)\phi d\Omega - \int_\Gamma q^* \phi d\Gamma + \int_\Gamma u^* \frac{\partial \phi}{\partial n} d\Gamma = \int_\Omega \frac{1}{\varepsilon}\left(\frac{\partial \phi}{\partial t} - h_1\right) u^* d\Omega. \quad (2.91)$$

To eliminate the domain integral on the left hand side of Equation (2.91), u^* is chosen as the fundamental solution of modified Helmholtz equation[3] [28]

$$u^* = \frac{1}{2\pi} K_0(sr) \quad (2.92)$$

with its normal derivative q^* given by

$$q^* = \frac{-s}{2\pi} K_1(sr) \frac{\partial r}{\partial n}. \quad (2.93)$$

Then, we obtain

$$c_i \phi_i + \int_\Gamma q^* \phi d\Gamma - \int_\Gamma u^* \frac{\partial \phi}{\partial n} d\Gamma = - \int_\Omega \frac{1}{\varepsilon}\left(\frac{\partial \phi}{\partial t} - h_1\right) u^* d\Omega \quad (2.94)$$

Following the DRBEM idea, the domain integral on the right hand side of Equation (2.94) is approximated by using radial basis functions f_j as

$$\frac{1}{\varepsilon}(\frac{\partial \phi}{\partial t} - h_1) \approx \sum_{j=1}^{N+L} \lambda_j(t) f_j(x, y) \quad (2.95)$$

in which $\lambda_j(t)$ is a set of time-dependent undetermined coefficients and the radial basis functions f_j are linked to the particular solutions $\hat{u}_j$ of modified Helmholtz equation now

$$\nabla^2 \hat{u}_j - s^2 \hat{u}_j = f_j. \quad (2.96)$$

Substitution of Equation (2.96) into Equation (2.95) results in

---

[3] u^* is chosen as the fundamental solution of modified Helmholtz equation. That is, u^* satisfies

$$\nabla^2 u^* - s^2 u^* = -\Delta(r - r_i).$$

$$\frac{1}{\varepsilon}(\frac{\partial\phi}{\partial t} - h_1) = \sum_{j=1}^{N+L} \lambda_j(t)(\nabla^2 \hat{u}_j - s^2 \hat{u}_j) \tag{2.97}$$

and further substitution of Equation (2.97) into Equation (2.94) gives

$$c_i\phi_i + \int_\Gamma q^*\phi d\Gamma - \int_\Gamma u^* \frac{\partial\phi}{\partial n} d\Gamma = -\sum_{j=1}^{N+L} \lambda_j(t) \int_\Omega (\nabla^2 \hat{u}_j - s^2 \hat{u}_j) u^* d\Omega \tag{2.98}$$

at the source point i with $\phi_i = \phi(x_i, y_i)$. When the Green's second identity is also applied to the right hand side of Equation (2.98), it will be an integral equation defined only on Γ

$$c_i\phi_i + \int_\Gamma q^*\phi d\Gamma - \int_\Gamma u^* \frac{\partial\phi}{\partial n} d\Gamma = \sum_{j=1}^{N+L} \lambda_j(t)(c_i\hat{u}_{ji} + \int_\Gamma q^*\hat{u}_j d\Gamma - \int_\Gamma u^*\hat{q}_j d\Gamma). \tag{2.99}$$

There are some different ways to find suitable functions f_j which satisfy the non-homogeneous modified Helmholtz Equation (2.96). First, we start by taking $\hat{u}$ as a polynomial

$$\hat{u}_j = a_0 + a_1 r + a_2 r^2 + a_3 r^3 + \cdots + a_m r^m$$

then we calculate the corresponding normal derivative $\hat{q} = \frac{\partial\hat{u}}{\partial n}$ and f_j (using Equation (2.96)). For example, by taking $a_0 = a_1 = 0$ [63], f_j, $\hat{u}$ and $\hat{q}$ are obtained as

$$f_j = 4a_2 + 9a_3 r_j + \cdots + m^2 a_m r_j^{m-2} - s^2(a_2 r_j^2 + a_3 r_j^3 + \cdots + a_m r_j^m), \tag{2.100}$$

$$\hat{u}_j = a_2 r_j^2 + a_3 r_j^3 + \cdots + a_m r_j^m, \tag{2.101}$$

$$\hat{q}_j = (2a_2 r_j + 3a_3 r_j^2 + \cdots + m a_m r_j^{m-1})\frac{\partial r}{\partial n}. \tag{2.102}$$

Equations (2.100)-(2.102) show that there are several possibilities of f_j, $\hat{u}_j$ and $\hat{q}_j$ depending on the choice of a_m.

On the other hand, a linear combination of thin plate splines [65] can be also used to obtain the logarithmic type radial basis functions $f_j = r_j^{2n} \log r_j$ for $n = 1, 2, 3, 4, 5$ [66].

The use of constant boundary elements for the discretization of the boundary (see Figure 2.3) leads to the corresponding matrix-vector form of Equation (2.99)

$$H\phi - G\frac{\partial\phi}{\partial n} = (H\hat{U} - G\hat{Q})\lambda \tag{2.103}$$

where λ is the vector which contains $\lambda_j(t)$. Using Equation (2.95), λ can be written as

$$\lambda = F^{-1}(\frac{1}{\varepsilon}\frac{\partial\phi}{\partial t} - \frac{1}{\varepsilon}h_1) \tag{2.104}$$

and then we obtain the system

$$H\phi - G\frac{\partial\phi}{\partial n} = (H\hat{U} - G\hat{Q})F^{-1}(\frac{1}{\varepsilon}\frac{\partial\phi}{\partial t} - \frac{1}{\varepsilon}h_1). \tag{2.105}$$

Here, the components of H and G are

$$H_{ij} = c_i\delta_{ij} - \frac{1}{2\pi}\int_{\Gamma_j} sK_1(sr)\frac{\partial r}{\partial n}d\Gamma_j, \tag{2.106}$$

$$G_{ij} = \frac{1}{2\pi}\int_{\Gamma_j} K_0(sr)d\Gamma_j. \tag{2.107}$$

The diagonal entries H_{ii} are equal to c_i (i.e. $H_{ii} = c_i$) since $\frac{\partial r}{\partial n} = 0$ in Equation (2.106) as the normal $\vec{n}$ and the distance r from the source point are always perpendicular to each other, whereas the diagonal entries of G matrix are calculated analytically in a similar manner given in Section 2.1.2 thorough Equations (2.80-2.83). Thus, they are obtained as

$$G_{ii} \approx \frac{l}{2\pi}(\ln\frac{2}{l} - \ln\frac{s}{2} - \gamma + 1). \tag{2.108}$$

When the time derivative in Equation (2.105) is discretized by using the implicit backward finite difference approximation (see Equation (2.51)), the DRBEM discretized system of equations becomes

$$(H + \frac{C}{\varepsilon\Delta t})\phi^{(m+1)} - G\frac{\partial\phi}{\partial n}^{(m+1)} = \frac{C}{\varepsilon\Delta t}\phi^{(m)} + \frac{C}{\varepsilon}h_1^{(m)} \tag{2.109}$$

m denoting the time level t_m and

$$C = -(H\hat{U} - G\hat{Q})F^{-1}. \tag{2.110}$$

Here the coordinate matrix F is computed by using one of the type of the aforementioned radial basis functions. The insertion of boundary conditions results in a linear system $Az = d$, where A is a full matrix. Once this system is solved, the interior values of ϕ at the selected internal nodes, and the unknown values of ϕ and $\frac{\partial \phi}{\partial n}$ on the boundary according to given boundary conditions are obtained. Finally, the original unknown is obtained by using the transformation given in Equation (2.88).

2.2 The Domain Boundary Element Method (DBEM)

The application of the DBEM, which is another type of boundary element method, will be given for the discretization of the unsteady convection-diffusion-reaction Equations (2.1). DBEM also aims to transform the given differential equation into equivalent integral equation by weighting the equation with the fundamental solution that corresponds to the steady-state problem as in the case of DRBEM. Thus, the basic integral equation of the method involves a domain integral of the time derivative. If the domain integral is kept in the integral equations and is computed numerically, then the DBEM arises [28]. The DBEM discretization with different fundamental solutions, namely fundamental solution of convection-diffusion-reaction equation and fundamental solution of modified Helmholtz equation, will be explained in Section 2.2.1 and Section 2.2.2, respectively.

2.2.1 DBEM with the fundamental solution of convection-diffusion-reaction equation

Here, the application of DBEM with the fundamental solution of convection-diffusion-reaction equation to Equation (2.1) is explained. Similar to DRBEM application with the fundamental solution convection-diffusion-reaction equation explained in Section 2.1.2, one can obtain the same BEM integral Equation (2.58) through the weighted residual method. Equation (2.58) can be written in matrix-vector form as

$$Hu - Gq = -\int_{\Omega} u^* \frac{\partial u}{\partial t} d\Omega + \int_{\Omega} h u^* d\Omega \tag{2.111}$$

where H and G are the same matrices of which entries are given in Equations (2.75)-(2.85).

Unlikely of DRBEM, the domain integral on the right hand side of Equation (2.111) will be kept and it will be computed numerically by using the composite trapezoidal rule taking the end points of the constant elements as integration points (see Section 2.2.1.1).

When the time derivative on the right hand side of Equation (2.111) is discretized by using again backward finite difference approximation (see Equation (2.51)), Equation (2.111) becomes

$$(H + \frac{1}{\Delta t} M_1) u^{(m+1)} - G \frac{\partial u}{\partial n}^{(m+1)} = \frac{1}{\Delta t} M_1 u^{(m)} + M_2 \tag{2.112}$$

where M_1 is the diagonal matrix for which the diagonal entries $(M_1)_{ii}$ are computed by

$$(M_1)_{ii} = \int_{\Omega} u^* d\Omega \tag{2.113}$$

and M_2 is a vector with the entries

$$(M_2)_i = \int_{\Omega} h u^* d\Omega. \tag{2.114}$$

at each node i. Finally, after the insertion of boundary conditions to the system (2.112) we obtain a linear system of equations which needs to be solved iteratively for increasing time levels.

2.2.1.1 Composite trapezoidal rule in 2-D

We consider the double integral

$$I = \iint_{\Omega} f(x, y) dx dy, \tag{2.115}$$

where $\Omega = \{(x, y) \in \mathbb{R}^2 \ : \ a \leq x \leq b, \ r(x) \leq y \leq s(x)\}$.

The integral can be written in iterated form as

$$I = \int_a^b \left(\int_{r(x)}^{s(x)} f(x,y)dy \right) dx. \tag{2.116}$$

At first, we approximate the inner integral with the one-dimensional composite trapezoidal rule in which x is fixed and then we approximate the outer integral also by one-dimensional rule. More precisely, we apply the composite trapezoidal rule in 2-D.

$$F(x) := \int_{r(x)}^{s(x)} f(x,y)dy \quad \Rightarrow \quad I = \int_a^b F(x)dx. \tag{2.117}$$

Then, I is approximated by composite trapezoidal rule as [67]

$$I \approx T(F,h) = \frac{h}{2}\sum_{j=1}^{n}(F(x_{j-1}) + F(x_j)) \tag{2.118}$$

where $x_j = a + jh$ and $h = \frac{b-a}{n}$. To be able to calculate $F(x_j)$ we approximate again

$$\begin{aligned} F(x_j) &= \int_{r(x_j)}^{s(x_j)} f(x_j,y)dy \approx T(f(x_j),h_j) \\ &= \frac{h_j}{2}\sum_{k=1}^{n_j}(f(x_j,y_{j,k-1}) + f(x_j,y_{j,k})) \end{aligned} \tag{2.119}$$

where

$$y_{j,k} = r(x_j) + kh_j \qquad h_j = \frac{s(x_j) - r(x_j)}{n_j} \tag{2.120}$$

In general, n_j is chosen such that $h \approx h_j$ for all j, to minimize the computational cost. The general formula can be written as

$$I \approx \frac{hh_j}{4}\sum_{j=0}^{n}\sum_{k=0}^{n_j} w_{j,k} f(x_j, y_{j,k}) \tag{2.121}$$

where $w_{j,k}$ is equal to 4 in the interior, equal to 2 on the boundary, and equal to 1 at the corner points. The points $(x_j, y_{j,k})$ are taken as the end points of the constant elements.

2.2.2 DBEM with the fundamental solution of modified Helmholtz equation

Similar to the application of DRBEM with the fundamental solution of modified Helmholtz equation (Section 2.1.3), first we transform the time-dependent CDR Equation (2.1) into the following inhomogeneous modified Helmholtz equation

$$\nabla^2\phi - s^2\phi = \frac{1}{\varepsilon}(\frac{\partial\phi}{\partial t} - h_1) \tag{2.122}$$

where

$$h_1 = h\exp(-\frac{a_1 r_x + a_2 r_y}{2\varepsilon}), \qquad s = \sqrt{\frac{\sigma}{\varepsilon} + \frac{a_1^2 + a_2^2}{4\varepsilon^2}} \tag{2.123}$$

by using time-dependent exponential type transformation (2.88). When the fundamental solution of modified Helmholtz Equation (2.92) is employed to weight the Equation (2.122), we end up with the integral Equation (2.94) which contains a domain integral involving a time derivative. However, in DBEM this domain integral is preserved [28] and it is computed by numerical integration. Thus, Equation (2.94) takes the form

$$H\phi - G\frac{\partial\phi}{\partial n} = \frac{-1}{\varepsilon}(\int_\Omega u^*\frac{\partial\phi}{\partial t}d\Omega - \int_\Omega h_1 u^* d\Omega) \tag{2.124}$$

where H and G are the same BEM matrices given in Equations (2.106)-(2.108). When the time derivative is discretized by using implicit backward finite difference approximation (2.51), Equation (2.124) results in

$$(H + \frac{1}{\Delta t}M_1)\phi^{(m+1)} - G\frac{\partial\phi}{\partial n}^{(m+1)} = \frac{1}{\Delta t}M_1\phi^{(m)} + M_2 \tag{2.125}$$

where M_1 is constructed as a diagonal matrix of which the diagonal entries $(M_1)_{ii}$ are computed from

$$(M_1)_{ii} = \frac{1}{\varepsilon}\int_\Omega u^* d\Omega \tag{2.126}$$

while M_2 is a vector with entries

$$(M_2)_i = \frac{1}{\varepsilon}\int_\Omega h_1 u^* d\Omega. \tag{2.127}$$

at each node i. The domain integrals are computed numerically by using composite trapezoidal rule as explained in Section 2.2.1.1. Insertion of the boundary conditions results in a linear system to be solved iteratively for increasing time levels. The solution in the original variable u is obtained by back substitution of ϕ into Equation (2.88) as in the application of DRBEM (see Section 2.1.3).

CHAPTER 3

NUMERICAL SOLUTION OF TIME-DEPENDENT CONVECTION-DIFFUSION-REACTION TYPE EQUATIONS WITH CONSTANT COEFFICIENTS

Solving the CDR type equation always attracts the researchers due to its various applications in biology, ecology, engineering and medicine. These equations describes physical systems in which either particles, energy or other physical quantities are transferring. The time-dependent CDR equations include the time derivative of the unknown and its first and second-order space derivatives making the solution procedure a challenging task. According to the magnitude of diffusion coefficient, the CDR equation can be either diffusion-dominated or convection-dominated. The later is difficult to solve due to the oscillations in the solutions. These cases are considered and solved by numerical techniques through this chapter.

The general time-dependent CDR equation is given in Equation (2.1) as

$$\frac{\partial u}{\partial t} - \varepsilon \nabla^2 u + \vec{a} \cdot \nabla u + \sigma u = h \tag{3.1}$$

where $u(x, t)$ is the unknown function, h is the source function; and ε, $\vec{a} = (a_1, a_2)$, σ are diffusion, convection and reaction coefficients, respectively.

The general boundary and initial conditions are

$$\alpha u + \mu \frac{\partial u}{\partial n} = g \quad \text{on} \quad (0, T] \times \Gamma; \quad u(x, 0) = u_0, \quad x \in \Omega \tag{3.2}$$

where α, μ are constants and $g = g(x, y, t)$ is a given function as mentioned previously in Chapter 2.

This chapter is devoted on the numerical solution of Equation (3.1) by both DRBEM and DBEM which make use of various type of fundamental solutions, namely fundamental solutions of Laplace, convection-diffusion-reaction and modified Helmholtz equations, in spatial discretization. On the other hand, an implicit backward finite difference scheme is applied for the time discretization. Equation (3.1) is kept in its original form in the cases when the fundamental solutions of Laplace and convection-diffusion-reaction equations are taken into account. However, it is transformed into the modified Helmholtz equation by using the time-dependent exponential type transformation

$$u(x,y,t) = \exp(\frac{a_1 r_x + a_2 r_y}{2\varepsilon})\phi(x,y,t) \tag{3.3}$$

which is given in Equation (2.88) to be able to use the fundamental solution of modified Helmholtz equation through the application of DRBEM and DBEM. Thus, the resulting reduced modified Helmholtz equation becomes

$$\nabla^2\phi - s^2\phi = \frac{1}{\varepsilon}(\frac{\partial \phi}{\partial t} - h_1) \tag{3.4}$$

as given in Equation (2.89). Here, $h_1 = h\exp(-\frac{a_1 r_x + a_2 r_y}{2\varepsilon})$ and $s = \sqrt{\frac{\sigma}{\varepsilon} + \frac{a_1^2 + a_2^2}{4\varepsilon^2}}$.

Furthermore, another application area that one can face with the convection-diffusion type equations is the magnetohydrodynamics (MHD) which studies the flow resulting from the interaction between the magnetic field and electrically conducting moving fluids. The governing equations of MHD flow coupled in the velocity and the induced magnetic field are derived from the Navier-Stokes equations of fluid dynamics and Maxwell's equations of electromagnetism through Ohm's law [8, 9, 10]. The MHD flow problem in channels has also a wide range of engineering applications such as power generation, acceleration, geothermal energy extraction, conducting plasma in physics, producing liquid metals, nuclear fusion, etc.

In this chapter, we consider specifically the MHD duct flow which is governed by the transient flow of an incompressible, viscous, electrically conducting fluid in a rectangular duct subject to an externally applied uniform inclined magnetic field of intensity B_0 making an angle β with the positive y-axis. The flow is driven by a constant pressure gradient in the axial direction. Thus, the non-dimensional form of the time-dependent MHD duct flow equations given in Equation (1.7) is [10, 68]

$$
\begin{aligned}
\nabla^2 V + M_x \frac{\partial B}{\partial x} + M_y \frac{\partial B}{\partial y} &= -1 + \frac{\partial V}{\partial t} \\
& \qquad\qquad\qquad \text{in} \quad \Omega \\
\nabla^2 B + M_x \frac{\partial V}{\partial x} + M_y \frac{\partial V}{\partial y} &= \frac{\partial B}{\partial t}
\end{aligned}
\tag{3.5}
$$

for $t > 0$. The general boundary conditions for variable wall conductivity λ and no-slip walls are given as

$$
\frac{\partial B}{\partial n} + \lambda B = 0 \quad \text{and} \quad V = 0 \qquad \text{on} \qquad [0, T] \times \Gamma \tag{3.6}
$$

where $V(x, y)$ is the velocity and $B(x, y)$ is the induced magnetic field. Hartmann number M is the modulus of the vector $\overrightarrow{M} = (M_x, M_y)$ ($M_x = M \sin\beta$ and $M_y = M \cos\beta$). The walls of the duct are insulated (i.e. $B = 0$) when λ tends to infinity and they are perfectly conducting (i.e. $\frac{\partial B}{\partial n} = 0$) when $\lambda = 0$ on the walls. The walls which are perpendicular to applied magnetic field are called Hartmann walls, while the walls which are parallel to the magnetic field are called side walls.

The system (3.5), which is coupled in velocity and induced magnetic field, can be transformed into two decoupled convection-diffusion equations as follows

$$
\begin{aligned}
\nabla^2 w_1 + M_x \frac{\partial w_1}{\partial x} + M_y \frac{\partial w_1}{\partial y} &= -1 + \frac{\partial w_1}{\partial t} \\
& \qquad\qquad\qquad \text{in} \qquad \Omega, \\
\nabla^2 w_2 - M_x \frac{\partial w_2}{\partial x} - M_y \frac{\partial w_2}{\partial y} &= -1 + \frac{\partial w_2}{\partial t}
\end{aligned}
\tag{3.7}
$$

for $t > 0$, and by defining

$$
w_1 = V + B \quad \text{and} \quad w_2 = V - B. \tag{3.8}
$$

Then, the corresponding boundary conditions become

$$
\begin{aligned}
\text{For insulated walls} \quad &: \quad w_1 = 0, \quad w_2 = 0, \\
\text{For variable conductivity walls} \quad &: \quad w_2 = -w_1, \quad \frac{\partial w_2}{\partial n} = \frac{\partial w_1}{\partial n} + 2\lambda w_1.
\end{aligned}
\tag{3.9}
$$

It is noted that, the equations for w_1 and w_2 in Equation (3.7) are the convection-diffusions equations which are compatible with Equation (3.1) where $\varepsilon = 1$, $\vec{a} = (\mp M_x, \mp M_y)$, $\sigma = 0$ and $h = 1$.

The resulting convection-diffusion equations (3.7), can be further transformed into two transient modified Helmholtz equations by using the exponential type transformation given in Equation (3.3), that is,

$$w_1 = \exp(-\frac{M_x r_x + M_y r_y}{2})u_1 \quad \text{and} \quad w_2 = \exp(\frac{M_x r_x + M_y r_y}{2})u_2 \tag{3.10}$$

with $\vec{a} = (a_1 = \mp M_x, a_2 = \mp M_y)$ and $\varepsilon = 1$. Thus, the equations in the new variables u_1, u_2, and the corresponding boundary conditions become

$$\begin{aligned} \nabla^2 u_1 - s^2 u_1 &= -\exp(\frac{M_x r_x + M_y r_y}{2}) + \frac{\partial u_1}{\partial t} \\ \nabla^2 u_2 - s^2 u_2 &= -\exp(-\frac{M_x r_x + M_y r_y}{2}) + \frac{\partial u_2}{\partial t} \end{aligned} \quad \text{in} \quad \Omega, \tag{3.11}$$

$$\begin{aligned} \text{For insulated walls} \quad &: \quad u_1 = 0, \quad u_2 = 0, \\ \text{For variable conductivity walls} \quad &: \quad u_2 = -\exp(-(M_x r_x + M_y r_y))u_1, \\ &\quad\ \frac{\partial u_2}{\partial n} = \exp(-(M_x r_x + M_y r_y))(\frac{\partial u_1}{\partial n} + 2\lambda u_1). \end{aligned} \tag{3.12}$$

The equations for u_1 and u_2 in (3.11) are also compatible with the modified Helmholtz equation (3.4) with $s = \sqrt{\frac{M_x^2 + M_y^2}{4}}$ and $h_1 = \exp(\mp\frac{M_x r_x + M_y r_y}{2})$. Here, the boundary conditions are coupled in u_1 and u_2 for the case when the walls have variable conductivity. Once Equation (3.7) or Equation (3.11) is solved for (w_1, w_2) or (u_1, u_2), respectively, the original unknowns V and B can be obtained with the back substitutions

$$V = \frac{1}{2}(w_1 + w_2), \qquad B = \frac{1}{2}(w_1 - w_2)$$

for the system of convection-diffusion type Equations (3.7) and

$$\begin{aligned} V &= \frac{1}{2}(u_1 \exp(-\frac{M_x r_x + M_y r_y}{2}) + u_2 \exp(\frac{M_x r_x + M_y r_y}{2})), \\ B &= \frac{1}{2}(u_1 \exp(-\frac{M_x r_x + M_y r_y}{2}) - u_2 \exp(\frac{M_x r_x + M_y r_y}{2})) \end{aligned} \tag{3.13}$$

for the system of modified Helmholtz equations (3.11).

To conclude, the MHD duct flow equations are basically convection-diffusion type equations which can be treated in the same manner with the general convection-diffusion-reaction equation (3.1) by using the present techniques explained elaborately in Chapter 2. Thus, the MHD duct flow problem, which is an attractive research area, is also taken as an application in the present chapter.

In the first part of the chapter (Section 3.1) the applications of the dual reciprocity and domain boundary element methods for the general time-dependent CDR equation are briefly explained for each type of fundamental solutions. The numerical simulations are carried out for two test problems in Section 3.2. First, the time-dependent CDR equation, for which the exact solutions is available, is solved by both DRBEM and DBEM with each aforementioned fundamental solutions in Section 3.2.1. Then, the time-dependent MHD flow, which is governed by the coupled convection-diffusion type equations in terms of velocity and induced magnetic field, is solved by both DRBEM and DBEM in Section 3.2.2. The results are analyzed according to the values of Hartmann number under the no-slip velocity, insulated and/or variable conductivity wall conditions. Moreover, the calculations are performed not only in a regular problem domain of square duct but also in an irregular domain of a duct with a perturbed boundary, which enables a comparative study on the effect of the computational domain on MHD flow.

3.1 Application of DRBEM and DBEM to CDR Equation with Constant Coefficients

The details how to dicsretize the general time-dependent CDR equation (3.1) by a combined technique namely, DRBEM and DBEM with different fundamental solutions in space, and implicit backward finite difference approximation in time, are given in Chapter 2. Thus, in this section only basics steps through the application of the numerical methods will be given. The boundary element approach transforms the differential Equation (3.1) into the following equivalent integral equations

$$\varepsilon c_i u_i + \varepsilon \int_\Gamma q^* u d\Gamma - \varepsilon \int_\Gamma u^* q d\Gamma = - \int_\Omega b u^* d\Omega \tag{3.14}$$

and

$$c_i u_i + \varepsilon \int_\Gamma q^* u d\Gamma - \varepsilon \int_\Gamma u^* \frac{\partial u}{\partial n} d\Gamma + \int_\Gamma (a_1 u^* n_x u + a_2 u^* n_y u) d\Gamma = - \int_\Omega b u^* d\Omega. \tag{3.15}$$

by weighting Equation (3.1) with the fundamental solution $u^*(=\frac{1}{2\pi}\ln\frac{1}{|r-r_i|})$ of the Laplace equation and the fundamental solution $u^*(=\frac{1}{2\pi\varepsilon}\exp(-\frac{a_1r_x+a_2r_y}{2\varepsilon})K_0(sr))$ of the convection-diffusion-reaction equation, respectively, over the whole domain Ω and applying the Green's second identity. Similarly, Equation (3.4), which is the modified Helmholtz equation form of Equation (3.1), reduces to

$$c_i\phi_i + \int_\Gamma q^*\phi d\Gamma - \int_\Gamma u^*\frac{\partial\phi}{\partial n}d\Gamma = -\int_\Omega bu^*d\Omega \tag{3.16}$$

when the fundamental solution $u^*(=\dfrac{1}{2\pi}K_0(sr))$ of modified Helmholtz equation is employed through the Green's second identity.

In (3.14)-(3.16), b involves the leftover terms in Equation (3.1) and in Equation (3.4) according to the used fundamental solution u^*, that is the terms except the Laplacian, the convection-diffusion-reaction and the modified Helmholtz operators, respectively. As mentioned previously, the domain integrals on the right hand side of Equations (3.14, 3.15, 3.16) are transformed into boundary integrals by means of radial basis functions f_j in DRBEM while they are preserved and evaluated by the use of numerical integration in DBEM.

3.1.1 DRBEM formulation

In order to transform the domain integrals in Equations (3.14), (3.15) and (3.16) into boundary integrals, the inhomogeneity b is approximated as

$$b \approx \sum_{j=1}^{N+L}\alpha_j(t)f_j(x,y) \tag{3.17}$$

by radial basis functions f_j where $\alpha_j(t)$ is a set of time-dependent coefficients as given in Equation (2.16). When the Green's second identity is also applied to the right hand sides of Equations (3.14), (3.15) and (3.16), one ends up with the following boundary-only integral equations:

$$\varepsilon c_iu_i+\varepsilon\int_\Gamma q^*ud\Gamma-\varepsilon\int_\Gamma u^*qd\Gamma = \sum_{j=1}^{N+L}\alpha_j(t)(c_i\hat{u}_{ji}+\int_\Gamma q^*\hat{u}_jd\Gamma-\int_\Gamma u^*\hat{q}_jd\Gamma), \tag{3.18}$$

and

$$c_i u_i + \varepsilon \int_\Gamma q^* u d\Gamma - \varepsilon \int_\Gamma u^* \frac{\partial u}{\partial n} d\Gamma + \int_\Gamma (a_1 u^* n_x u + a_2 u^* n_y u) d\Gamma \tag{3.19}$$
$$= \sum_{j=1}^{N+L} \alpha_j(t)(c_i u_{ji} + \varepsilon \int_\Gamma q^* \hat{u} d\Gamma - \varepsilon \int_\Gamma u^* \frac{\partial \hat{u}}{\partial n} d\Gamma + \int_\Gamma (a_1 u^* n_x \hat{u} + a_2 u^* n_y \hat{u}) d\Gamma)$$

and

$$c_i \phi_i + \int_\Gamma q^* \phi d\Gamma - \int_\Gamma u^* \frac{\partial \phi}{\partial n} d\Gamma = \sum_{j=1}^{N+L} \alpha_j(t)(c_i \hat{u}_{ji} + \int_\Gamma q^* \hat{u}_j d\Gamma - \int_\Gamma u^* \hat{q}_j d\Gamma) \tag{3.20}$$

as given, respectively in Equation (2.20), Equation (2.62) and Equation (2.99).

In DRBEM application, we consider three types of fundamental solutions namely, fundamental solutions of Laplace, convection-diffusion-reaction and modified Helmholtz equations. Thus, $\hat{u}_j$ are the particular solutions which are linked to f_j through the equations

$$\nabla^2 \hat{u}_j = f_j, \quad \varepsilon \nabla^2 \hat{u}_j - a_1 \frac{\partial \hat{u}_j}{\partial x} - a_2 \frac{\partial \hat{u}_j}{\partial y} - \sigma \hat{u}_j = f_j, \quad \nabla^2 \hat{u}_j - s^2 \hat{u}_j = f_j \tag{3.21}$$

respectively, when the fundamental solution of Laplace, convection-diffusion-reaction and modified Helmholtz equations are employed. In approximations, the polynomial or logarithmic type radial basis functions, the corresponding particular solutions and their normal derivatives are taken as follows for each fundamental solutions:

• **Case 1** (Fundamental solution of Laplace equation):

$$f_j = 1 + r_j, \qquad \hat{u} = \frac{r_j^2}{4} + \frac{r_j^3}{9}, \qquad \hat{q} = (\frac{r_j}{2} + \frac{r_j^2}{3})\frac{\partial r}{\partial n}. \tag{3.22}$$

• **Case 2** (Fundamental solution of CDR equation) [29]:

$$f_j = \varepsilon(1 + r_j) - (\frac{1}{2} + \frac{r_j}{3})(a_1 r_x + a_2 r_y) - \frac{\sigma}{36}(9r_j^2 + 4r_j^3), \tag{3.23}$$
$$\hat{u}_j = \frac{r_j^2}{4} + \frac{r_j^3}{9}, \qquad \hat{q}_j = (\frac{r_j}{2} + \frac{r_j^2}{3})\frac{\partial r}{\partial n}.$$

• **Case 3** (Fundamental solution of modified Helmholtz (mH) equation) [63]:
The polynomial type radial basis functions:

$$f_j = 1 - r_j + r_j^2 - r_j^3 - s^2(\frac{r_j^2}{4} - \frac{r_j^3}{9} + \frac{r_j^4}{16} - \frac{r_j^5}{25}), \tag{3.24}$$
$$\hat{u}_j = \frac{r_j^2}{4} - \frac{r_j^3}{9} + \frac{r_j^4}{16} - \frac{r_j^5}{25}, \qquad \hat{q}_j = (\frac{r_j}{2} - \frac{r_j^2}{3} + \frac{r_j^3}{4} - \frac{r_j^4}{5})\frac{\partial r}{\partial n}.$$

The logarithmic type radial basis functions:

$$\hat{u}_j = \begin{cases} -\dfrac{4}{s^4}(K_0(sr) + \log r) - \dfrac{r^2 \log r}{s^2} - \dfrac{4}{s^4}, & r > 0 \\ \dfrac{4}{s^4}(\gamma + \log(\dfrac{s}{2})) - \dfrac{4}{s^4}, & r = 0 \end{cases} \tag{3.25}$$

$$\hat{q}_j = \begin{cases} (\dfrac{4}{s^4}(sK_1(sr) - \dfrac{1}{r}) - \dfrac{1}{s^2}(2r \log r + r))\dfrac{\partial r}{\partial n}, & r > 0 \\ 0, & r = 0 \end{cases} \tag{3.26}$$

$$f_j = \begin{cases} r^2 \log r, & r > 0 \\ 0, & r = 0 \end{cases} \tag{3.27}$$

Finally, by the use of constant elements in the discretization of the boundary and employing properly the backward finite difference approximation for the time derivative (as explained in Sections (2.1.1), (2.1.2) and (2.1.3), respectively for each case mentioned above), one can obtain the general matrix-vector form of the discretized DRBEM equations as follows

$$(\bar{H} + \frac{C}{\Delta t})\bar{u}^{(m+1)} - \bar{G}\frac{\partial \bar{u}}{\partial n}^{(m+1)} = \frac{C}{\Delta t}\bar{u}^{(m)} + C\bar{h}^{(m)}. \tag{3.28}$$

Here, m denotes the time iteration, $\bar{u}$ is the unknown and the analogous of the matrices $\bar{H}$, $\bar{G}$, C and the vector $\bar{h}$ are given in:

• Equation (2.52) for **Case 1**, when we apply the fundamental solution of Laplace equation. Thus, the above variables correspond to

$$C = -(\bar{H}\hat{U} - \bar{G}\hat{Q})F^{-1}, \quad \bar{u} = u, \quad \bar{H} = \widetilde{H}, \quad \bar{G} = \widetilde{G} \quad \text{and} \quad \bar{h} = h \tag{3.29}$$

in Equation (2.52).

• Equation (2.86) for **Case 2** when the fundamental solution of CDR equation is applied. For this case:

$$C = -(\bar{H}\hat{U} - \bar{G}\hat{Q})F^{-1}, \quad \bar{u} = u, \quad \bar{H} = H, \quad \bar{G} = G \quad \text{and} \quad \bar{h} = h. \tag{3.30}$$

• Equation (2.109) for the **Case 3** when the fundamental solution of mH equation is employed. The corresponding terms for the above variables are as follows:

$$C = -\frac{1}{\varepsilon}(\bar{H}\hat{U} - \bar{G}\hat{Q})F^{-1}, \quad \bar{u} = \phi, \quad \bar{H} = H, \quad \bar{G} = G \quad \text{and} \quad \bar{h} = h_1. \tag{3.31}$$

Here, F is the coordinate matrix taking f_j as columns, $\hat{U}$ and $\hat{Q}$ are the matrices which take the particular solutions $\hat{u}_j$ and their normal derivatives $\hat{q}_j$ (given in Equations (3.22)-(3.24)) as columns, respectively.

3.1.2 DBEM formulation

In DBEM application, the domain integral on the right hand side of the Equations (3.14), (3.15) and (3.16) are kept and computed numerically by composite trapezoidal rule (see Section 2.2.1.1). When we follow the procedure given in Sections 2.2.1 and 2.2.2, we obtain the following equation in matrix-vector form

$$(\bar{H} + \frac{1}{\Delta t}M_1)\bar{u}^{(m+1)} - \bar{G}\frac{\partial \bar{u}}{\partial n}^{(m+1)} = \frac{1}{\Delta t}M_1\bar{u}^{(m)} + M_2 \tag{3.32}$$

where M_1 is a diagonal matrix and M_2 is a vector.

The analogous of the unknown $\bar{u}$, the matrices $\bar{H}$, $\bar{G}$, M_1 and the vector M_2 are given in:

• Equation (2.112) when the fundamental solution of CDR equation is used. That is, the above variables correspond to

$$\bar{u} = u, \quad \bar{H} = H, \quad \bar{G} = G, \quad (M_1)_{ii} = \int_\Omega u^* d\Omega \quad \text{and} \quad (M_2)_i = \int_\Omega h u^* d\Omega \tag{3.33}$$

in Equation (2.112).

• Equation (2.125) when the fundamental solution of mH equation is employed. Thus, the corresponding terms in Equation (2.125) for the above variables are as follows:

$$\bar{u} = \phi, \quad \bar{H} = H, \quad \bar{G} = G, \quad (M_1)_{ii} = \frac{1}{\varepsilon}\int_\Omega u^* d\Omega \quad \text{and} \quad (M_2)_i = \frac{1}{\varepsilon}\int_\Omega h_1 u^* d\Omega. \tag{3.34}$$

In each case, after the insertion of boundary conditions, the system (3.32) is transformed into a linear system of equations which will be solved iteratively for increasing time levels.

3.2 Numerical Results for the Time-dependent CDR type Equation with Constant Coefficients

In this section, we present the applications of DRBEM and DBEM to the CDR type equations and investigate the effects of the use of different fundamental solutions on the accuracy and the efficiency of the solution process. Two test problems governed by the time-dependent CDR equations are considered. In Section 3.2.1, the time-dependent CDR equation is solved and the obtained numerical results are compared with the analytical solutions in order to validate our numerical codes for DBEM and DRBEM with various fundamental solutions. Then in Section 3.2.2, the unsteady MHD flow is solved again by DBEM and DRBEM in ducts with straight and perturbed walls of different conductivity for several values of Hartmann number.

3.2.1 CDR equation with exact solution

The problem of transient convection-diffusion-reaction given by

$$\begin{aligned}\frac{\partial u}{\partial t} - \varepsilon \nabla^2 u + \vec{a} \cdot \nabla u + \sigma u &= h, \quad \text{in} \quad (0,T] \times \Omega, &(3.35)\\ u &= 0 \quad \text{on} \quad [0,T] \times \Gamma, &(3.36)\\ u(0,x) &= u_0(x) \quad \text{in} \quad \Omega &(3.37)\end{aligned}$$

is considered. Here, $\{\Omega = (x,y) : 0 \leq x, y \leq 1\}$ and $(0,T) = (0,0.5)$, $\vec{a} = (a_1,a_2)^T = (2,3)^T$ and $\sigma = 1$. The exact solution of the problem is [20]

$$\begin{aligned}u(t,x,y) = {} & 16\sin(\pi t)x(1-x)y(1-y)\\ & \times \left[\frac{1}{2} + \frac{\arctan(2\varepsilon^{-1/2}(0.25^2 - (x-0.5)^2 - (y-0.5)^2))}{\pi}\right]. \qquad (3.38)\end{aligned}$$

The forcing term h and the initial condition u_0 are set such that Equation (3.38) satisfies the boundary value problem.

The solution to this problem obtained by DRBEM with the fundamental solution of Laplace Equation is visualized in Section 3.2.1.1. Then, the results not only by DRBEM but also by DBEM with the fundamental solutions of CDR and mH equations are given in Sections 3.2.1.2 and 3.2.1.3, respectively.

3.2.1.1 DRBEM with the fundamental solution of Laplace equation

First, the comparison of present result with the exact solution is shown in Figure 3.1 in terms of time evolution of the solutions up to $T = 7.5$ along the points at the center and close to the corners. In Figure 3.1, Node 1 represents the center point $(0.5, 0.5)$, Node 2 represents the corner points: $(0.74, 0.74)$, $(0.26, 0.26)$, $(0.74, 0.26)$, $(0.26, 0.74)$; and Node 3 represents the corner points: $(0.86, 0.86)$, $(0.14, 0.14)$, $(0.86,$ $0.14)$, $(0.14, 0.86)$. It is well observed that at each points the oscillating analytical solution agrees very well with the obtained DRBEM solution with an relative error of 23×10^{-4} as time advances. The relative error is evaluated by $\left|\dfrac{u_i^{exact} - u_i}{u_i^{exact}}\right|$, where $i = 1, ..., N + L$.

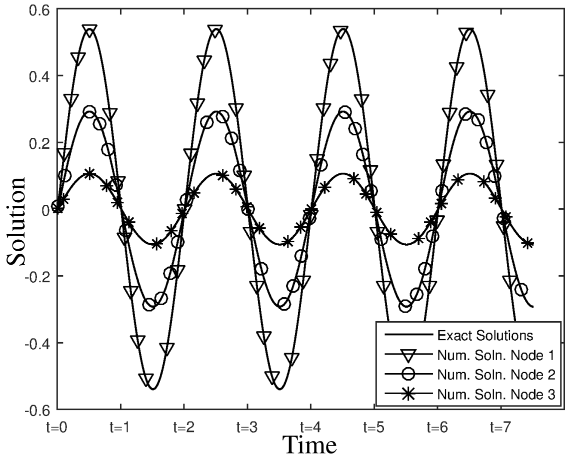

Relative error=23×10^{-4}

Figure 3.1: Time evolution of the exact and DRBEM solutions at central point (Node 1) and at some corner points (Node 2, Node 3) up to $T = 7.5$: $\varepsilon = 1$.

Then, the effect of diffusion coefficient ε on the numerical solution is investigated. For the discretization of the computational domain, $N = 100$ constant boundary elements and $L = 625$ interior nodes are taken for ε = 10, 1, 10^{-1}, 10^{-2} while $N =$ $200, L = 1600$ and $N = 300, L = 9025$ are used for smaller values of $\varepsilon = 10^{-3}$ and ε =10^{-4}, respectively. The comparison of the exact and DRBEM solutions at $T = 0.5$ for several values of diffusion coefficient are displayed along the horizontal centerline ($y = 0.5$, $0 \leq x \leq 1$) in Figure 3.2. It is observed that the DRBEM solutions are in good agreement with the corresponding exact ones, especially when $\varepsilon = 10$, 1, 10^{-1}, 10^{-2}, 10^{-3}. However, as ε decreases to 10^{-4}, slight differences between the exact and DRBEM solutions, especially where u takes its maximum and minimum values, arise following the fact that the equation becomes convection-dominated for smaller values of ε. Thus, the DRBEM code which uses the fundamental solution of diffusion equation (i.e. Laplacian equation), loses its efficiency. Moreover, a decrease in the diffusion coefficient ε has an increasing effect on the values of concentration u.

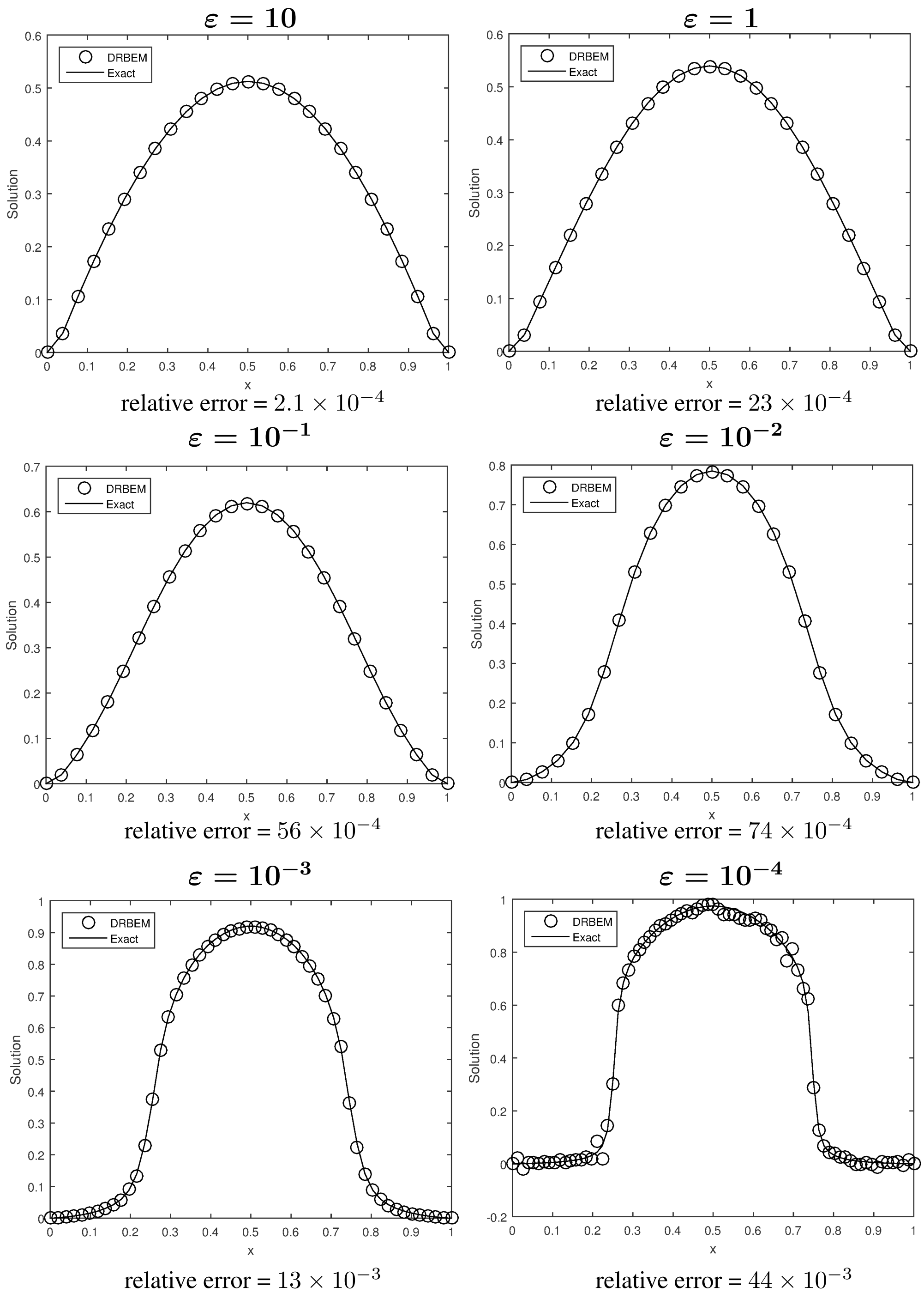

Figure 3.2: Effect of ε on the DRBEM solution with the fundamental solution of Laplace equation along horizontal centerline $y = 0.5$ at $T = 0.5$.

3.2.1.2 DBEM and DRBEM with the fundamental solution of CDR equation

As in Section 3.2.1.1, we investigate the effect of diffusion coefficient ε (= 10, 1, 10^{-1}, 10^{-2}) on the solution u. In Figure 3.3, the obtained results by both DBEM and DRBEM with the fundamental solution of CDR equation are drawn along the horizontal centerline ($y = 0.5$, $0 \leq x \leq 1$) to compare them with the analytical solution. Maximum $N = 180$ and $L = 2025$ nodes are used in discretization through the application of DBEM and DRBEM. It is observed that for ε = 10, the results obtained by both DBEM and DRBEM are in good agreement with the exact ones. However, when $\varepsilon \leq 1$, DBEM has difficulties in giving accurate results compared to DRBEM. Furthermore, for smaller values of $\varepsilon \leq 10^{-3}$, Equation (3.35) becomes more convection-dominated, and thus both DBEM and DRBEM suffer to give reasonable results.

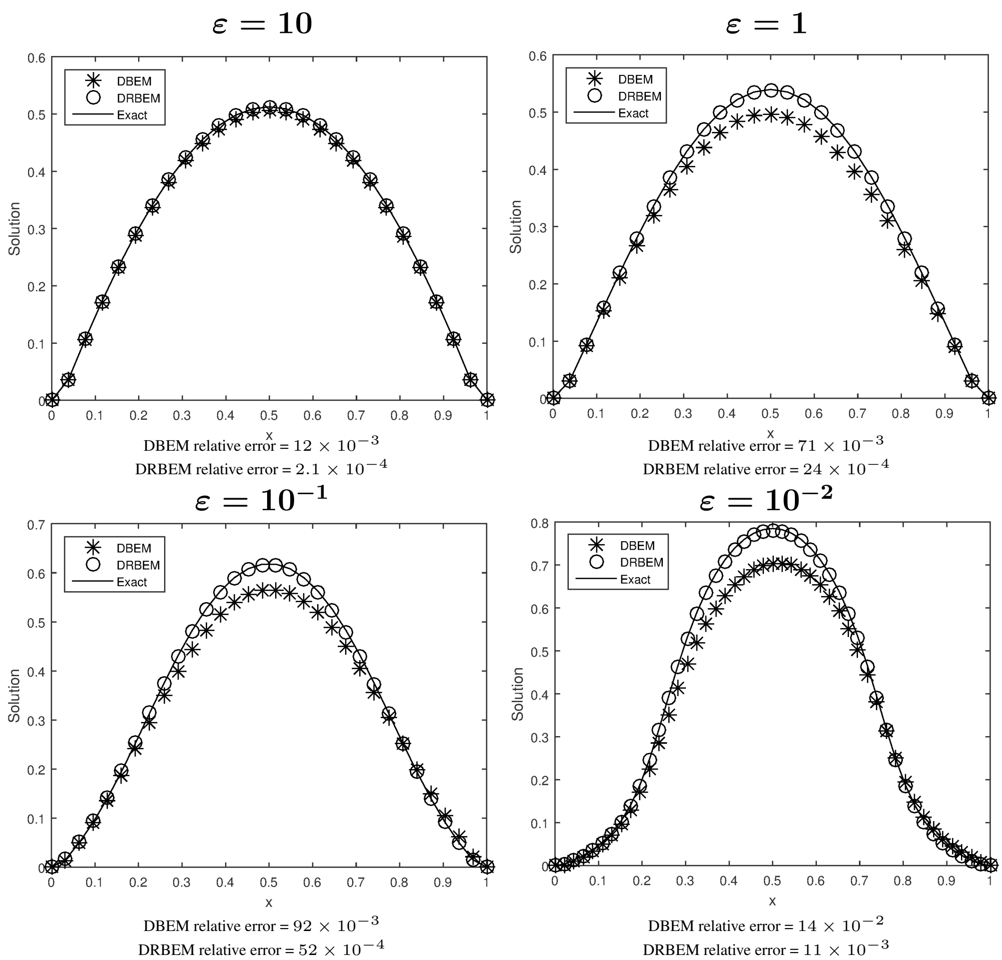

Figure 3.3: Effect of ε on the DBEM and DRBEM solutions with the fundamental solution of CDR equation along horizontal centerline $y = 0.5$ at $T = 0.5$.

3.2.1.3 DBEM and DRBEM with the fundamental solution of modified Helmholtz equation

Finally, to investigate the effect of the diffusion coefficient ε (= 10, 1, 10^{-1}, 10^{-2}) on the solution when the fundamental solution of mH equation is used in DBEM and DRBEM, the variation of u along the horizontal centerline $y = 0.5$, $0 \leq x \leq 1$ is drawn in Figure 3.4 at $T = 0.5$. For the smallest value of ε, maximum $N = 300$, $L = 5625$ and $N = 100$, $L = 625$ points are used in the discretization with DBEM and DRBEM, respectively. As expected we need to take more number of boundary elements for smaller values of ε (i.e. in the convection-dominated case) to deal with the resulting discrepancies between the exact and present numerical results.

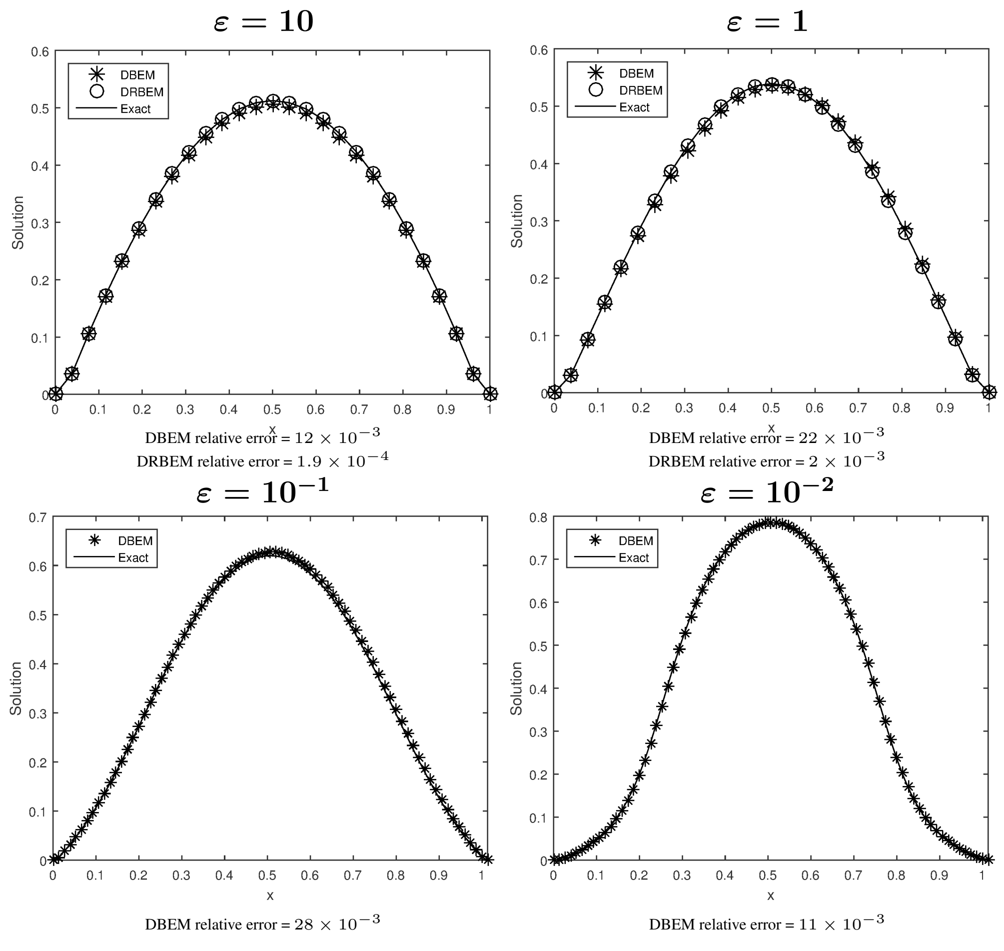

Figure 3.4: Effect of ε on the DBEM and DRBEM solutions with the fundamental solution of mH equation along horizontal centerline $y = 0.5$ at $T = 0.5$.

Figure 3.4 show that the DBEM gives quite compatible results with the analytical solution not only for high but also small values of ε ($= 10^{-1}$, 10^{-2}) while DRBEM gives reasonable results only for $\varepsilon \geq 1$. On the other hand, for smaller values of $\varepsilon \leq 10^{-3}$, both techniques suffer from computational difficulties due to the overflow of the argument in the exponential function located in the exponential type transformation (3.3).

In this section which is devoted to solve the transient CDR type equations, we are able to validate our computer codes by testing the problems with available exact solutions. One can notice that, DRBEM with fundamental solution of Laplace equation gives the most accurate results for even smaller values of ε. On the other hand, the use of the fundamental solution of CDR equation results in better accuracy than the use of the fundamental solution of mH equation by DRBEM while in DBEM a reverse situation is observed.

3.2.2 Magnetohydrodynamic Duct Flow

As mentioned previously, the problem of MHD duct flow given in Equations (3.5-3.6) is taken as the second test problem since the MHD equations are basically convection-diffusion type equations coupled in the velocity of the fluid and induced magnetic field. For the solution of these equations, DBEM and DRBEM are employed by using the fundamental solutions of convection-diffusion (CD) and modified Helmholtz equations.

In this section, we focus on the solution of MHD flow problems in two different problem domains namely, regular square duct with straight walls in Section 3.2.2.1 and irregular duct with a perturbed upper wall in Section 3.2.2.2, subject to various boundary conditions for the induced magnetic field under an externally applied magnetic field at different inclination angles.

3.2.2.1 MHD Flow in a Regular Square Cavity with Straight Walls

The MHD duct flow problem is solved in a computational domain of a regular square duct to analyze the effects of various combination of wall conductivities and inclination angle on the flow and magnetic fields for increasing values of Hartmann number. The physical configuration of the MHD duct flow with straight walls is displayed in Figure 3.5.

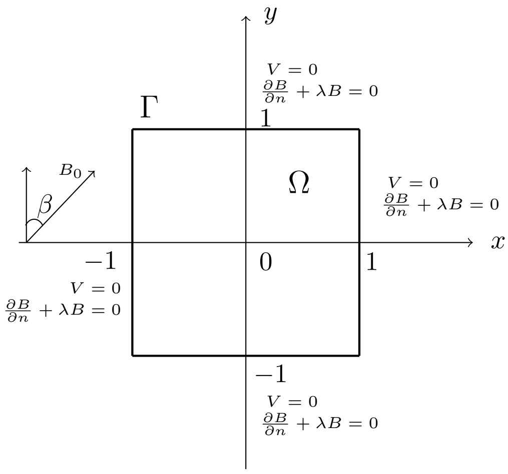

Figure 3.5: Geometry of MHD duct flow with straight walls and boundary conditions.

To discretize the boundary of the square duct with straight boundaries, maximum $N = 360$ constant boundary elements and $L = 8100$ interior nodes are taken for the highest value of Hartmann number $M = 200$ used in the application of DBEM with both CD and mH fundamental solutions. On the other hand, in the application of DRBEM maximum $N = 300$, $L = 5625$ nodes are used to discretize the computational domain when $M = 80$.

3.2.2.1.1 Insulated duct walls under horizontal magnetic field

First, we investigate the MHD duct flow with insulated walls ($B = 0$) under a uniform transverse magnetic field ($\beta = \pi/2$) for which the steady-state exact solution is available [10] in order to compare the present DBEM and DRBEM results with the corresponding analytical solutions at the steady-state. Thus, we specifically consider the MHD flow subject to a uniform horizontally applied external magnetic field (i.e. $\beta = \pi/2$, $M_x = M$ and $M_y = 0$ in Equation (3.5)) which is given by

$$\left.\begin{aligned} \nabla^2 V + M\frac{\partial B}{\partial x} &= -1 + \frac{\partial V}{\partial t} \\ \nabla^2 B + M\frac{\partial V}{\partial x} &= \frac{\partial B}{\partial t} \end{aligned}\right. \qquad \text{in} \quad \Omega, \tag{3.39}$$

under no-slip ($V = 0$) boundary conditions for the velocity.

The decoupled form of Equation (3.39) is obtained by using transformation (3.8) and considering $M_x = M$ and $M_y = 0$ in Equation (3.7). Thus, we have the following governing convection-diffusion type equations

$$\left.\begin{aligned} \nabla^2 w_1 + M\frac{\partial w_1}{\partial x} &= -1 + \frac{\partial w_1}{\partial t} \\ \nabla^2 w_2 - M\frac{\partial w_2}{\partial x} &= -1 + \frac{\partial w_2}{\partial t} \end{aligned}\right. \quad \text{in} \quad \Omega \tag{3.40}$$

with the boundary conditions

$$w_1 = w_2 = 0 \quad \text{on} \quad \Gamma. \tag{3.41}$$

On the other hand, Equation (3.40) is further transformed into two transient modified Helmholtz equations as given in Equation (3.11) by using the transformation (3.10). Thus, the Equations (3.40) become

$$\left.\begin{aligned} \nabla^2 u_1 - \frac{M^2}{4}u_1 &= -\exp(\frac{M}{2}r_x) + \frac{\partial u_1}{\partial t} \\ \nabla^2 u_2 - \frac{M^2}{4}u_2 &= -\exp(-\frac{M}{2}r_x) + \frac{\partial u_2}{\partial t} \end{aligned}\right. \quad \text{in} \quad \Omega \tag{3.42}$$

with

$$u_1 = u_2 = 0 \quad \text{on} \quad \Gamma \tag{3.43}$$

which enables one to use the fundamental solution of modified Helmholtz equation in DBEM and DRBEM applications.

To be able to compare the present numerical results with the steady-state exact solutions, the numerical results are obtained at different time levels to determine when the steady-state is reached at a fixed $M = 10$. Thus, the velocity and the induced magnetic field along the horizontal centerline $y = 0$, $0 \leq x \leq 1$ as time advances are drawn in Figure 3.6 when the fundamental solutions of both CD and mH equations are used in DBEM. It is well observed that, the values of the velocity and the induced magnetic field show no significant change at approximately $T = 0.9$ and $T = 0.4$, respectively for the fundamental solutions of CD and mH, which indicates that the steady-state is reached for both V and B. Furthermore, the time evolutions of equivelocity and current lines are also drawn in Figure 3.7 for the same case, and the visualized results confirm the obtained time levels $T \approx 0.9$ and $T \approx 0.4$ when the steady-state is reached for V and B. Thus, in the subsequent numerical computations of the present section, the equivelocity and current lines are drawn at time level $T = 1$ when the steady-state has been already reached. On the other hand, the time evolution of V and B when DRBEM is employed is not displayed here since the application of DRBEM gives very similar results compared to DBEM.

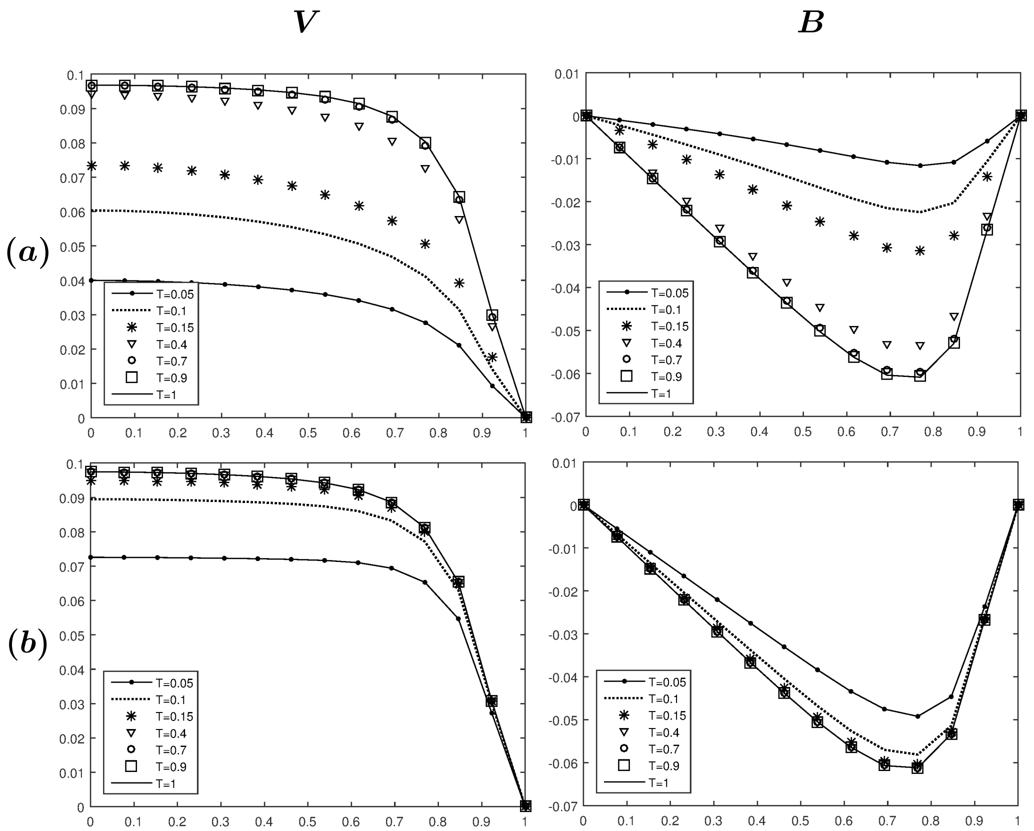

Figure 3.6: Velocity and induced magnetic field along horizontal centerline $y = 0$ at increasing time levels by DBEM with the fundamental solutions of (a) CD and (b) mH equations: $M = 10$, $\beta = \frac{\pi}{2}$.

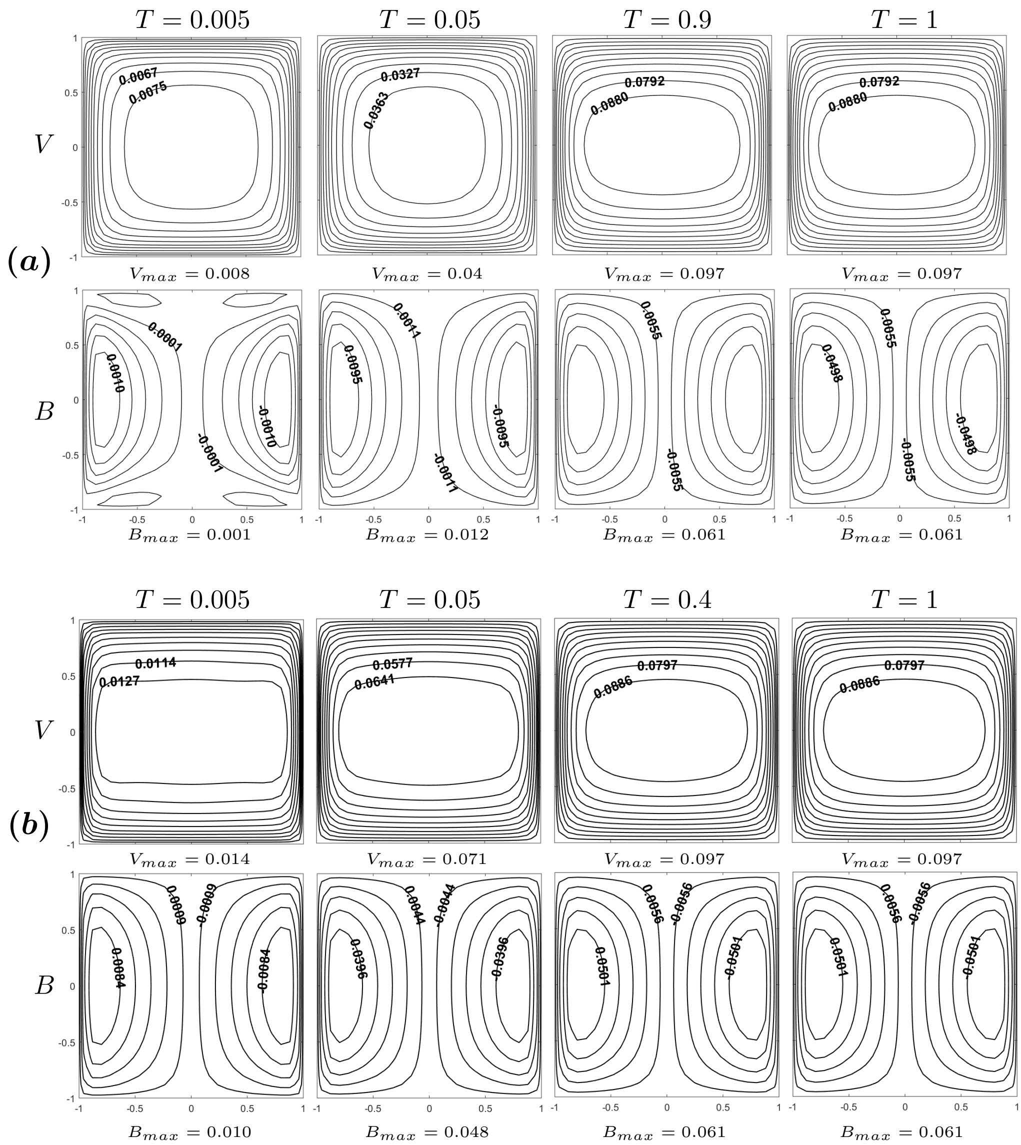

Figure 3.7: Time evolutions of the velocity and induced current by DBEM with the fundamental solutions of (a) CD and (b) mH equations: $M = 10$, $\beta = \frac{\pi}{2}$.

The effect of Hartmann number M $(= 40, 80, 200)$ on the steady-state velocity and induced magnetic field obtained by DBEM and DRBEM with the fundamental solutions of CD and mH equations is shown in Figure 3.8 and Figure 3.9, respectively. The corresponding exact solutions are also illustrated in order to compare them qualitatively with the present numerical results, and a quantitative error is given in terms of relative error calculated on the entire domain. As Hartmann number increases, it is seen from Figure 3.8 that the velocity become stagnant at the center of the duct and the boundary layers are formed along the walls of the duct. Moreover, the velocity decreases indicating the well-known retarding effect of the intensity of the magnetic field as M increases. On the other hand, Figure 3.9 shows that, an increase in M results in formation of boundary layers along the horizontal walls especially in the regions close to the corners of the duct for the induced magnetic field.

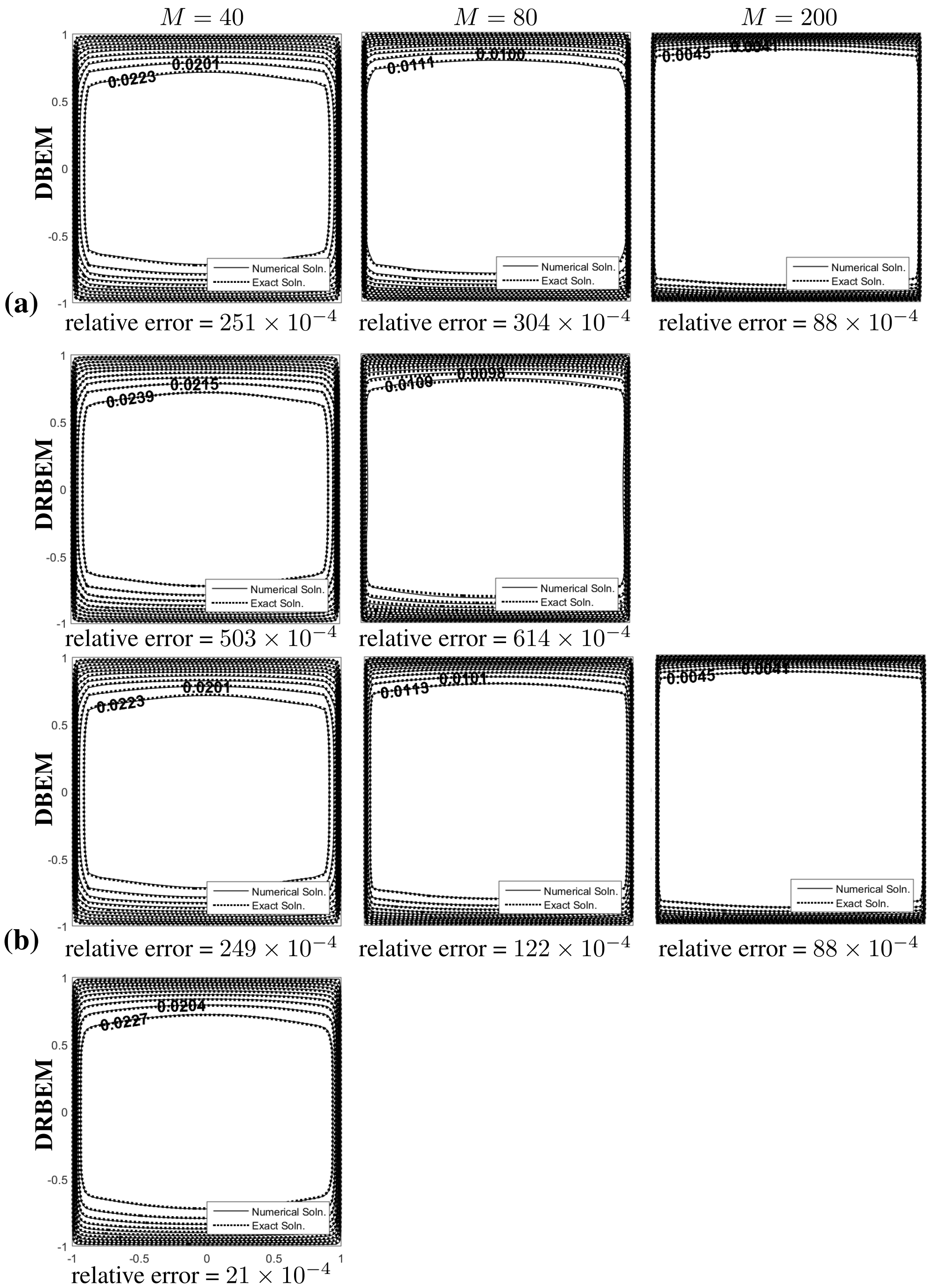

Figure 3.8: Effect of M on the velocity obtained by DBEM and DRBEM with the fundamental solution of (a) CD and (b) mH equations: $M = 40, 80, 200$, $\beta = \frac{\pi}{2}$, $T = 1$.

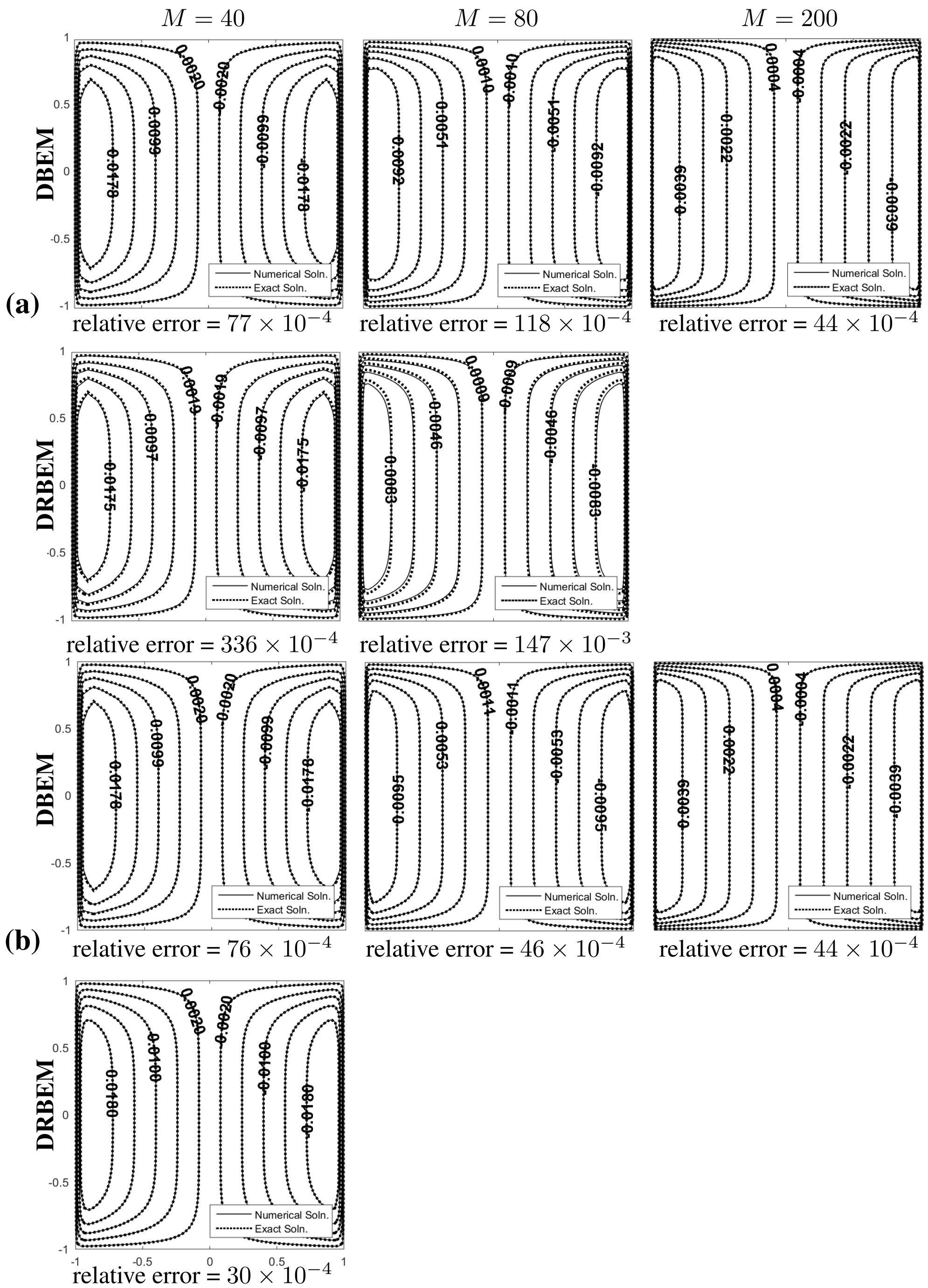

Figure 3.9: Effect of M on the induced current obtained by DBEM and DRBEM with the fundamental solution of (a) CD and (b) mH equations: $M = 40, 80, 200$, $\beta = \frac{\pi}{2}$, $T = 1$.

Furthermore, using the fundamental solutions of either CD or mH equations in either DBEM or DRBEM does not cause a significant change in the profiles of equivelocity and current lines; and an accuracy of order 10^{-4} is obtained between the exact and numerical solutions in terms of relative error for each value of M for which the numerical solutions can be obtained. Moreover, the DBEM with both of the fundamental solutions enables one to obtain accurate solutions for the values of Hartmann number up to 200 whereas DRBEM suffers from computational difficulties for high values of M. That is, reasonably well results for V and B can be obtained using DRBEM for small values of $M \leq 40$ by the use fundamental solution of mH equation, while the use of fundamental solution of CD equation increases the Hartmann number up to moderate values of $M \leq 80$. The reason for this observation is that, the exponential terms $(\exp(-\frac{a_1 r_x + a_2 r_y}{2\varepsilon}))$ are computed in domain integrals when the fundamental solution of CD is employed, which results in some computational advantage in DRBEM especially at higher values of M. On the other hand, these exponential terms are involved by the exponential transformation (3.3) when the fundamental solution of mH equation is used, and hence they are computed outside the domain integral treated as coefficients. This may results in very large values causing overflows in computations, that the DRBEM results are obtained for smaller values of M when compared with the results of DBEM.

3.2.2.1.2 Insulated duct walls under oblique magnetic field

This section studies the effect of the oblique external magnetic field on the velocity and induced magnetic field behaviors for the MHD flow in a duct with insulated walls (i.e. $B = 0$, $\lambda \to \infty$). That is, the equations and the corresponding boundary conditions of the problem are taken as given in Equations (3.7-3.9) and Equations (3.11-3.12), respectively, when the fundamental solution of CD and mH are employed. As in the previous Section 3.2.2.1.1, the solutions are drawn at $T = 1$ since for this insulated duct problem the steady-state is also reached before $T = 1$ as expected.

The effect of inclination angle $\beta(= \frac{\pi}{6}, \frac{\pi}{4}, \frac{\pi}{3})$ on the velocity and induced magnetic field is displayed respectively in Figure 3.10 and Figure 3.11 for a fix $M = 30$. It is observed that the equivelocity lines extend and form a circulation in the direction of externally applied magnetic field. The velocity increases as β decreases from $\frac{\pi}{3}$ to $\frac{\pi}{4}$, and a further decrease to $\beta = \frac{\pi}{6}$ results in a decrease in the velocity. On the other hand, two vortices are formed in the profiles of current lines, however, the symmetry about the y-axis observed when $\beta = \frac{\pi}{2}$ (see Figure 3.9) is deteriorated with the application of the inclined magnetic field. It is observed that at $M = 30$, DRBEM and DBEM results obtained by using both of the fundamental solutions are compatible to each other for each β.

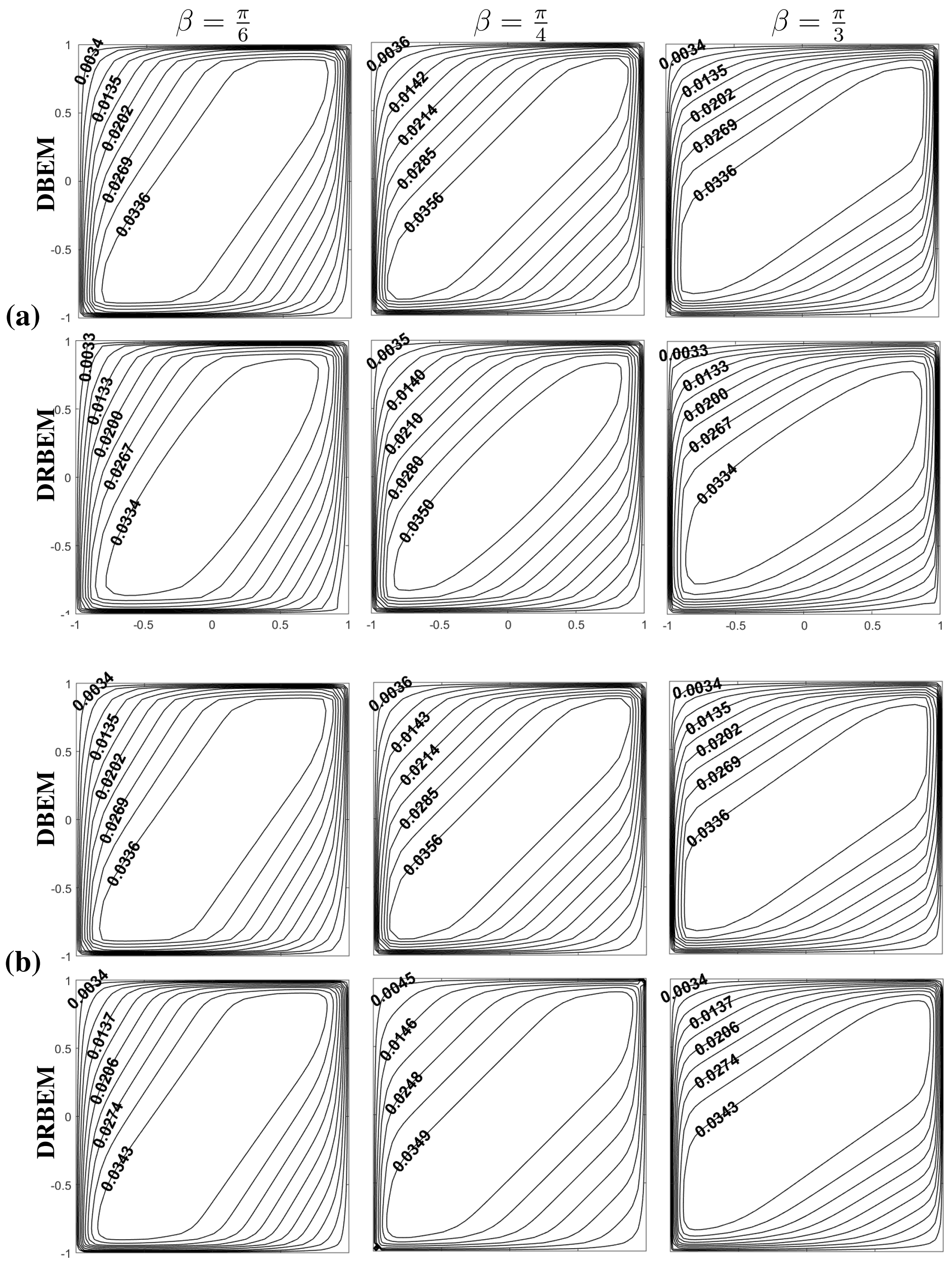

Figure 3.10: Effect of β on the velocity obtained by DBEM and DRBEM with the fundamental solution of (a) CD and (b) mH equations: $\beta = \frac{\pi}{6}, \frac{\pi}{4}, \frac{\pi}{3}$, $M = 30$, $T = 1$.

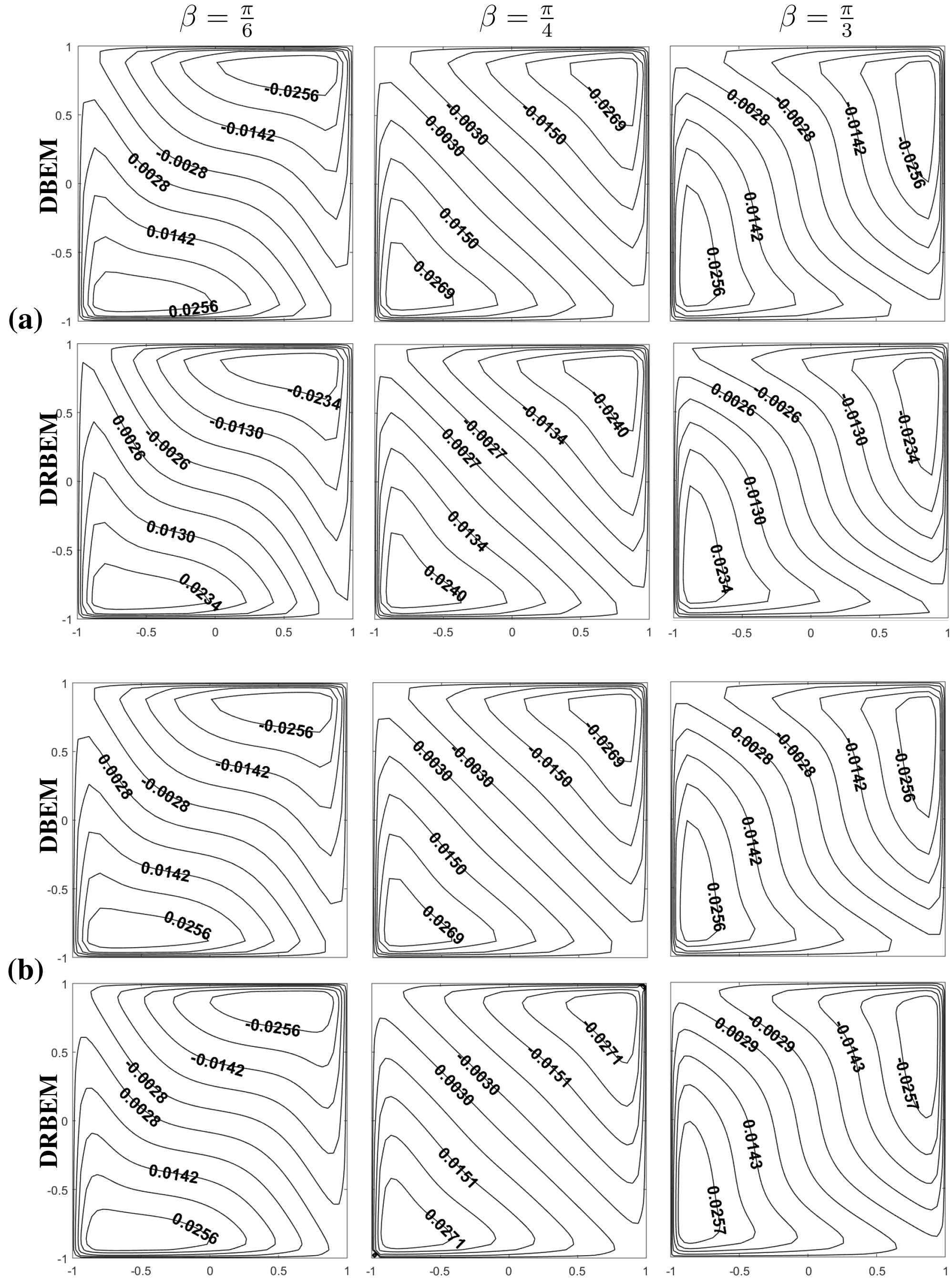

Figure 3.11: Effect of β on the induced current obtained by DBEM and DRBEM with the fundamental solution of (a) CD and (b) mH equations: $\beta = \frac{\pi}{6}, \frac{\pi}{4}, \frac{\pi}{3}$, $M = 30$, $T = 1$.

Figures 3.12 and 3.13 display the DBEM and DRBEM solutions in terms of equivelocity and current lines, respectively for increasing values of Hartmann number ($30 \leq M \leq 200$) at a fixed $\beta = \frac{\pi}{3}$, $T = 1$. The well-known characteristics of the velocity and the induced magnetic field are well-captured by both DBEM and DRBEM at the computed values of M. That is, as M increases the velocity decreases and the fluid becomes stagnant at the center of the duct. Thus, boundary layers are formed near the corners and the flow is aligned in the direction of applied magnetic field. Moreover, the flattening tendency of the flow and induced magnetic field is still well-observed as M increases. As in Section 3.2.2.1.1, the DBEM results are almost invariant to the type of the fundamental solutions for each M up to $M \leq 200$.

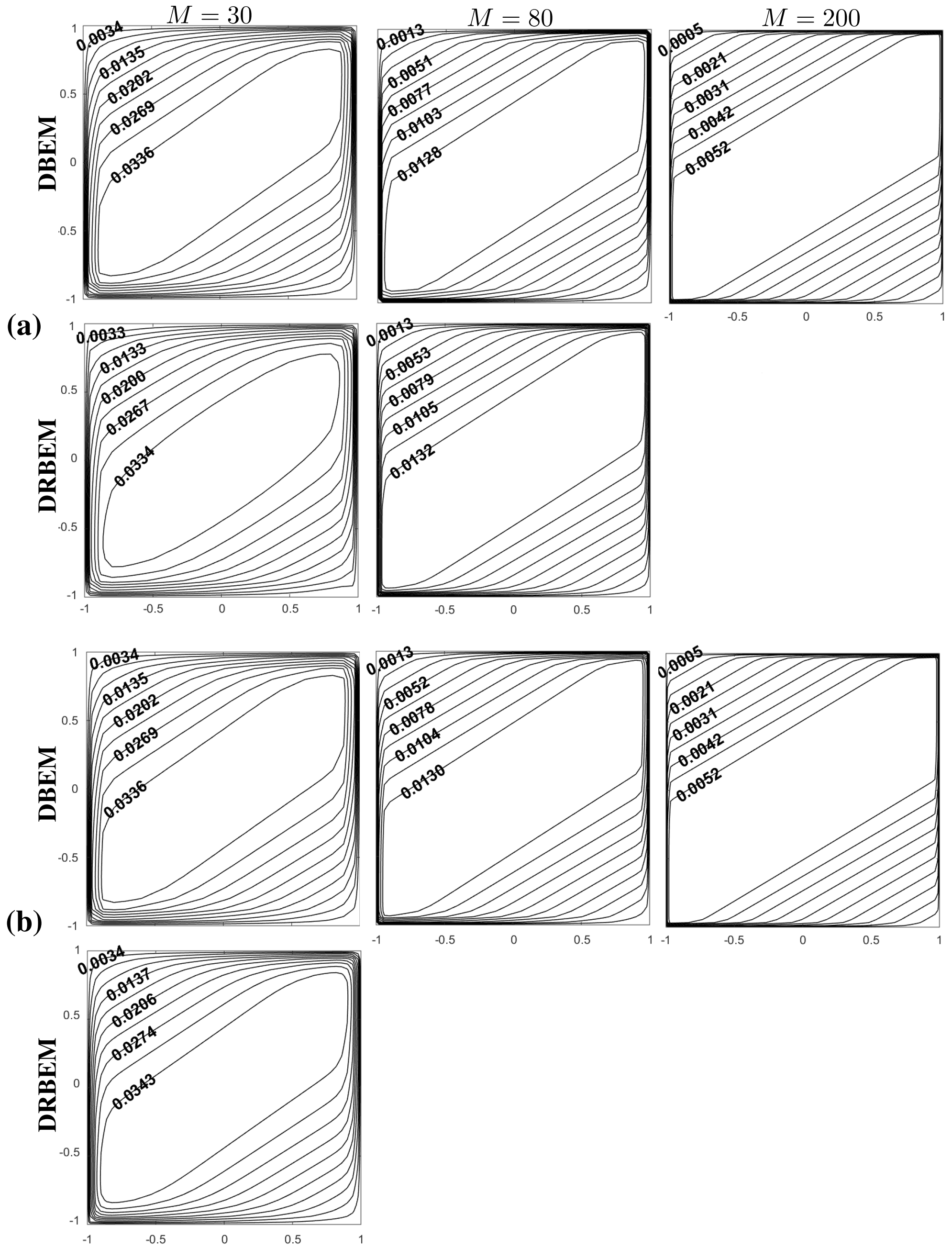

Figure 3.12: Effect of M on the velocity obtained by DBEM and DRBEM with the fundamental solution of (a) CD and (b) mH equations: $M = 30, 80, 200$, $\beta = \dfrac{\pi}{3}$, $T = 1$.

On the other hand, it restricts the results by DRBEM up to $M \leq 30$ when the fundamental solution of mH equation is employed while one can obtain reasonably well results up to $M \leq 80$ with the use of fundamental solution of CD equation in DRBEM. Thus, DRBEM works more properly with the use of the fundamental solution of CD equation.

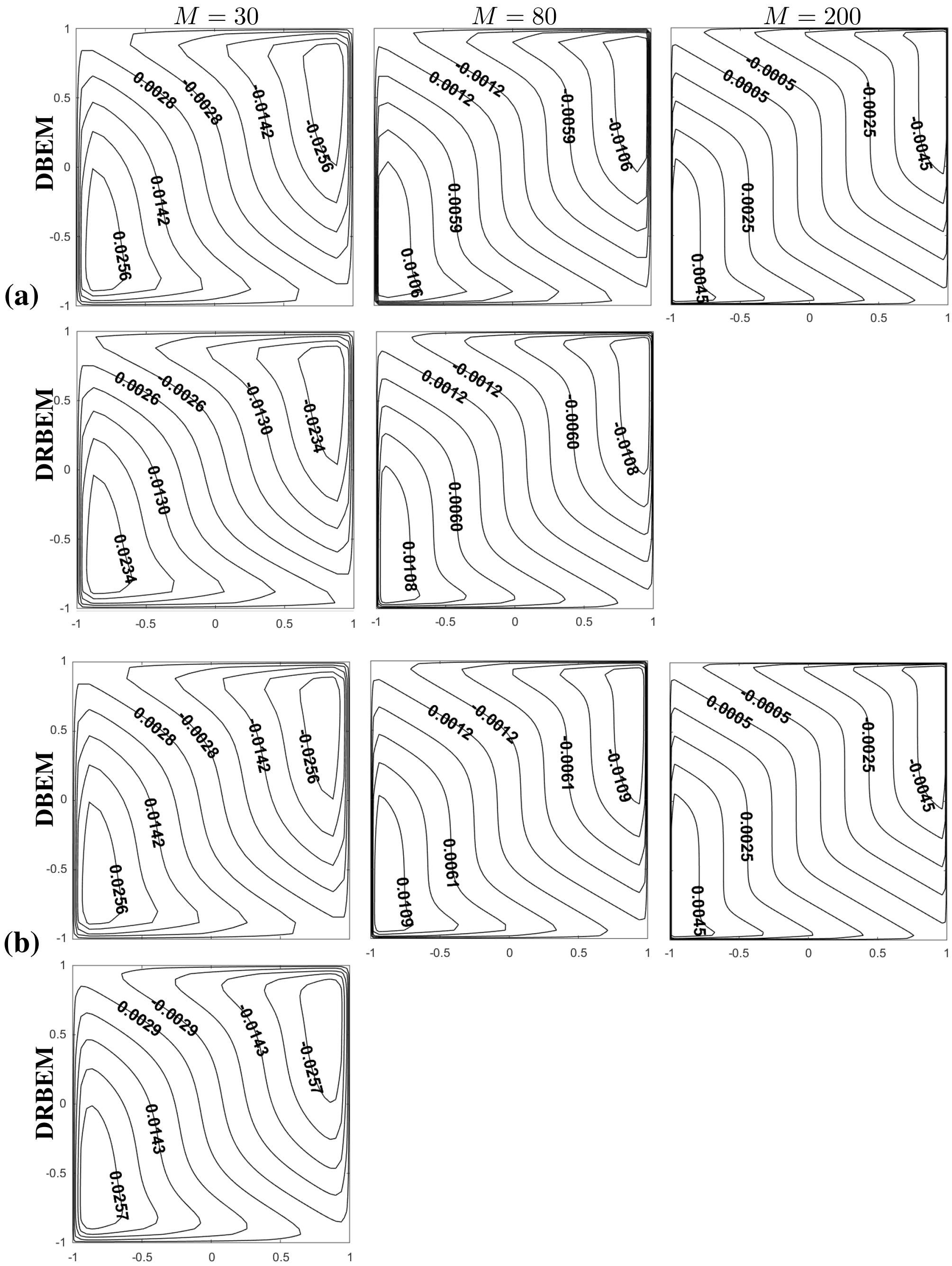

Figure 3.13: Effect of M on the induced current obtained by DBEM and DRBEM with the fundamental solution of (a) CD and (b) mH equations: $M = 30, 80, 200$, $\beta = \frac{\pi}{3}, T = 1$.

3.2.2.1.3 Variably conducting duct walls under oblique magnetic field

In this section, we consider the MHD duct flow problem (3.5) when the duct walls have variable conductivity (i.e. $\dfrac{\partial B}{\partial n} + \lambda B = 0$). That is, the MHD equations given by Equation (3.7) in CD form and by Equation (3.11) in mH form are solved with variable wall conductivity conditions given in Equations (3.9) and (3.12), respectively. The DBEM and DRBEM solutions with the fundamental solutions of the convection-diffusion and the modified Helmholtz equations will be given for several values of λ at a fixed $\beta = \dfrac{\pi}{2}$ in order to see the pure effect of wall conductivity on the solution.

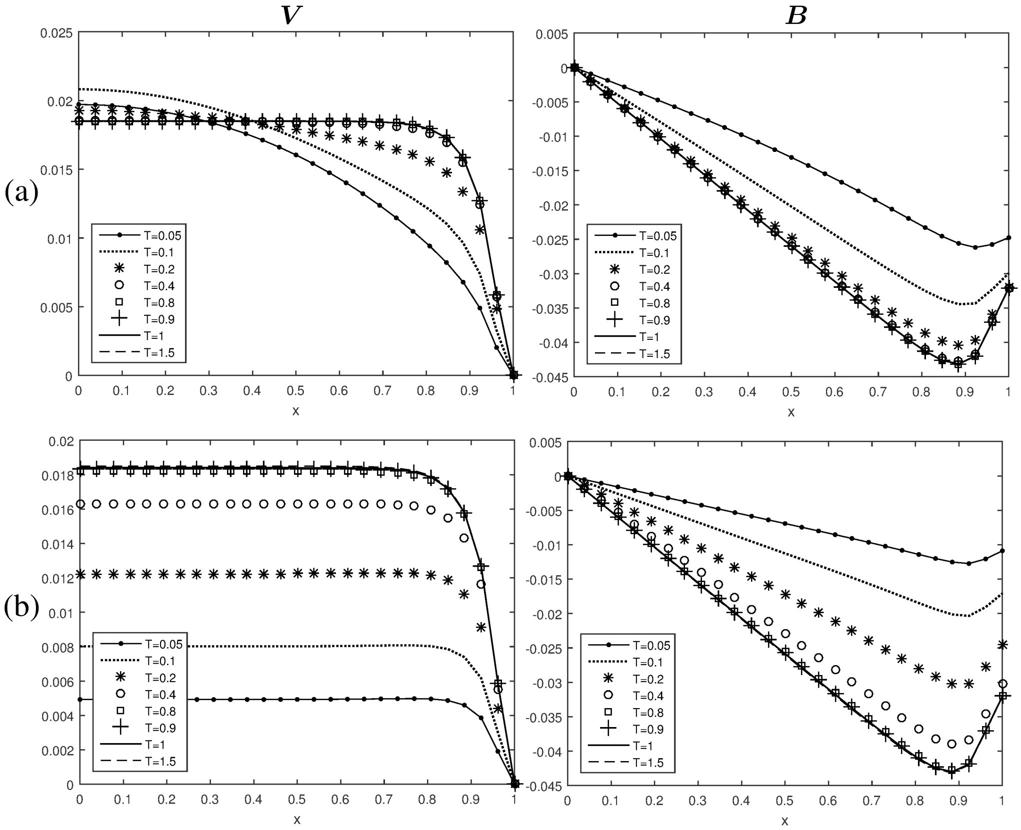

Figure 3.14: Velocity and induced magnetic field along horizontal centerline $y = 0$ at increasing time levels by DBEM with the fundamental solution of (a) CD and (b) mH equations: $M = 20$, $\lambda = 10$, $\beta = \frac{\pi}{2}$.

The velocity and induced magnetic field obtained from the application of DBEM with fundamental solutions of convection-diffusion and modified Helmholtz equations along the horizontal centerline ($y = 0$, $0 \leq x \leq 1$) at $M = 20$, $\lambda = 10$, $\beta = \dfrac{\pi}{2}$ are displayed in Figure 3.14 at increasing time levels $(0.05 \leq T \leq 1.5)$ in order to see when the steady-state is reached. It is noticed that after $T \approx 0.9$, the values of velocity and induced magnetic field are not changing significantly, which indicates that the steady-state is reached for both of the cases. The results of $T \approx 0.9$ are also confirmed by the behavior of equivelocity and current lines drawn in Figure 3.15 for the same fundamental solution cases. Thus, in all the subsequent computations the steady-state is taken as $T = 1$.

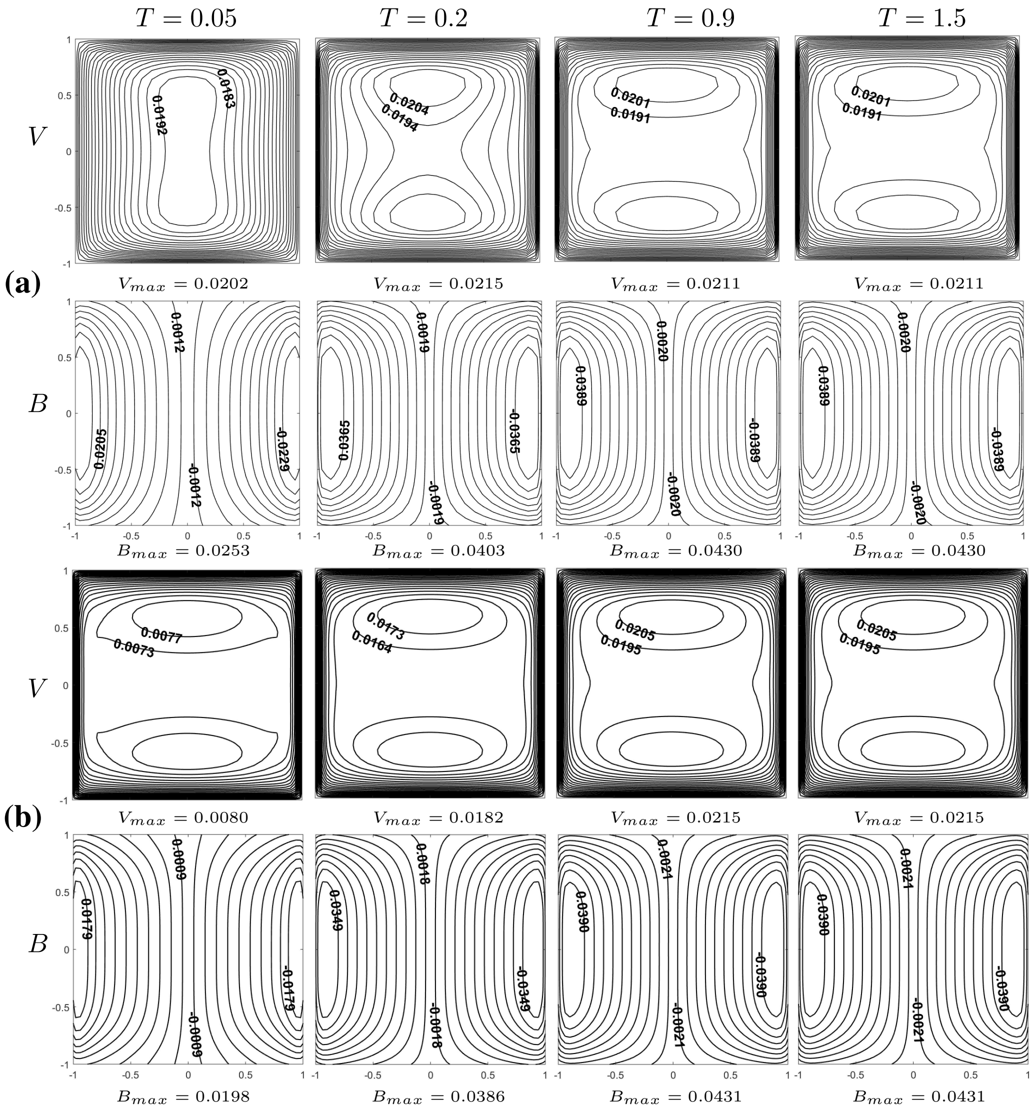

Figure 3.15: Time evolutions of velocity and induced current by DBEM with the fundamental solution of (a) CD and (b) mH equations: $M = 20$, $\lambda = 10$, $\beta = \frac{\pi}{2}$.

The effect of the wall conductivity parameter $\lambda(= 0, 10, 100)$ is displayed at $M = 20$, $\beta = \dfrac{\pi}{2}$ in terms of equivelocity lines in Figure 3.16 and current lines in Figure 3.17, respectively. The current lines are perpendicular to the horizontal walls $y = \mp 1$ in the case of perfectly conducting duct walls ($\lambda = 0$). As λ increases they circulate forming two oppositely signed vortices symmetrically along the vertical centerline and behave as if the solution of the MHD flow with insulated walls ($\lambda \to \infty$). On the other hand, from the equivelocity lines, we observe that the flow has the circular behavior at the center of the duct and separated symmetrically about the horizontal centerline $y = 0$ in the case of perfectly conducting duct walls ($\lambda = 0$). As λ increases, the vortices disappear gradually and we obtain the behavior of the solution of MHD flow with insulated walls ($\lambda \to \infty$: see Figure 3.8 at $T = 1$). As in the previous cases, DBEM enables one to obtain similar results by the use of different fundamental solutions while DRBEM fails to obtain accurate results by the use of the fundamental solution of mH equation. Therefore, in Figures 3.16 and 3.17 the DRBEM results are only given for the case in which the fundamental solution of CD equation is used.

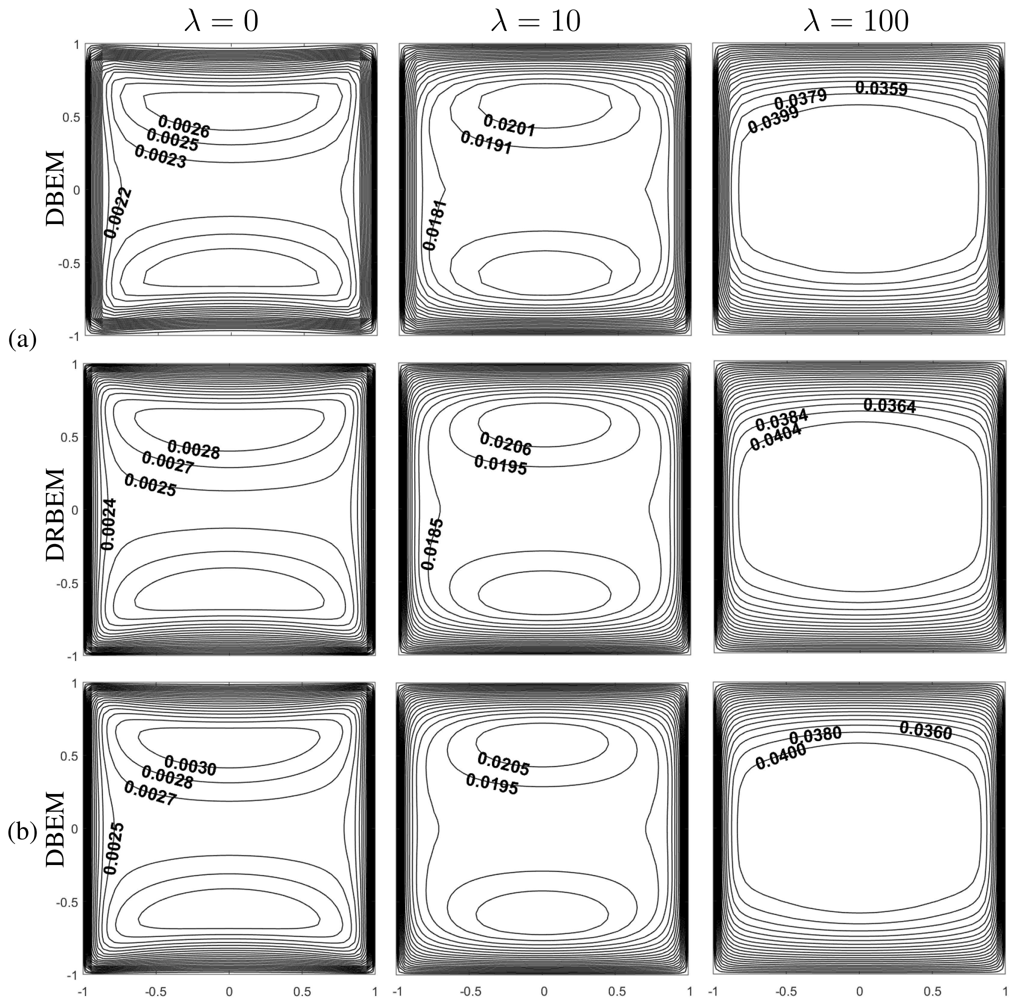

Figure 3.16: Effect of λ on the velocity obtained by DBEM and DRBEM with the fundamental solution of (a) CD and (b) mH equations: $\lambda = 0, 10, 100$, $M = 20$, $\beta = \frac{\pi}{2}$, $T = 1$.

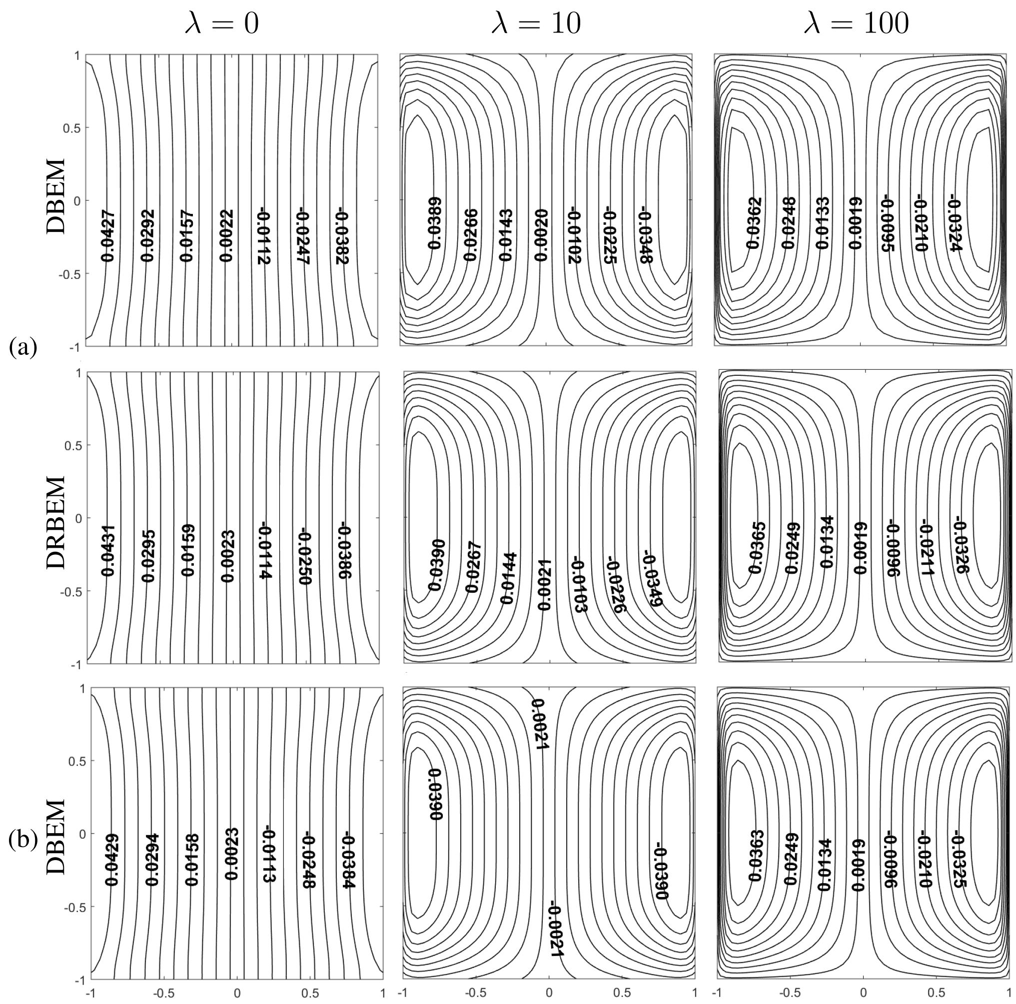

Figure 3.17: Effect of λ on the induced current obtained by DBEM and DRBEM with the fundamental solution of (a) CD and (b) mH equations: $\lambda = 0, 10, 100$, $M = 20$, $\beta = \frac{\pi}{2}$, $T = 1$.

A comparison between DBEM and DRBEM with the fundamental solutions of CD is also displayed in terms of equivelocity lines in Figure 3.18 and current lines in Figure 3.19, respectively, for several values of M at a fix $\lambda = 10$ and $\beta = \dfrac{\pi}{2}$. The DBEM solution with the fundamental solution of modified Helmholtz equation is also included in terms of equivelocity and current lines in Figure 3.18 and Figure 3.19, respectively. One can notice that DBEM is more efficient for higher values of M (up to $M = 150$) than DRBEM (up to $M = 20$), when the fundamental solution of convection-diffusion equation is applied. On the other hand, with the use of fundamental solution of mH equation, DBEM gives results for only smaller values of M (up to $M = 20$) while DRBEM fails to give reasonably well results even for small values of M. It is observed that as M increases, the flow is separated symmetrically in the y-direction as a result of both the variable conductivity ($\lambda = 10$) and the direction of the applied magnetic field ($\beta = \dfrac{\pi}{2}$). Moreover, with an increase in M the separation is more pronounced and the fluid becomes stagnant at the center of the duct while boundary layers are formed close to the horizontal walls. On the other hand, the boundary layers observed along the vertical walls when $\lambda \to \infty$ (see Figure 3.9) in current lines disappear with the conducting walls. Moreover, the vortices occurred in the current line profiles extend vertically becoming dense at the corners of horizontal walls.

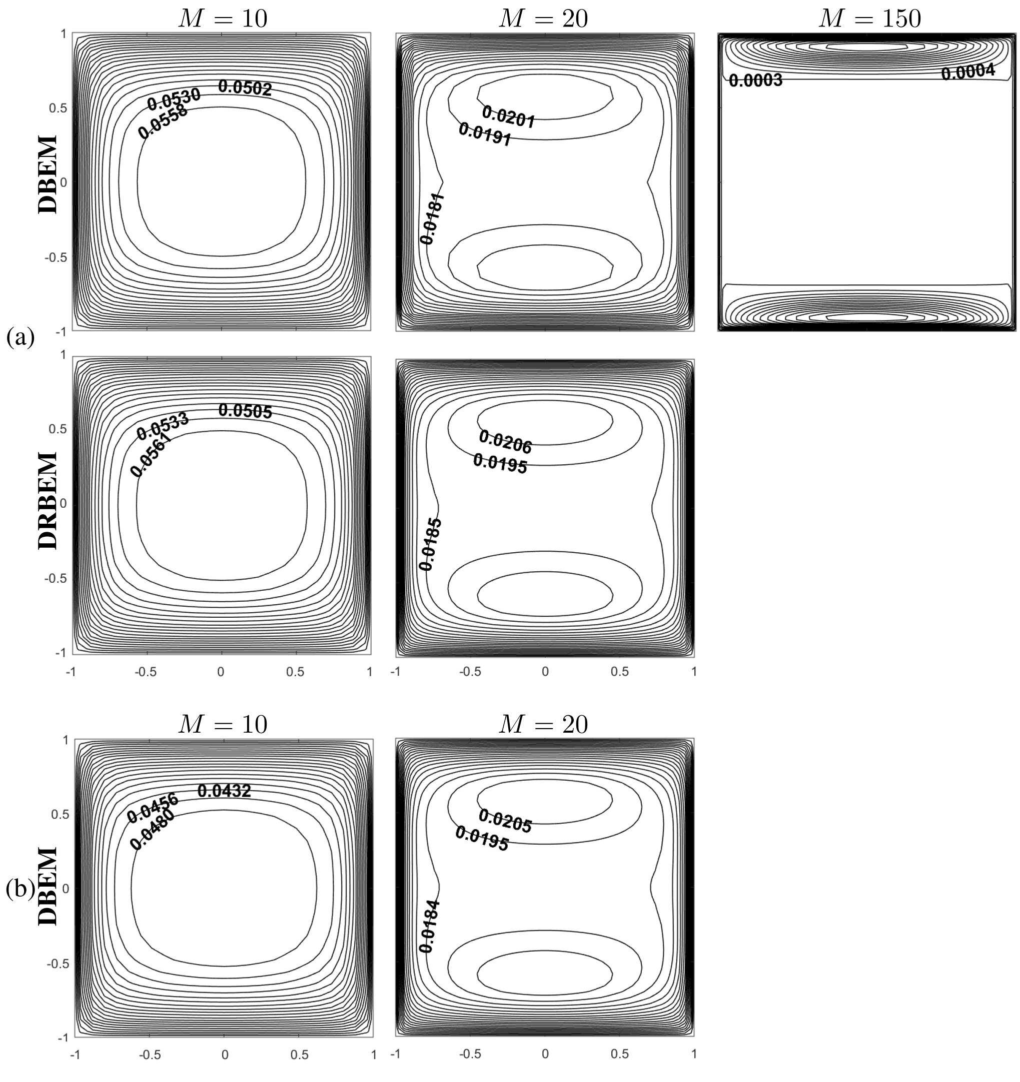

Figure 3.18: Effect of M on the velocity obtained by DBEM and DRBEM with the fundamental solution of (a) CD and (b) mH equations: $M = 10, 20, 150$, $\lambda = 10$, $\beta = \frac{\pi}{2}$, $T = 1$.

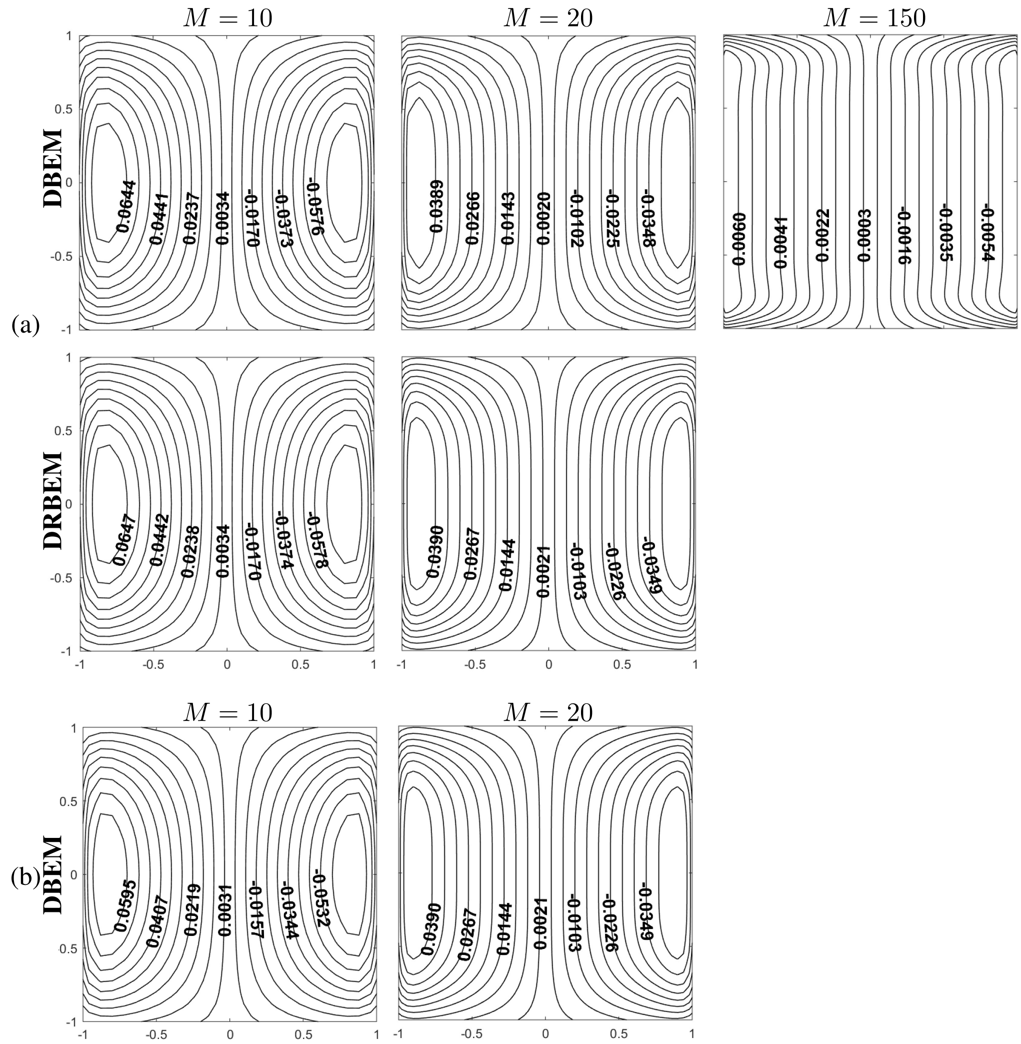

Figure 3.19: Effect of M on the induced current obtained by DBEM and DRBEM with the fundamental solution of (a) CD and (b) mH equations: $M = 10, 20, 150$, $\lambda = 10$, $\beta = \frac{\pi}{2}$, $T = 1$.

To summarize, the numerical results reveal that, MHD flow in a rectangular duct with insulated and/or variably conducting walls under an oblique external magnetic field, can be solved with DBEM to a good accuracy for high values of Hartmann number. In addition, there is no significant difference observed in the results between the use of the fundamental solution of CD or mH equations. On the other hand, DRBEM gives reasonably well results for rather small values of Hartmann number observing that the use of fundamental solution of CD equation is better than employing the fundamental solution of mH equation in the sense of increasing Hartmann number.

3.2.2.2 MHD Flow in an Irregular Duct with a Perturbed Wall

In this section, MHD flow is solved numerically in an irregular duct with a perturbed upper wall in order to analyze the effect of computational domain on the behavior of velocity and induced magnetic field. The unsteady MHD duct flow subject to a uniform vertically applied external magnetic field (i.e. taking $\beta = 0$, $M_x = 0$ and $M_y = M$ in Equation (3.5)) is considered. Thus, the governing equations become

$$\left.\begin{aligned} \nabla^2 V + M\frac{\partial B}{\partial y} &= -1 + \frac{\partial V}{\partial t} \\ \nabla^2 B + M\frac{\partial V}{\partial y} &= \frac{\partial B}{\partial t} \end{aligned}\right\} \quad \text{in} \quad \Omega \tag{3.44}$$

with the no-slip velocity boundary conditions $V = 0$ on Γ. The side walls (which are parallel to the applied magnetic field) are taken to be insulated $(B = 0)$, while the Hartmann walls (which are perpendicular to the applied magnetic field) are perfectly conducting ($\frac{\partial B}{\partial n} = 0$). The upper wall of the duct is perturbed as shown in Figure 3.20, [45]. Thus, the duct Ω is defined as

$$\Omega = \{(x, y) \in \mathbb{R}^2 : -c < x < c, -1 < y < 1 - \xi f(x)\} \tag{3.45}$$

where ξ is the perturbation parameter arbitrarily small ($0 < \xi \ll 1$), while f is assumed to be an arbitrary smooth perturbation function and c is a constant.

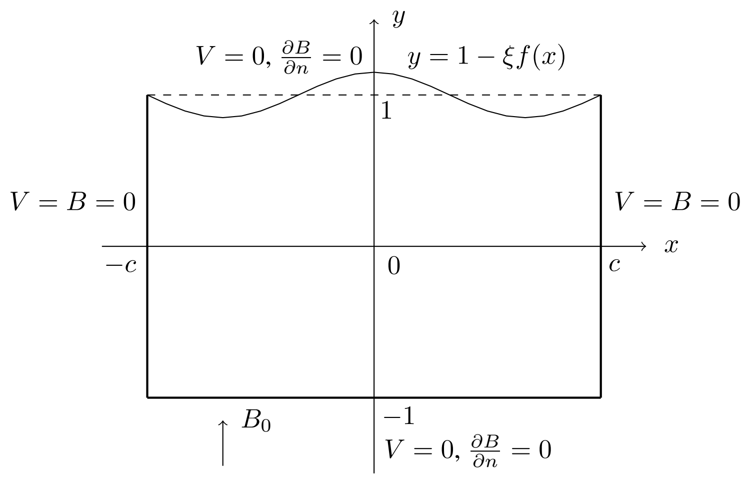

Figure 3.20: Cross-section of a perturbed duct with boundary conditions

The present techniques DBEM and DRBEM are employed for the discretization of Equation (3.44) in either CD form given in Equation (3.7) or mH form as in Equation

(3.11) by taking $M_x = 0$ and $M_y = M$ with the corresponding boundary conditions. The main concentration will be on the use of DBEM with both of these fundamental solutions as a tool for the solution of the problem under consideration, since it is observed in previous Section 3.2.2.1 that the DBEM gives more accurate results compared to DRBEM for moderate and large values of Hartmann number.

First, the accuracy of the results obtained by DBEM either with the fundamental solution of modified Helmholtz or convection-diffusion equations is validated by comparing the obtained results with the ones given in the work [45] in terms of surface plots of velocity V and induced magnetic field B in Figure 3.21. In this test problem, the perturbation function is taken as $f = -\cos(\frac{\pi x}{4})$ for $\xi = 0.1$ and $M = 5$. The results are in well agreement with the results given in [45] (see Figure 14 and Figure 18 in [45]).

(a) Modified Helmholtz (b) Convection-Diffusion

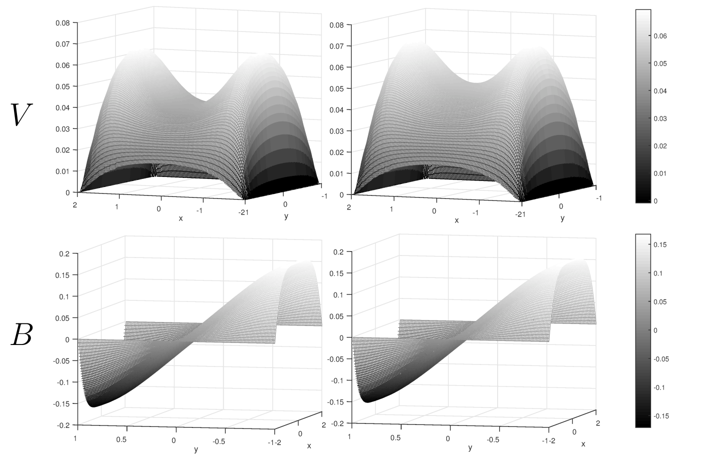

Figure 3.21: The level curves of velocity and induced current obtained by DBEM with the fundamental solution of (a) mH and (b) CD equations: $M = 5$, $\xi = 0.1$, $f = -\cos(\frac{\pi x}{4})$, $T = 1$.

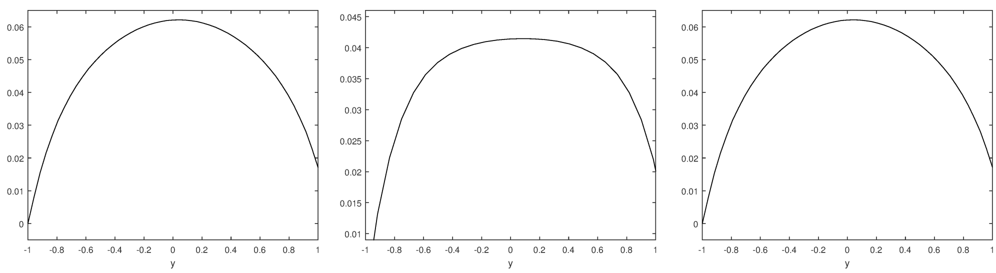

Figure 3.22: Velocity profile along the vertical lines $x = -1.0$ (left), $x = 0$ (middle) and $x = 1.0$ (right).

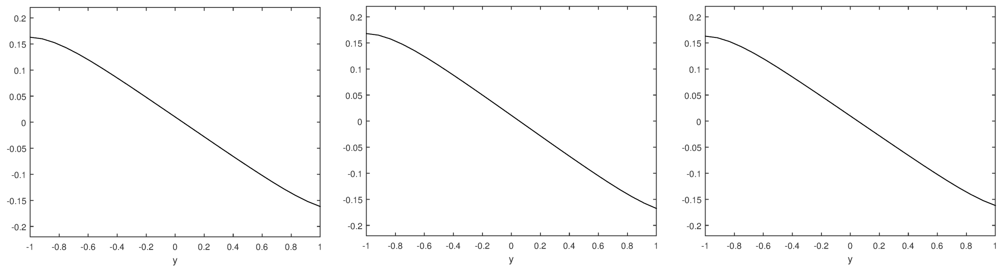

Figure 3.23: Induced magnetic field profile along the vertical lines $x = -1.0$ (left), $x = 0$ (middle) and $x = 1.0$ (right).

Furthermore, for the same test problem the variations of the velocity and the induced magnetic field along the vertical lines $x = \mp 1.0, 0$ are drawn in Figure 3.22 and Figure 3.23, respectively. The agreement of the present results with the ones given in [45] (see Figures 12,13,16,17 in [45]) is also well observed.

In the rest of the present section, we will focus on the effect of the perturbation function f $(= -\cos(\frac{2\pi x}{3}))$ with several perturbation parameters $\xi (= 0, 0.1, 0.3, 0.5)$ and Hartmann numbers ($5 \leq M \leq 150$) on the flow and the induced magnetic field. In order to determine, when the solution reaches to the steady-state, the velocity and induced magnetic field are drawn along the horizontal centerline ($y = 0$, $0 \leq x \leq 2$) in Figure 3.24 for $M = 30$ and $\xi = 0$ at several time levels ($0.05 \leq T \leq 1$) with straight walls by DBEM. It is clear that, after $T \geq 0.4$ the steady-state is reached for both the velocity and induced magnetic field.

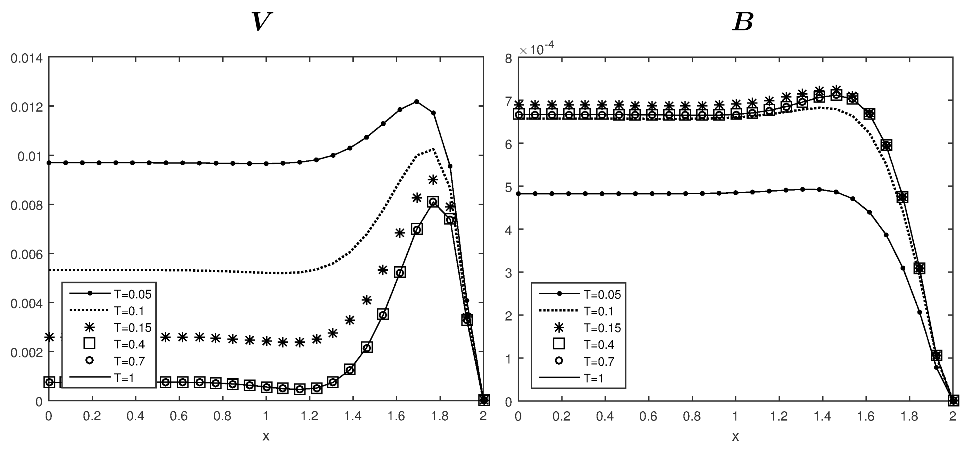

Figure 3.24: Velocity and induced magnetic field along horizontal centerline $y = 0$ at transient levels by DBEM with the fundamental solution of CD equation: $M = 30$, $\xi = 0$.

Further, the DBEM solutions with the fundamental solution of convection-diffusion equation are illustrated in Figure 3.25 for transient levels $T = 0.05, 0.1, 0.4, 1$ when $M = 30$, $f = -\cos(\frac{2\pi x}{3})$ and $\xi = 0.1$. It can also be seen from Figure 3.25 that the solution reaches steady-state when $T \geq 0.4$ which is compatible with centerline plots in Figure 3.24. Thus, all the subsequent graphs are drawn at $T = 1$ (as in the previous Section 3.2.2.1) which was also the steady-state for the MHD flow in a duct with straight walls.

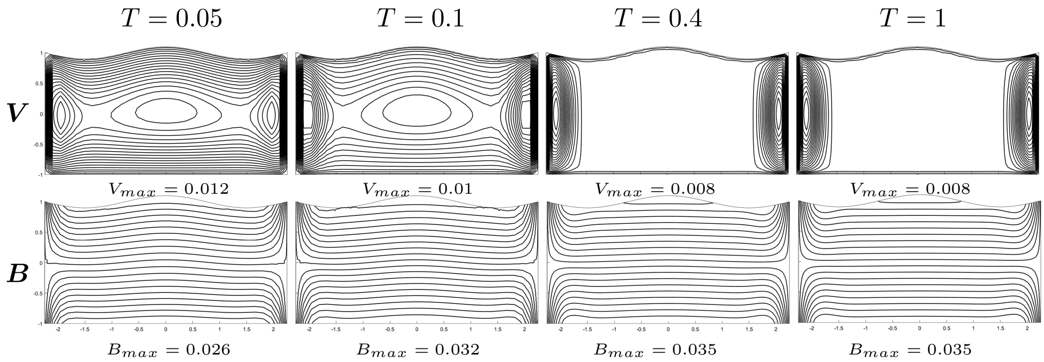

Figure 3.25: Time evolutions of velocity and induced current by DBEM with the fundamental solution of CD equation: $M = 30$, $f = -\cos(\frac{2\pi x}{3})$, $\xi = 0.1$.

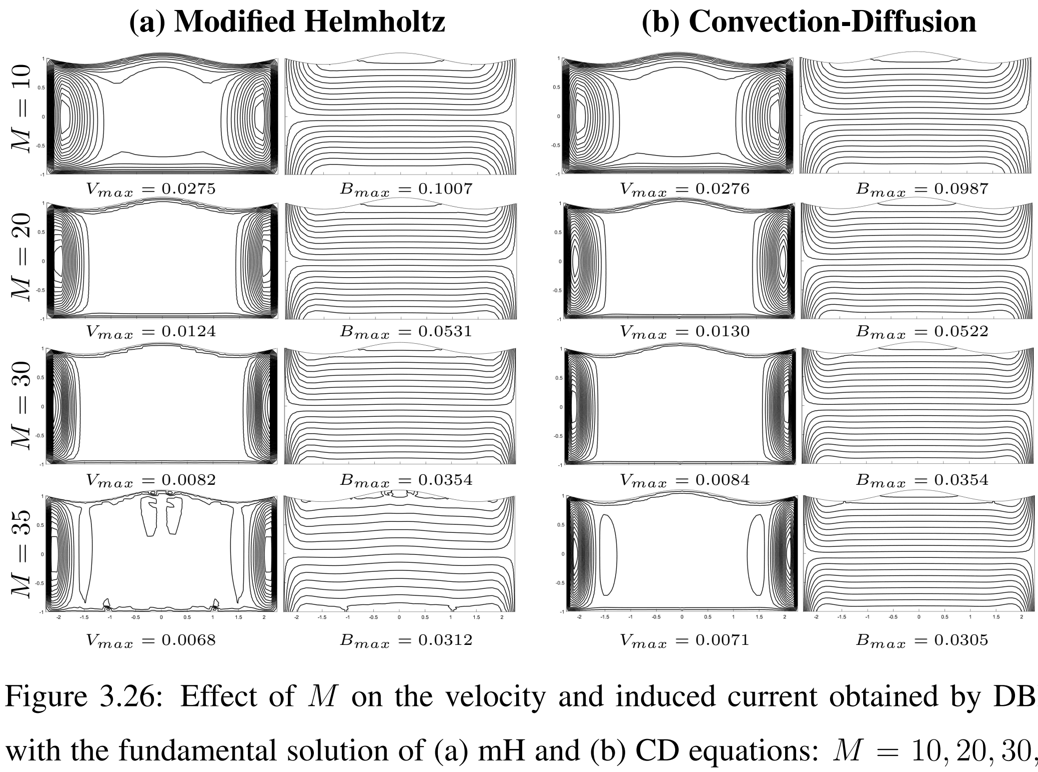

Figure 3.26: Effect of M on the velocity and induced current obtained by DBEM with the fundamental solution of (a) mH and (b) CD equations: $M = 10, 20, 30, 35$, $f = -\cos(\frac{2\pi x}{3})$, $\xi = 0.1$, $T = 1$.

First, the effect of the use of different fundamental solutions in the application of DBEM on the velocity and induced magnetic field is depicted in Figure 3.26 for M=10, 20, 30, 35 by taking $f = -\cos(\frac{2\pi x}{3})$ and $\xi = 0.1$. When $M \leq 30$, both of the fundamental solutions provide the same results with a good accuracy. However, when $M > 30$ DBEM with the fundamental solution of modified Helmholtz equation has difficulties in giving accurate results and some disruptions occur along the perturbed wall while the use of the fundamental solution of convection-diffusion results in acceptable results. Thus, the subsequent computations are performed by using DBEM with the fundamental solution of convection-diffusion equation.

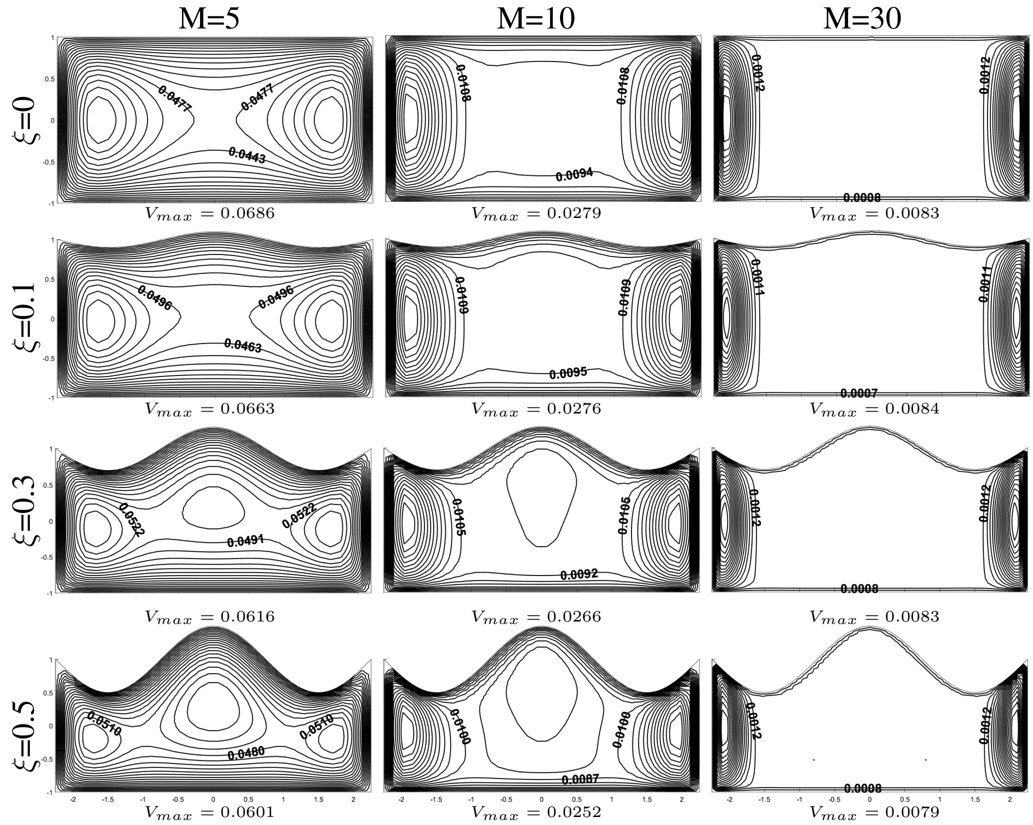

Figure 3.27: Effect of ξ on the velocity obtained by DBEM with the fundamental solution of CD equation: $\xi = 0, 0.1, 0.3, 0.5$, $M = 5, 10, 30$, $f = -\cos(\frac{2\pi x}{3})$, $T = 1$.

The effect of the perturbation parameter ξ on the velocity and the induced magnetic field is displayed, respectively, in Figures 3.27 and 3.28. It is seen that the magnitude of the induced magnetic field increases with an increase in ξ, whereas there is a decrease in the velocity when M=5, 10. When $M = 30$ the increase rate in the magnitude of induced magnetic field becomes very small compared to the cases when $M = 5, 10$; and there is almost no change in the velocity. Moreover, the fluid flows in terms of two eddies close to the side walls. It is well observed that at small values of Hartmann number ($M = 5, 10$) an additional vortex is formed at the center of the cavity and this vortex moves upwards due to the expansion of the computational domain with an increase in ξ. A further increase in Hartmann number results in a retardation in the fluid flow at the center of the cavity and the fluid flows completely in terms of two side layers weakening the effect of the perturbation. On the other hand, current lines fill the region due to the perturbed upper boundary obeying its boundary conditions, and start to form side layers as M increases.

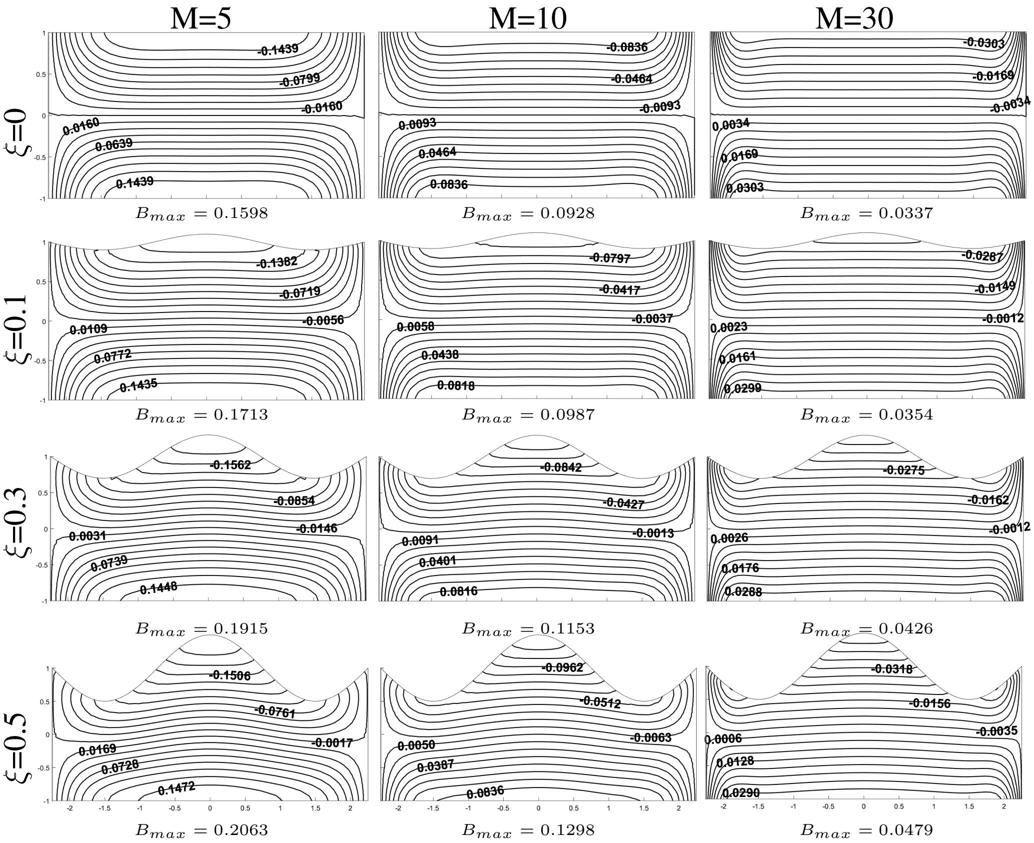

Figure 3.28: Effect of ξ on the induced current obtained by DBEM with the fundamental solution of CD equation: $\xi = 0, 0.1, 0.3, 0.5$, $M = 5, 10, 30$, $f = -\cos(\frac{2\pi x}{3})$, $T = 1$.

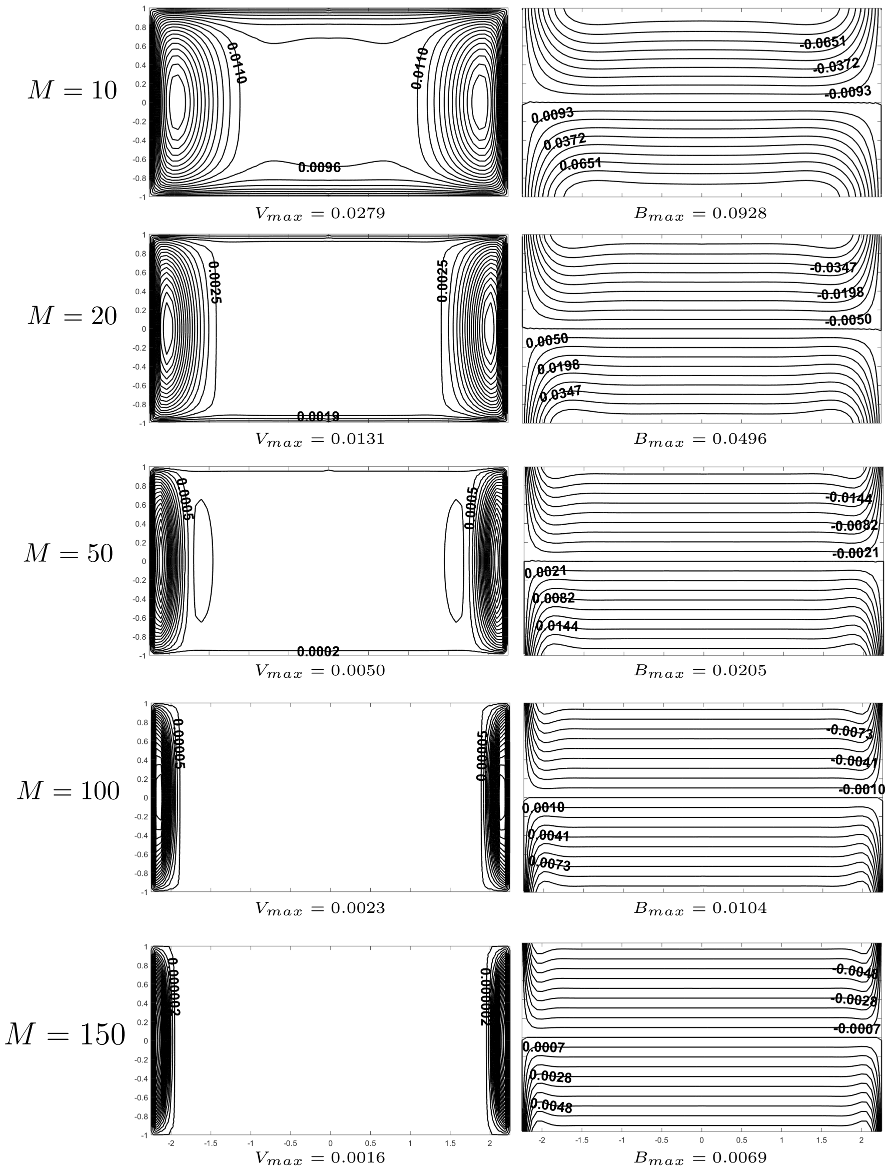

Figure 3.29: Effect of M on the velocity and induced current in a rectangular duct with straight walls obtained by DBEM with the fundamental solution of CD equation: $M = 10, 20, 50, 100, 150$, $T = 1$.

Further, the effect of the Hartmann number on the velocity and the induced magnetic field is presented in Figure 3.29 for a rectangular duct with straight walls and in Figure 3.30 for a duct with perturbed upper wall ($f = -\cos(\frac{2\pi x}{3})$), respectively. It is observed that, for straight or perturbed upper wall cases, as M increases the flow is separated into two vortices near the side walls, the velocity drops and the fluid becomes stagnant at the center of the duct. Moreover, boundary layer formation is observed on the insulating parts of the boundary for both the velocity and the induced magnetic field as M increases. As Hartmann number increases to $M = 50$, Hartmann layers are developed for the equivelocity lines, however, with a further increase in M to 150 the Hartmann layers are weakened and finally vanish. Moreover, the induced

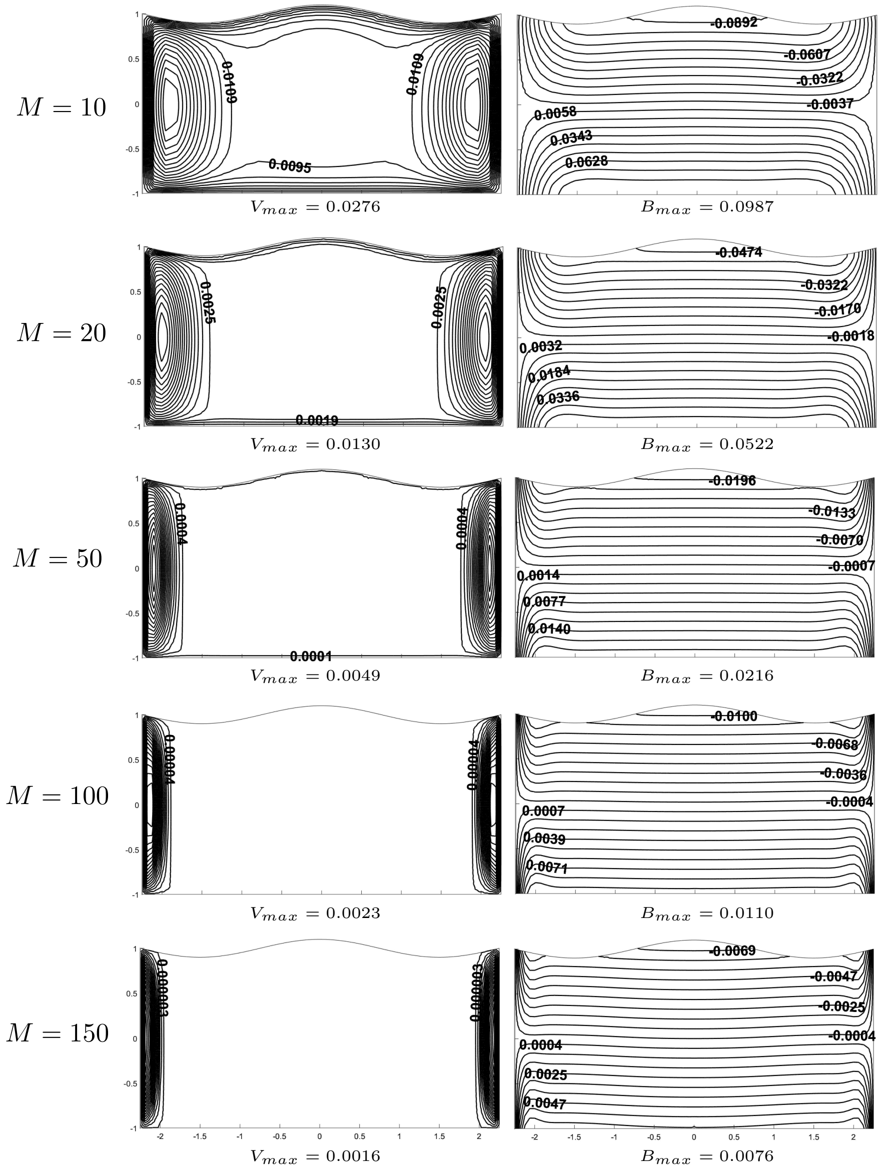

Figure 3.30: Effect of M on the velocity and induced current in a rectangular duct with perturbed upper wall obtained by DBEM with the fundamental solution of CD equation: $M = 10, 20, 50, 100, 150$, $f = -\cos(\frac{2\pi x}{3})$, $\xi = 0.1$, $T = 1$.

magnetic field is antisymmetric with respect to x-axis and the current lines are perpendicular to the conducting walls as expected. The magnitude of the induced magnetic field increases for each Hartmann number when the upper wall of the duct is perturbed. On the other hand, a decrease in the velocity is well-observed for moderate values of $M(\leq 50)$ in the perturbed duct when compared to the velocity in the duct with regular straight walls. This velocity drop is not seen for Hartmann number values $M > 50$ since the flattening flow is the dominating case as M increases.

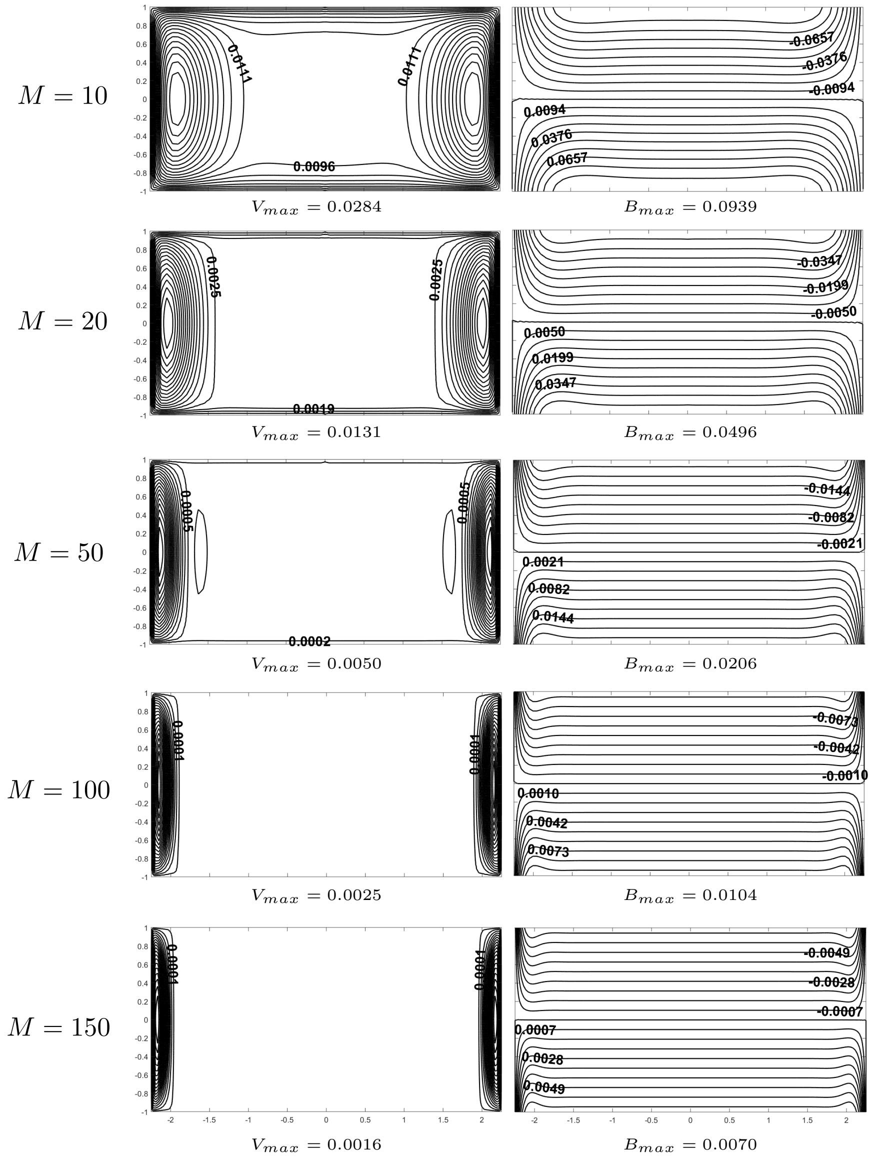

Figure 3.31: Effect of M on the velocity and induced current in a rectangular duct with straight walls obtained by DRBEM with the fundamental solution of CD equation: $M = 10, 20, 50, 100, 150$, $T = 1$.

In addition, DRBEM is also employed to solve the unsteady MHD flow with perturbed boundary by using the fundamental solution of convection-diffusion equation. As mentioned before, the previous Section (3.2.2.1) shows that the DRBEM with the fundamental solution of modified Helmholtz equation performs poorly in all cases, and hence, in DRBEM the numerical simulations are performed only with the fundamental solution of convection-diffusion equation. The results are obtained for several values of Hartmann number, and are presented in Figure 3.31 and Figure 3.32, for rectangular duct with straight walls and with a perturbed upper wall, respectively. The results are almost the same with the DBEM results for straight and perturbed upper wall with $f = -\cos(\frac{2\pi x}{3})$ and $\xi = 0.1$. Maximum 1200 boundary elements are used in DRBEM for highest value of Hartmann number, while 500 boundary elements are taken in DBEM. Thus, DRBEM is in need of using more boundary elements than the DBEM to achieve accurate results. This indicates that the DRBEM is computationally less efficient than DBEM as Hartmann number increases.

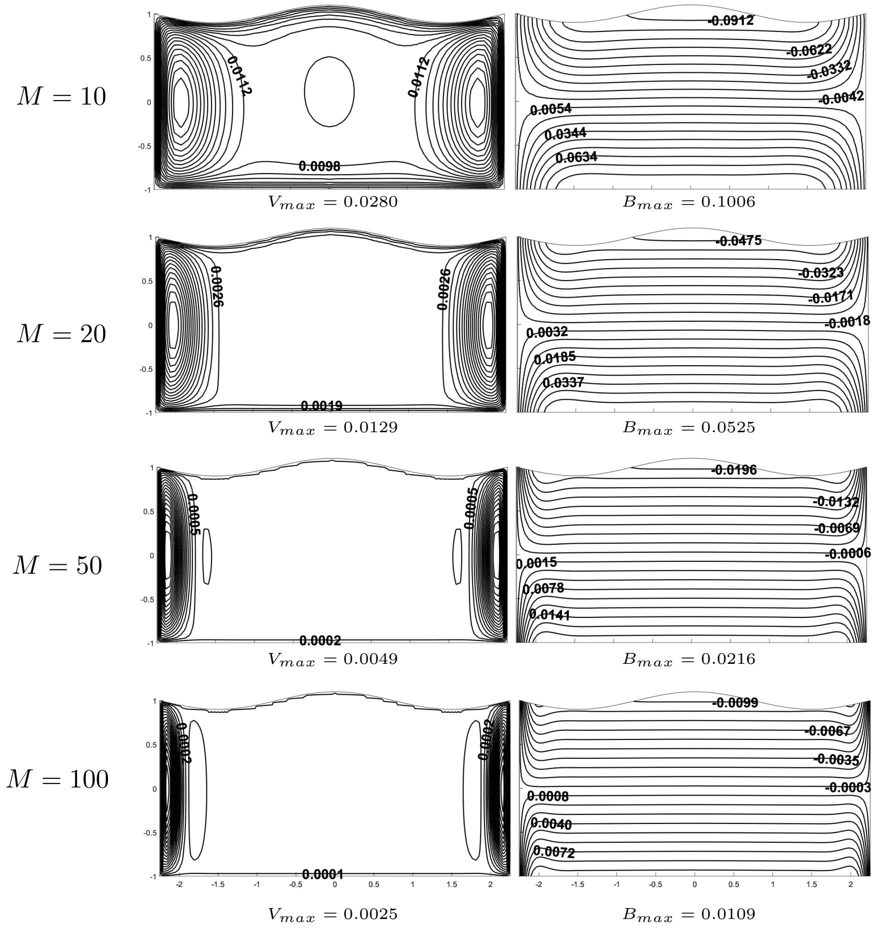

Figure 3.32: Effect of M on the velocity and induced current in a rectangular duct with perturbed upper wall obtained by DRBEM with the fundamental solution of CD equation: $M = 10, 20, 50, 100$, $f = -\cos(\frac{2\pi x}{3})$, $\xi = 0.1$, $T = 1$.

Finally, we obtain the solution of MHD duct flow in duct with a different shape of upper boundary which is determined by the perturbation function f. We consider basically two different shapes of upper wall, that is either concave down or concave up around vertical centerline of the duct. Figure 3.33 shows that the flow is divided into two vortices forming side layers and becoming stagnant at the center when the upper curve boundary is concave down at its middle part (for $f = -\cos(\frac{\pi x}{4})$ and $f = -\cos(\frac{2\pi x}{3})$). On the other hand when the curved boundary is concave up (i.e. $f = \cos(2\pi(1-x^2))$ and $f = \sin(2\pi(1-x^2))$) at the middle part, the flow covers almost all the duct and the side layer formation is retarded. However, the induced magnetic field profiles are not altered much in both cases.

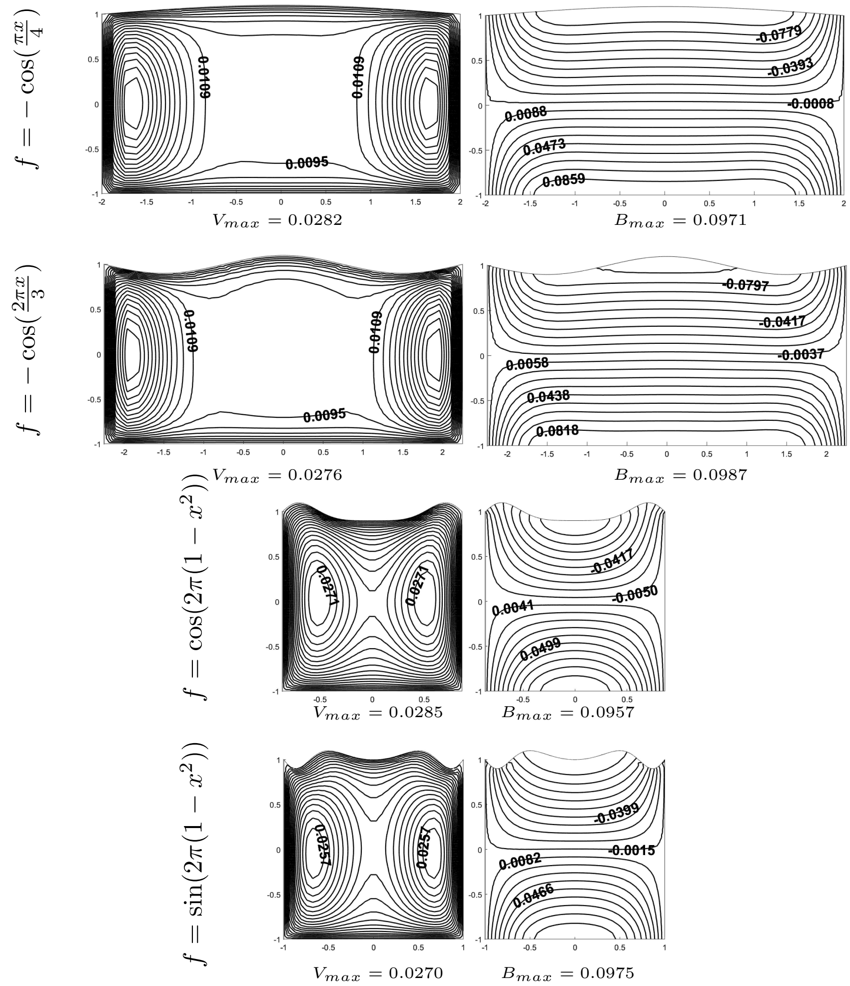

Figure 3.33: Effect of perturbation function f on the velocity and induced current in a rectangular duct with perturbed upper wall obtained by DBEM with the fundamental solution of CD equation: $M = 10, \xi = 0.1, T = 1$.

3.3 Summary of the Obtained Results in Chapter 3

In this chapter, the CDR type equations are solved numerically by using DBEM and DRBEM approaches which employ basically either the fundamental solution of CD or mH equations. The results obtained for two test problems, namely concentration and MHD duct flow problems, are visualized in terms of qualitative comparison between the use of fundamental solutions of CD and mH equations. It is found that:

- For the CDR equation (concentration problem), the fundamental solution of CDR equation with both DRBEM and DBEM gives results with good accuracy while the fundamental solution of mH equation gives reasonably well results with only DBEM in the sense of decreasing diffusion parameter which makes the system convection dominated.
- Similarly, for the second test problem (namely, MHD duct flow), the DBEM results are almost invariant to the use of fundamental solution of either CD or mH equations, especially in the case of duct with straight walls, while DRBEM with the fundamental solution of CD equation gives reasonably well results for increasing values of M, β and λ. Moreover, in some cases (i.e. for the MHD flow in a duct with variably conducting walls), DRBEM with the fundamental solution of mH equation fails to obtain results even for small values of M.
- At small values of $M(= 5, 10)$, in a perturbed duct the velocity drops while the magnitude of induced magnetic field increases when compared to the case in ducts with straight walls. The effect of perturbation on the flow and magnetic field is weakened for higher values of $M(\geq 30)$. On the other hand, current lines fill the region due to the perturbed upper boundary obeying its boundary conditions, and start to form side layers as M increases.
- The well-known physical characteristics of MHD flow , namely flattening tendency of the flow and the formation of boundary layers for both the velocity and induced current as M increases, are well-captured by both DBEM and DRBEM especially with the fundamental solution of CD equation.

CHAPTER 4

NUMERICAL SOLUTION OF TIME-DEPENDENT CONVECTION-DIFFUSION TYPE EQUATION WITH VARIABLE COEFFICIENTS

In this chapter we deal with the time-dependent convection-diffusion type equations with variable coefficients. The main difference from Chapter 3 is that the coefficients of the convection terms vary with respect to either only space variables or containing the unknown as well. That is, in the present chapter we consider the general time-dependent CDR equation given in Equation (3.1) which is reduced to

$$\frac{\partial u}{\partial t} - \varepsilon \nabla^2 u + \vec{a} \cdot \nabla u = h \tag{4.1}$$

with no reaction term (i.e. $\sigma = 0$) under suitable boundary conditions. Moreover, the coefficients of convection terms, $\vec{a}$, are not just constants but they are functions of space variables, unknown u and/or its spatial derivatives (i.e. $\vec{a} = (a_1(x, y, u, u_x, u_y), a_2(x, y, u, u_x, u_y)))$.

First, the applications of DBEM and DRBEM to Equation (4.1) with the fundamental solution of CD equation is explained in Section 4.1 giving attention basically on the differences encountered through the numerical procedures due to the variable convection terms. Then, the numerical results obtained for the problems governed by Equation (4.1) are given in Section 4.2 with some discussions. In this respect, we first consider the two-dimensional time-dependent heat conduction problem governed by Equation (4.1) with coefficients of convection terms depending on space variables only in Section 4.2.1. Then, the investigation is extended for the problems which are governed by Equation (4.1) with coefficients of convection terms depending on not only the space variables but also the unknown itself in Section 4.2.2. In this section, we consider some fluid dynamics problems which are mainly governed by the Navier-Stokes (NS) equations. Due to the nonlinearity of these equations, the analytical solution is not available. Thus, it is inevitable to employ some numerical techniques for the solution of the NS equations. We use the DBEM and DRBEM with the fundamental solution of CD equation to discretize the NS equations in different computational domains under various boundary conditions. Specifically, we first consider the unsteady NS equations in a square cavity for which the analytical solution is available in order to validate our computer codes in Section 4.2.2.1. Then, the lid-driven cavity flow of which the top-lid is moving with a constant velocity and the natural convection flow which is governed by the NS equation combined with the energy equation are considered in Section 4.2.2.2 and Section 4.2.2.3, respectively. Further, in Section 4.2.2.4, the pressure driven fluid flow in a channel between the two parallel plates is solved by DBEM. Finally, the MHD natural convection flow under the effect of an externally applied magnetic field is investigated in a square cavity filled with a porous medium in Section 4.2.2.5.

4.1 Applications of DRBEM and DBEM to CD Equation with Variable Coefficients

In Chapter 3, the applications of DRBEM and DBEM to the unsteady CDR equation with constant coefficients by using the fundamental solution of CD equation have been given. The present section is devoted to point out briefly the crucial steps which indicate the differences from Section 3.1 in the applications of DBEM and DRBEM to the CD type equations due to the variable coefficients. Thus, when Equation (4.1) is weighted by the fundamental solution u^* of the CD equation

$$u^* = \frac{1}{2\pi\varepsilon}\exp(-\frac{a_1 r_x + a_2 r_y}{2\varepsilon})K_0(sr) \tag{4.2}$$

where $s = \sqrt{\frac{a_1^2+a_2^2}{4\varepsilon^2}}$, one can obtain the following integral equation (as given in Equation (3.15))

$$c_i u_i + \varepsilon\int_\Gamma q^* u d\Gamma - \varepsilon\int_\Gamma u^*\frac{\partial u}{\partial n}d\Gamma + \int_\Gamma (a_1 u^* n_x u + a_2 u^* n_y u)d\Gamma = -\int_\Omega b u^* d\Omega \tag{4.3}$$

after applying Green's second identity two times.

In Equation (4.3), b represents the leftover terms in Equation (4.1) except the CD operator, due to the employed fundamental solution u^*.

4.1.1 DRBEM formulation

In DRBEM application, the domain integral on the right hand side of Equation (4.3) is transformed into the equivalent boundary integral by means of radial basis functions f_j as follows (see Equation (3.19) in Section 3.1.1)

$$
\begin{aligned}
c_i u_i + \varepsilon \int_\Gamma q^* u d\Gamma - \varepsilon \int_\Gamma u^* \frac{\partial u}{\partial n} d\Gamma + \int_\Gamma (a_1 u^* n_x u + a_2 u^* n_y u) d\Gamma \qquad (4.4) \\
= \sum_{j=1}^{N+L} \alpha_j(t) (c_i u_{ji} + \varepsilon \int_\Gamma q^* \hat{u} d\Gamma - \varepsilon \int_\Gamma u^* \frac{\partial \hat{u}}{\partial n} d\Gamma + \int_\Gamma (a_1 u^* n_x \hat{u} + a_2 u^* n_y \hat{u}) d\Gamma).
\end{aligned}
$$

It is important to note here that, the fundamental solution u^* and its normal derivative q^* contain the variable coefficients a_1 and a_2 which are functions of x, y and/or u, u_x, u_y. However, when the boundary is discretized using constant elements, in each source point $i(= (x_i, y_i))$, these coefficients can be taken as constants when a_1 and a_2 are functions of space variables only, that is,

$$a_1 = a_1(x_i, y_i), \qquad a_2 = a_2(x_i, y_i). \qquad (4.5)$$

On the other hand, when they also depend on the unknown u, Equation (4.1) becomes nonlinear and an iterative scheme should be employed for the solution. Since Equation (4.1) is time-dependent, the iterative process is performed through the time integration denoted by m. Thus, to obtain the solution u at the $(m+1)$-st time level t_{m+1}, we use the values of u at the m-th time level t_m to remove the nonlinearity in Equation (4.1) due to the variable coefficients of convection terms. That is, a_1 and a_2 are evaluated as

$$
\begin{aligned}
a_1 &= a_1^{(m)}(x_i, y_i, u^{(m)}(x_i, y_i, t_m), u_x^{(m)}(x_i, y_i, t_m), u_y^{(m)}(x_i, y_i, t_m)), \qquad (4.6) \\
a_2 &= a_2^{(m)}(x_i, y_i, u^{(m)}(x_i, y_i, t_m), u_x^{(m)}(x_i, y_i, t_m), u_y^{(m)}(x_i, y_i, t_m)). \qquad (4.7)
\end{aligned}
$$

So, a_1 and a_2 again become constant at each node i and time level m. In this sense, Equation (4.4) is just reduced to Equation (3.19) which is its correspondence in Section 3.1.1. Therefore, after the discretization of time derivative by using the backward finite difference scheme (see Equation (2.51)), the matrix-vector form of the discretized DRBEM equation becomes

$$(H^{(m)} + \frac{C}{\Delta t}^{(m)}) u^{(m+1)} - G^{(m)} \frac{\partial u}{\partial n}^{(m+1)} = \frac{C}{\Delta t}^{(m)} u^{(m)} + C^{(m)} h^{(m)} \qquad (4.8)$$

as given in Equation (3.28). When the fundamental solution of CD equation is used, the components of $H^{(m)}$ and $G^{(m)}$ are

$$\begin{aligned} H_{ij} &= c_i\delta_{ij} - \frac{1}{2\pi}\int_{\Gamma_j} \exp(-\frac{a_1^{(m)}r_x + a_2^{(m)}r_y}{2\varepsilon}) \\ &\qquad \times[s^{(m)}K_1(s^{(m)}r)\frac{\partial r}{\partial n} - (\frac{a_1^{(m)}}{2\varepsilon}n_x + \frac{a_2^{(m)}}{2\varepsilon}n_y)K_0(s^{(m)}r)]d\Gamma_j, \end{aligned} \tag{4.9}$$

$$G_{ij} = \frac{1}{2\pi}\int_{\Gamma_j} \exp(-\frac{a_1^{(m)}r_x + a_2^{(m)}r_y}{2\varepsilon})K_0(s^{(m)}r)d\Gamma_j \tag{4.10}$$

and

$$H_{ii} \approx c_i + \frac{l}{2\pi}(\ln\frac{2}{l} - \ln\frac{s^{(m)}}{2} - \gamma + 1)(\frac{a_1^{(m)}n_x + a_2^{(m)}n_y}{2\varepsilon}), \tag{4.11}$$

$$G_{ii} \approx \frac{l}{2\pi}(\ln\frac{2}{l} - \ln\frac{s^{(m)}}{2} - \gamma + 1) \tag{4.12}$$

and $C^{(m)} = -(H^{(m)}\hat{U} - G^{(m)}\hat{Q})F^{-1}$. The coordinate matrix F is obtained by using the radial basis functions f_j [29]

$$f_j = \varepsilon(1 + r_j) - (\frac{1}{2} + \frac{r_j}{3})(a_1r_x + a_2r_y) \tag{4.13}$$

which are linked to the convection-diffusion equation

$$\varepsilon\nabla^2\hat{u}_j - a_1\frac{\partial\hat{u}_j}{\partial x} - a_2\frac{\partial\hat{u}_j}{\partial y} = f_j. \tag{4.14}$$

The corresponding particular solution and its normal derivative are taken as follows

$$\hat{u}_j = \frac{r_j^2}{4} + \frac{r_j^3}{9}, \qquad \hat{q}_j = (\frac{r_j}{2} + \frac{r_j^2}{3})\frac{\partial r}{\partial n}. \tag{4.15}$$

Here, matrices $\hat{U}$ and $\hat{Q}$ are obtained by taking each of the vectors $\hat{u}$ and $\hat{q}$ as columns, respectively. However, in Equation (4.8) the matrices H and G on the left hand side and the matrix C are changing at each iteration level when $\vec{a}$ is a function of u, and hence they are recalculated at each iteration. For that reason, we also put (m) on top of the matrices H, G and C as superscript. On the other hand, when $\vec{a}$ is a function of space variables, the matrices H and G are not changing at each iteration as in the case when the convection terms have constant coefficients.

To conclude, we use an initial guess for the unknown and for its space derivatives, i.e. $u^{(0)}$, $u_x^{(0)}$, $u_y^{(0)}$, to start the iterative process, and the coefficient $\vec{a}$ is computed at each node i as a constant. The iteration is terminated when a required time or a preassigned tolerance between two successive iteration is reached.

4.1.2 DBEM formulation

The variable coefficients a_1 and a_2 occurring in Equation (4.3) and in the fundamental solution (4.2), are also treated as explained in Section 4.1.1. The only difference in DBEM application is that the domain integrals on the right hand side of Equation (4.3) is preserved and calculated by using composite trapezoidal rule (see Section 2.2.1.1). When the constant elements are used for the discretization of the boundary and the backward finite difference scheme is employed for the time integration, the resulting DBEM matrix-vector equation becomes

$$(H^{(m)} + \frac{1}{\Delta t}M_1^{(m)})u^{(m+1)} - G^{(m)}\frac{\partial u}{\partial n}^{(m+1)} = \frac{1}{\Delta t}M_1^{(m)}u^{(m)} + M_2^{(m)} \tag{4.16}$$

as given in Equation (3.32). The matrices $H^{(m)}$ and $G^{(m)}$ are the same with the ones given in Section 4.1.1 and recalculated at each iteration. Similarly, the domain integrals $(M_1)_{ii}^{(m)} = \int_\Omega u^{*(m)} d\Omega$ and $(M_2)_i^{(m)} = \int_\Omega hu^{*(m)} d\Omega$, which also change at each time level, are calculated by using composite trapezoidal rule at each iteration when the convection term coefficients depend on the unknown u.

4.2 Numerical Results for the Time-dependent CD Equation with Variable Coefficients

The present section is devoted to the applications of DRBEM and DBEM to the CD type equations with variable coefficients. In Section 4.2.1, the time-dependent heat conduction problems which are governed by CD equation with variable coefficients containing only space variables, are solved to validate our numerical codes for DBEM and DRBEM, since their analytical solutions are available. Then, in Section 4.2.2 some fluid dynamics problems, which are governed mainly by the Navier-Stokes equations, are investigated again by the present numerical schemes. In these problems, the coefficients of the convection terms contain not only space variables but also the unknown function.

4.2.1 Two-Dimensional Heat Conduction Problems with Variable Coefficients

The unsteady 2-D heat conduction problem which is mathematically modelled as [69]

$$a(x,y)\nabla^2 u + a_x \frac{\partial u}{\partial x} + a_y \frac{\partial u}{\partial y} = h(x,y,t) + D(x,y,t)\frac{\partial u}{\partial t} \tag{4.17}$$

is considered in an isotropic non-homogeneous medium. Here, $u(x,y)$ is the unknown temperature, $a(x,y)$ is a known variable thermo-conductivity coefficient with components $a_x = \frac{\partial a}{\partial x}$ and $a_y = \frac{\partial a}{\partial y}$, $D(x,y,t)$ is a given function and $h(x,y,t)$ is a known heat source. The general boundary conditions are taken as

$$u(x,y,t) = \bar{u}(x,y,t), \qquad x \in \Gamma_1 \tag{4.18}$$

$$q(x,y,t) = \frac{\partial u}{\partial n} = \bar{q}(x,y,t) \qquad x \in \Gamma_2 \tag{4.19}$$

where $\bar{u}$ and $\bar{q}$ are given functions.

The numerical simulations are carried out by considering two test problems by DBEM and DRBEM which employ the fundamental solution of CD equation. In order to validate our numerical codes, we specifically consider the problems for which the exact solutions are available. The coefficients $a(x,y)$, $D(x,y,t)$, the function $h(x,y,t)$ and the exact solutions are taken as given in Table 4.1 [69].

Table 4.1: The problem parameters used for the solution of the 2-D heat conduction problem

	Test Problem 1	**Test Problem 2**
$a(x,y) =$	$x+y$	$x+y$
$D(x,y,t) =$	1	$1+t$
$h(x,y,t) =$	$6(x+y)-4$	$9(x^2+y^2)+12xy-1-t$
$u_{exact} =$	x^2+y^2+4t	x^3+y^3+t

The corresponding boundary conditions and the initial values at $t = 0$ are obtained from the exact solutions, and the geometric configurations of the test problems are displayed in Figure 4.1.

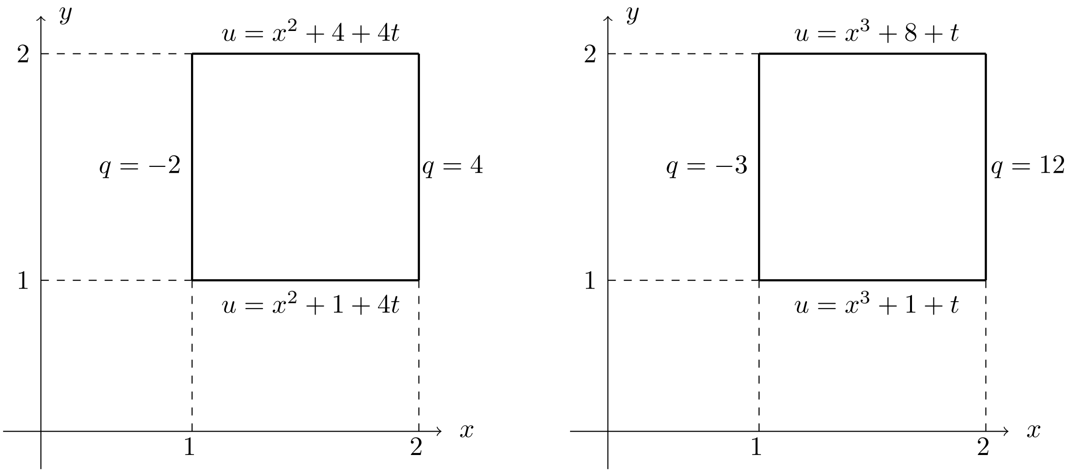

Test Problem 1 Test Problem 2

Figure 4.1: Geometries of the time-dependent heat conduction problems

In Figure 4.2, a qualitative comparison of the exact solution with numerical results obtained by both DBEM and DRBEM are visualized in terms of isotherms for Test Problem 1. Solutions are illustrated at a fixed time level $T = 1$ with the time step $\Delta t = 0.01$. It is well observed that the DBEM and DRBEM results are in quite well agreement with the exact solutions, which is also confirmed by the relative errors of order 10^{-3}, however, some deviations are observed especially along the walls which have Neumann type boundary conditions. Further, the temperature distribution along the horizontal centerline $y = 1.5$ ($1 \leq x \leq 2$) shown in Figure 4.3 confirms the accuracy of the present numerical results obtained by DBEM and DRBEM.

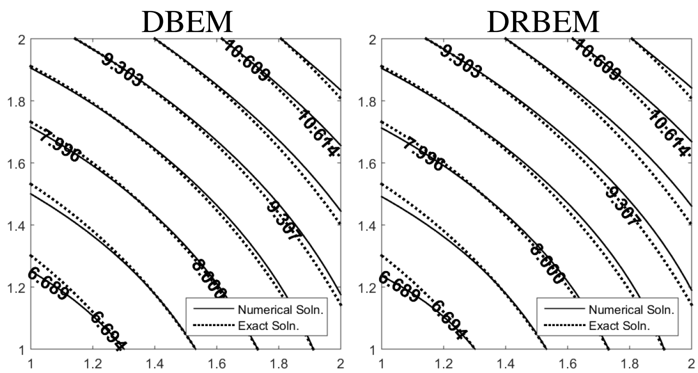

rel. error = 6×10^{-3} **rel. error =** 8×10^{-3}

Figure 4.2: Comparison of the exact solution with the results of DBEM and DRBEM in terms of isotherms.

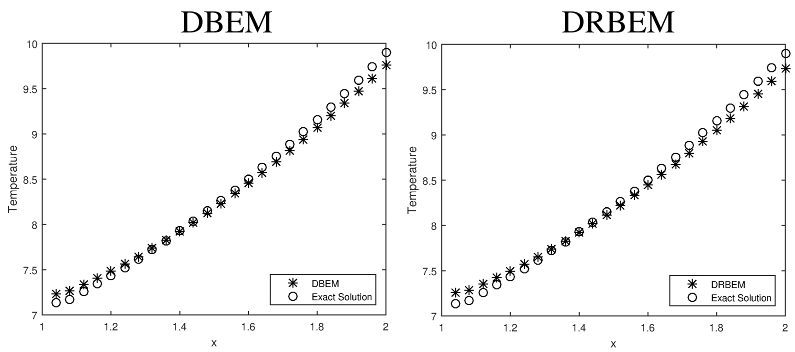

Figure 4.3: Temperature distribution along the line $y = 1.5$ by DBEM and DRBEM.

As a second test problem, the DBEM and DRBEM are employed to solve the heat transfer problem which involves time-dependent source function $h(x, y, t)$ and coefficient $D(x, y, t)$. As in Problem 1, the comparison of the exact solution with the

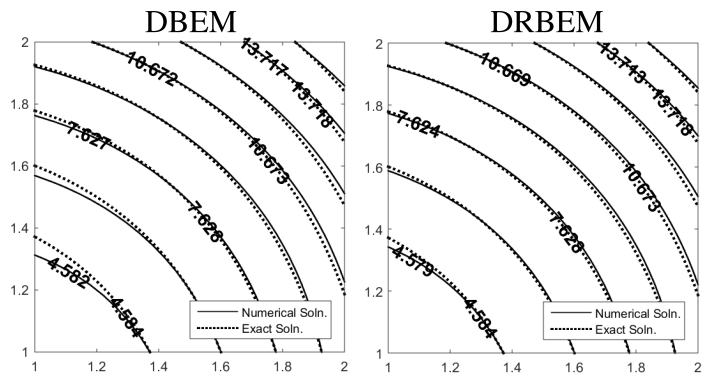

rel. error = 13×10^{-3} **rel. error =** 9×10^{-3}

Figure 4.4: Comparison of the exact solution with the results of DBEM and DRBEM in terms of isotherms.

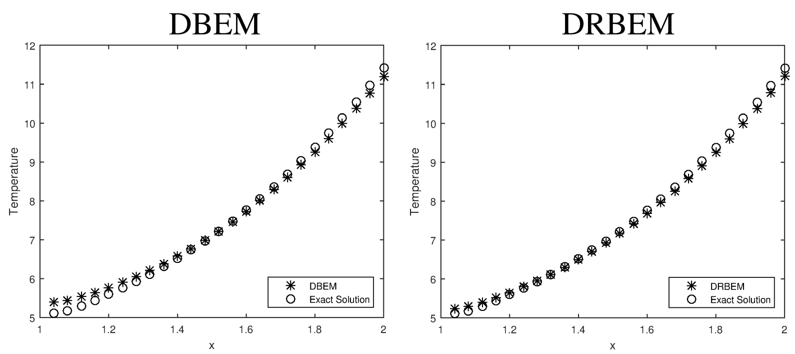

Figure 4.5: Temperature distribution along the line $y = 1.5$ by DBEM and DRBEM.

present numerical results are displayed in Figure 4.4 and Figure 4.5, respectively, in terms of isotherms and the temperature distribution along the horizontal centerline $y = 1.5$ of the problem domain. It is also well observed that, both DBEM and DRBEM results are in good agreement with the exact solution in each case which is compatible with the results of Problem 1.

4.2.2 Some Fluid Dynamics Problems

The time-dependent Navier-Stokes equations in terms of stream function-vorticity formulation subject to an external force f are given as (see Equations (1.27) -(1.28))

$$\begin{aligned} \nabla^2\psi &= -w && (4.20)\\ \frac{\partial w}{\partial t} + u\frac{\partial w}{\partial x} + v\frac{\partial w}{\partial y} &= \frac{1}{Re}\nabla^2 w + f && (4.21) \end{aligned}$$

when the stream function ψ and the vorticity w are defined as

$$u = \frac{\partial \psi}{\partial y}, \qquad v = -\frac{\partial \psi}{\partial x}, \tag{4.22}$$

$$w = \frac{\partial v}{\partial x} - \frac{\partial u}{\partial y}. \tag{4.23}$$

The vorticity equation can be thought as an unsteady CD type equation with variable coefficients containing the unknown ψ, i.e. $a_1 = u = \frac{\partial \psi}{\partial y}$ and $a_2 = v = -\frac{\partial \psi}{\partial x}$, which is the reason to consider the NS equations in the present chapter. The NS equations are coupled and highly nonlinear equations which require an iterative numerical solution between the stream function and vorticity equations by taking an initial value for the vorticity.

In the iterative solution procedure, the stream function equation is discretized by using DRBEM with the fundamental solution of Laplace equation while the vorticity equation which is the CD type equation with variable coefficients is solved by using both DRBEM and DBEM with the fundamental solution of CD equation as explained in Section 4.1.1 and Section 4.1.2, respectively.

Numerical algorithm:

(i) First, we solve the stream function equation (4.20) by using DRBEM with the fundamental solution of Laplace equation with an initial value of vorticity, $w^{(0)}$. Thus, the matrix-vector form of DRBEM is as follows

$$\tilde{H}\psi^{(m)} - \tilde{G}\frac{\partial\psi}{\partial n}^{(m)} = (\tilde{H}\hat{U} - \tilde{G}\hat{Q})\tilde{F}^{-1}(-w^{(m)}) \quad (4.24)$$

where the components of $\tilde{G}$ and $\tilde{H}$ are as given in Equations (2.25-2.28) in Chapter 2. The coordinate matrix $\tilde{F}$ is obtained by taking the radial basis functions $f_j = 1 + r_j$, which are linked to Poisson equation $\nabla^2\hat{u}_j = f_j$, as columns. The solution of Equation (4.24) gives the values of the stream function at the m-th iteration, i.e. we obtain $\psi^{(m)}$.

(ii) After obtaining the values of stream function for all boundary and interior nodes, the x and y-derivatives of ψ at each node (x_i, y_i), $i = 1, ..., N + L$, are obtained numerically by using the coordinate matrix $\tilde{F}$, that is: $u^{(m)} = \frac{\partial\psi}{\partial y}^{(m)} = \frac{\partial\tilde{F}}{\partial y}\tilde{F}^{-1}\psi^{(m)}$ and $v^{(m)} = -\frac{\partial\psi}{\partial x}^{(m)} = -\frac{\partial\tilde{F}}{\partial x}\tilde{F}^{-1}\psi^{(m)}$ as given in Chapter 2 (see Equation 2.40).

(iii) Once the vorticity equation (4.21) is weighted by the fundamental solution of CD equation (4.2) with $a_1 = u = \frac{\partial\psi}{\partial y}$, $a_2 = v = -\frac{\partial\psi}{\partial x}$ and $\varepsilon = \frac{1}{Re}$, and Green's second identity is employed, Equation (4.21) becomes

$$\begin{aligned} c_i w_i + \frac{1}{Re}\int_\Gamma q^* w d\Gamma - \frac{1}{Re}\int_\Gamma u^*\frac{\partial w}{\partial n}d\Gamma \quad &+ \quad \int_\Gamma (uu^* n_x w + vu^* n_y w)d\Gamma \\ &= \quad -\int_\Omega (\frac{\partial w}{\partial t} - f)u^* d\Omega. \quad (4.25) \end{aligned}$$

The above integral equation is nonlinear since the unknown w is multiplied by the derivatives of the other unknown ψ. However, when the values of $u^{(m)} = \frac{\partial\psi}{\partial y}^{(m)}$ and $v^{(m)} = -\frac{\partial\psi}{\partial x}^{(m)}$ at the m-th iteration obtained in step (ii) are inserted in Equation (4.25), the nonlinearity is removed.

(iv) Finally, when we use the constant elements to discretize the boundary, and backward finite difference for the time integration, one can get the matrix-vector form of DRBEM discretized system

$$(H^{(m)} + \frac{C}{\Delta t}^{(m)})w^{(m+1)} - G^{(m)}\frac{\partial w}{\partial n}^{(m+1)} = \frac{C}{\Delta t}^{(m)} w^{(m)} + C^{(m)}f^{(m)} \quad (4.26)$$

for the vorticity as given in Equation (4.8), and the matrix-vector form of DBEM discretized system is

$$(H^{(m)} + \frac{1}{\Delta t} M_1^{(m)}) w^{(m+1)} - G^{(m)} \frac{\partial w}{\partial n}^{(m+1)} = \frac{1}{\Delta t} M_1^{(m)} w^{(m)} + M_2^{(m)} \quad (4.27)$$

as given in Equation (4.16). The coefficients of matrices $H^{(m)}$, $G^{(m)}$, $C^{(m)}$, $M_1^{(m)}$ and $M_2^{(m)}$ are the same as given in Section 4.1 in which the coefficients ε, a_1 and a_2 correspond to $\varepsilon = \frac{1}{Re}$, $a_1 = u^{(m)}$ and $a_2 = v^{(m)}$.

(v) **Boundary conditions for vorticity:** In general, the boundary conditions for the vorticity are not known physically. To obtain the vorticity boundary conditions, one can use coordinate matrix $\tilde{F}$ given in step (i) by considering the stream function equation (4.20) ($\nabla^2 \psi = -w$) as

$$w = -(\frac{\partial \tilde{F}}{\partial x} \tilde{F}^{-1} \frac{\partial \tilde{F}}{\partial x} \tilde{F}^{-1} + \frac{\partial \tilde{F}}{\partial y} \tilde{F}^{-1} \frac{\partial \tilde{F}}{\partial y} \tilde{F}^{-1}) \psi. \quad (4.28)$$

(vi) After the insertion of the vorticity boundary conditions into Equations (4.26) and (4.27), and the system is rearranged by moving the columns of H and G from one side to the other according to known boundary conditions. When all unknowns are passed to the left hand side, one can obtain a linear system of $AX = D$ in both DRBEM and DBEM. Here, the vector X contains only the unknown values of $\frac{\partial w}{\partial n}$ on the boundary and unknown interior w values, and D is the known right hand side vector containing the information from the m-th time level. Once this linear system is solved, the vorticity values at the interior nodes are obtained at the $(m+1)$-st time level.

(vii) In order to accelerate the convergence to steady-state, when Equations (4.26) and (4.27) are solved, a relaxation parameter $0 < \beta_w \leq 1$ is employed for variable w as follows

$$w^{(m+1)} = (1 - \beta_w) w^{(m)} + \beta_w w^{(m+1)}. \quad (4.29)$$

(viii) Then, the values of vorticity obtained in step (vii) are used in the solution of stream function equation (4.20), and the solution procedure is repeated starting from the step (i). The iterative process is performed up to a preassigned time level or a preassigned tolerance between two successive iterations is reached.

4.2.2.1 Navier-Stokes equations in a square cavity with exact solution

As mentioned before, we first consider the time-dependent Navier-Stokes equations governed by

$$\nabla^2\psi = w \tag{4.30}$$

$$\frac{\partial w}{\partial t} + u\frac{\partial w}{\partial x} + v\frac{\partial w}{\partial y} = \frac{1}{Re}\nabla^2 w + f \tag{4.31}$$

in a square cavity $\Omega = \{(x, y) : 0 \leq x \leq 1, 0 \leq y \leq 1\}$ for which the analytical solution is given in [70] as follows:

$$u = \pi \sin t \sin(2\pi y) \sin^2(\pi x) \tag{4.32}$$

$$v = -\pi \sin t \sin(2\pi x) \sin^2(\pi y) \tag{4.33}$$

when the force function f is taken as

$$\begin{aligned} f = & -\pi^2 \cos t(\cos 2\pi x + \cos 2\pi y - 2\cos 2\pi x \cos 2\pi y) \\ & +\pi^4 \sin^2 t \sin 2\pi x \sin 2\pi y(\cos 2\pi x - \cos 2\pi y) \\ & -\frac{4}{Re}\pi^4 \sin t(\cos 2\pi x + \cos 2\pi y - 4\cos 2\pi x \cos 2\pi y). \end{aligned} \tag{4.34}$$

The boundary conditions for ψ and w are taken from the analytical solution accordingly as follows

$$\psi = -\sin t \sin^2 \pi x \sin^2 \pi y \tag{4.35}$$

$$w = -\pi^2 \sin t(\cos 2\pi x + \cos 2\pi y - 2\cos 2\pi x \cos 2\pi y). \tag{4.36}$$

The numerical simulations are carried out for several values of Reynolds number ($Re = 500$, 1000, 2000) to analyze the effect of Re on the flow. The streamlines and vorticity contours obtained by DBEM and DRBEM with the fundamental solution of CD equation are drawn, respectively, in Figure 4.6 and Figure 4.7. To discretize the spatial domain, $N = 120$ constant boundary elements and $L = 900$ interior nodes are used for the highest value of Reynolds number with the time step $\Delta t = 0.001$ in the applications of both DBEM and DRBEM. The calculated relative errors between the numerical and exact solutions reveal that DBEM and DRBEM results are quite compatible with the analytical solutions. Although, there is no significant difference in the obtained DBEM and DRBEM results, the DBEM results are slightly more accurate than the ones obtained by DRBEM. Thus, in the subsequent problems of fluid flows we concentrate on the solution by DBEM with the fundamental solution of CD equation. Moreover, it is well-observed from figures that the results indicate that the obtained flow patterns are independent of the Reynolds number for both the stream function and the vorticity for the present fluid flow problem.

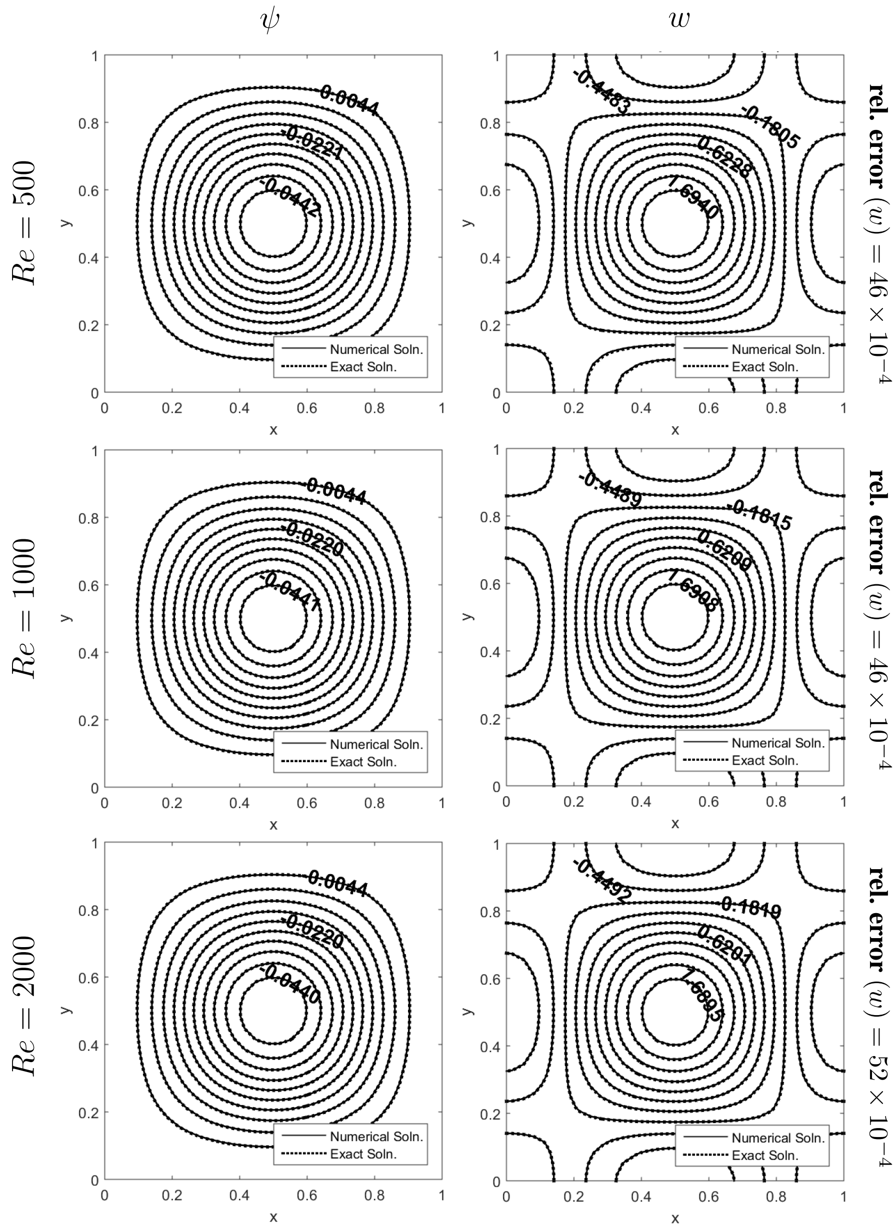

Figure 4.6: Effect of Re on the stream function and vorticity by DBEM: $Re = 500, 1000, 2000$, $T = 0.05$.

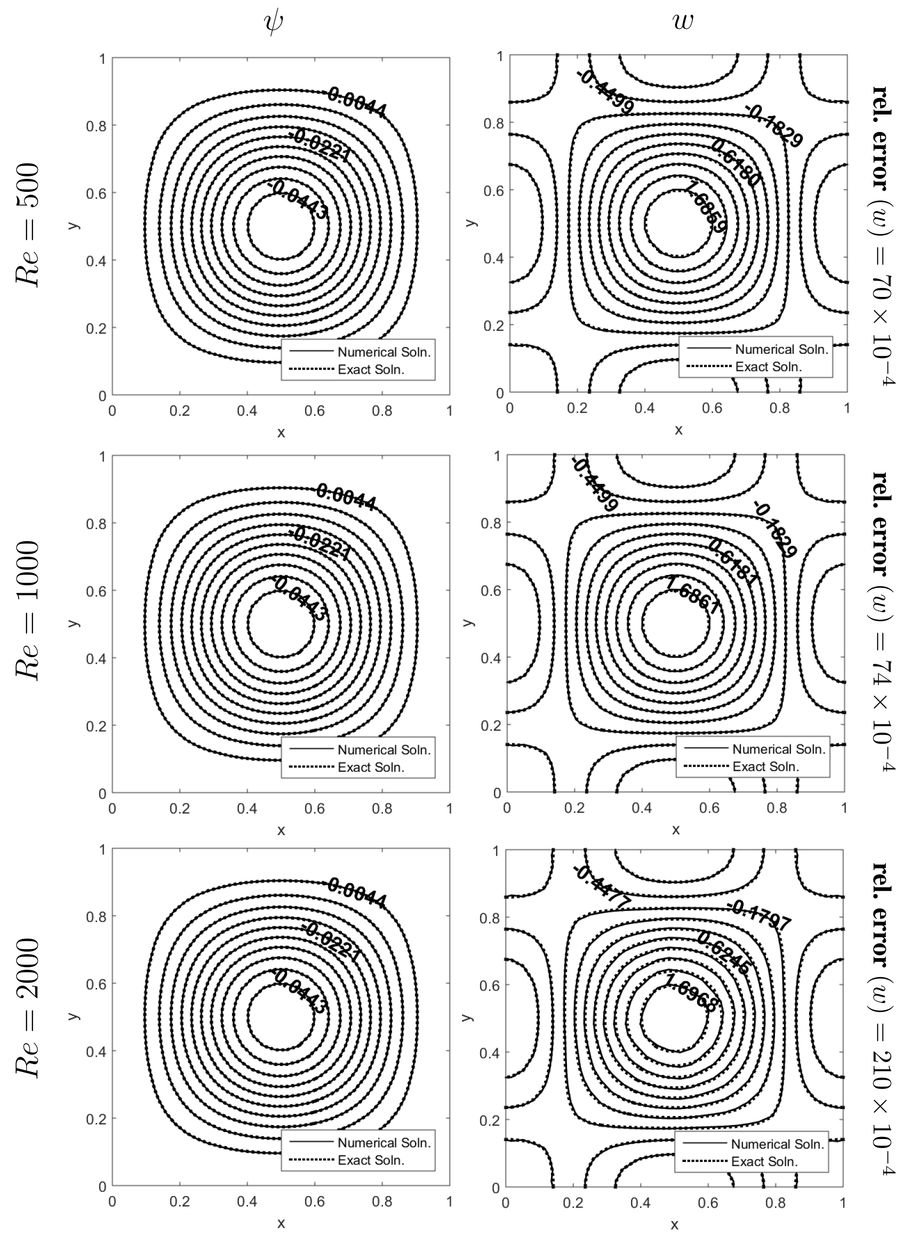

Figure 4.7: Effect of Re on the stream function and vorticity by DRBEM: $Re = 500, 1000, 2000$, $T = 0.05$.

4.2.2.2 Lid-driven cavity flow

The second problem governed by the NS equations (4.20) and (4.21) with $f = 0$, is a benchmark problem of fluid dynamics which is called the lid-driven cavity flow in a square domain $\Omega = \{(x, y) : 0 \leq x \leq 1, 0 \leq y \leq 1\}$. The upper wall of the cavity is moving with a constant horizontal velocity to the left ($u = -1$) while other three walls have no motion. The movement of the lid generates the fluid motion in the cavity. The corresponding boundary conditions for ψ and velocities are given in Figure 4.8. On the other hand, the unknown boundary conditions for the vorticity are obtained by using the coordinate matrix as given in Equation (4.28) through the application of the present numerical technique.

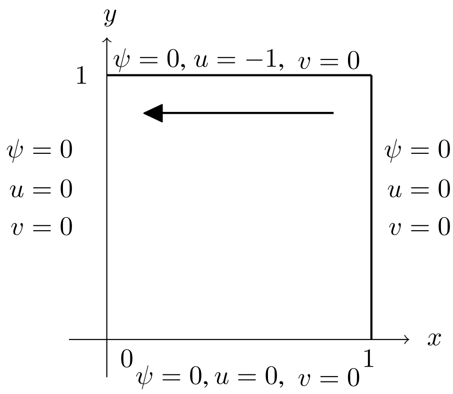

Figure 4.8: Geometry and the boundary conditions for the lid-driven cavity flow.

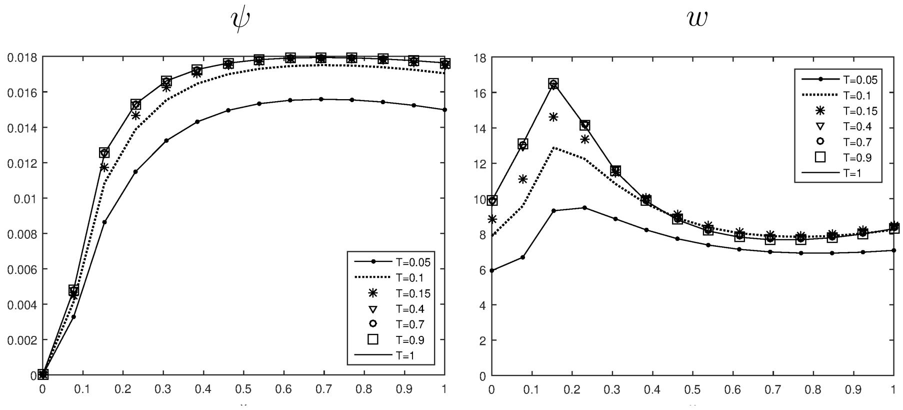

Figure 4.9: The stream function and vorticity along $y = 0.9$ at increasing time levels by DBEM with the fundamental solution of CD equation at $Re = 10$.

To determine when the steady-state is reached at fixed $Re = 10$, the numerical results are obtained at different time levels. The variations of the stream function and the vorticity along the line $y = 0.9$ as time advances are illustrated in Figure 4.9. It is observed that there is no change in the values of stream function and vorticity after $T = 0.4$, which indicates that the steady-state is reached for ψ and w at approximately $T = 0.4$.

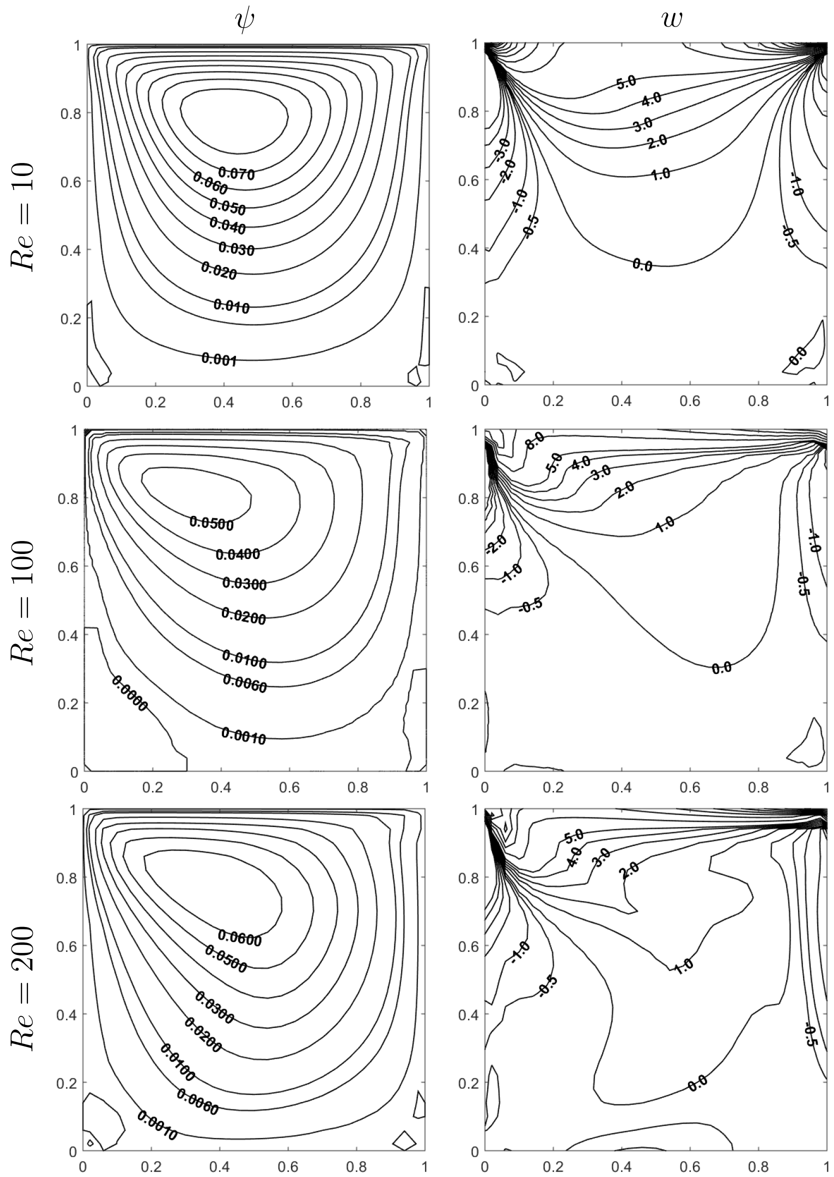

Figure 4.10: Effect of Re on the stream function and vorticity by DBEM: $Re = 10, 100, 200$.

In Figure 4.10, the streamlines and vorticity contours at steady-state (i.e. $T = 1$) are drawn for several values of $Re = 10, 100, 200$. In the application of DBEM with the fundamental solution of CD equation, $N = 100$ constant boundary elements and $L = 625$ interior nodes are used to discretize the computational domain while the time step is taken as $\Delta t = 0.01$. A primary vortex formed centrally close to the upper wall when $Re = 10$, moves to the left wall with an increase in Re to 100. Moreover, as Re increases to 100 the values of stream function decrease. In addition, secondary vortices start to form at the lover left and right corners of the cavity with an increase in Re, especially around $Re = 500$ as shown in Figure 4.11. On the other hand, the effect of the driven lid on vorticity is more pronounced at high values of Re. That is, the vorticity contours are almost symmetric at $Re = 10$ and this symmetry is deteriorated due to the strong vorticity gradient to the left at $Re = 100$ and $Re = 200$. These results are compatible with the available results given in [71, 72].

However, through the solution procedure of DBEM some difficulties arise in using the fundamental solution ($u^* = \frac{Re}{2\pi}\exp(-\frac{Re}{2}(ur_x + vr_y))K_0(sr)$) which contains the velocity components in the exponential terms, i.e. the unknowns u and v. Moreover, velocity components u and v are appearing as nonlinearity in the convection terms. Thus, the DBEM results which are in quite good agreement with results in [71, 72], can be obtained for the Reynolds number up to 200 when the iterative scheme is initiated with an arbitrary initial value for the vorticity. However, if we start with a well-educated initial value for the vorticity, which is obtained by using DRBEM with the fundamental solution of Laplace equation, one can obtain reasonably well results for higher values of Reynolds number, e.g. $Re = 500$, as shown in Figure 4.11.

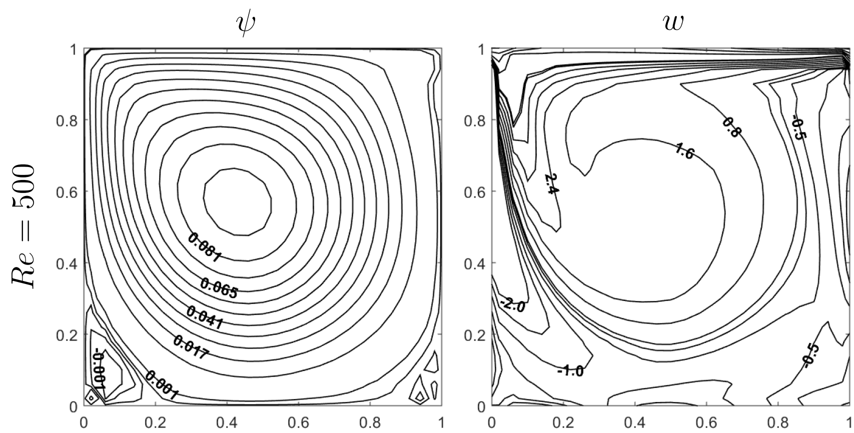

Figure 4.11: The streamlines and vorticity lines by DBEM when $Re = 500$.

4.2.2.3 Natural convection flow

In the case of heat flux, we need to extend the Navier-Stokes equations (given in Equations (4.20-4.21)) by adding the energy equation. Thus, the governing equations of the natural convection flow are given as (see Equations (1.29)-(1.31)) [15, 73]

$$
\begin{aligned}
\nabla^2\psi &= -w \qquad (4.37)\\
\frac{\partial T}{\partial t} + u\frac{\partial T}{\partial x} + v\frac{\partial T}{\partial y} &= \nabla^2 T \qquad (4.38)\\
\frac{\partial w}{\partial t} + u\frac{\partial w}{\partial x} + v\frac{\partial w}{\partial y} &= Pr\nabla^2 w + RaPr\frac{\partial T}{\partial x} \qquad (4.39)
\end{aligned}
$$

where T, Pr and Ra are the temperature, Prandtl number (see Equation (1.32)) and Rayleigh number (see Equation (1.33)), respectively. The energy equation is in the same form with the vorticity transport equation; and hence the discretization of it by DBEM can be performed in the same manner as given in Section 4.1.2.

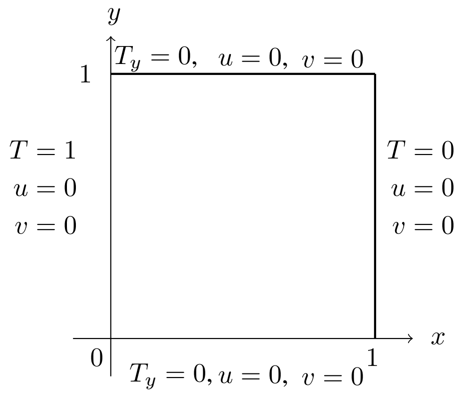

Figure 4.12: Geometry and the boundary conditions for the natural convection flow.

The boundary conditions of stream function and temperature are taken as

$$
\begin{aligned}
&\psi = 0, \ \frac{\partial \psi}{\partial x} = 0, \ T = 1 \qquad \text{at} \qquad x = 0, \ 0 \le y \le 1, \qquad (4.40)\\
&\psi = 0, \ \frac{\partial \psi}{\partial x} = 0, \ T = 0 \qquad \text{at} \qquad x = 1, \ 0 \le y \le 1, \qquad (4.41)\\
&\psi = 0, \ \frac{\partial \psi}{\partial y} = 0, \ \frac{\partial T}{\partial y} = 0 \qquad \text{at} \qquad y = 0, 1, \ 0 \le x \le 1 \qquad (4.42)
\end{aligned}
$$

while the boundary conditions of vorticity are derived from the coordinate matrix as given in Equation (4.28). The computational domain and the corresponding boundary conditions of the natural convection flow are displayed in Figure 4.12.

The iterative solution procedure:

- First, we solve the stream function equation (4.37) by DRBEM with the fundamental solution of Laplace equation to obtain $\psi^{(m)}$ by using $w^{(m)}$.

- At each iteration, u and v are computed at the m-th level by means of radial basis functions and are inserted into the energy equation (4.38) and vorticity transport equation (4.39) to remove the nonlinearity of these equations caused by the variable coefficients of convection terms. As a result of this insertion, the coefficients of Equation (4.38) and Equation (4.39) become constants at each node i and time level m.

- Further, energy equation (4.38) is solved by DBEM with the fundamental solution of CD equation as explained in Section 4.1.2; and as a result $T^{(m+1)}$ is obtained.

- The vorticity transport equation (4.39) involves the x-derivative of the temperature ($\frac{\partial T}{\partial x}$) which is computed by using the forward difference approximation as follows

$$\frac{\partial T}{\partial x} = \frac{T_{i+1,j} - T_{i,j}}{\Delta x} \tag{4.43}$$

  where Δx is the increment in the x-direction. Then, we solve the vorticity transport equation by DBEM with the fundamental solution of CD equation and we get $w^{(m+1)}$, as explained in Section 4.1.2.

- When we obtain w at the $(m+1)$-st time level, we use this value in the proceeding iterations to obtain the new value of the stream function in Equation (4.37). This process is repeated iteratively until we reach the desired time level or the preassigned convergence tolerance.

The streamlines, vorticity and temperature contours obtained by DBEM are drawn in Figure 4.13 for several values of $Ra(= 10^3, 10^4, 10^5)$ at $T = 3$ with $\Delta t = 0.01$. In computations, $N = 120$ constant boundary elements and $L = 900$ interior nodes are used for the highest value of Rayleigh number. A circular vortex formed at the center of the cavity for streamlines at $Ra = 10^3$ extends diagonally forming an elliptic shape with an increase in Ra up to 10^5. The isotherms which are almost vertical through the cavity tend to become horizontal especially at the center of the cavity as Ra increases, which indicates that the heat transfer is dominated by convection. Moreover, the vorticity becomes stagnant at the center of the cavity for higher values of Ra, which results in a boundary layer formation along the vertical walls. Similarly, one can observe the boundary layer formation along the vertical walls in isotherm profiles as well with an increasing Ra. It is also important to note here that obtained results are in good agreement with the results given in the literature [15, 73, 74].

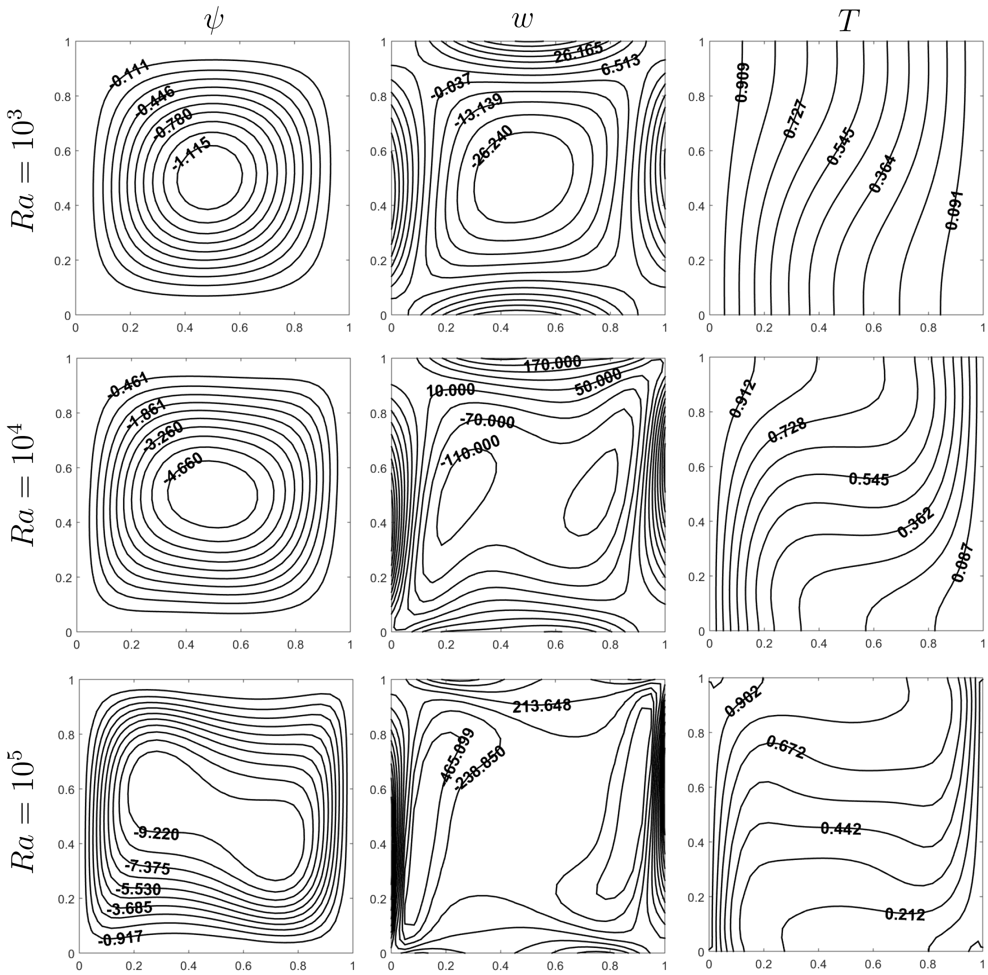

Figure 4.13: Effect of Ra on the stream function, vorticity and isotherms by DBEM: $Ra = 10^3, 10^4, 10^5$.

The results given in Figure 4.13 are obtained by taking the initial guess for the unknowns from the results of DRBEM solution using the fundamental solution of Laplace equation. If the iteration starts with an almost zero initial guess some difficulties arise in the use of the fundamental solution containing the velocity components in the exponential terms which cause nonlinearity through the convection terms.

4.2.2.4 Channel flow

The NS equations (4.20) and (4.21) with $f = 0$ is consider here for the fluid flow driven not in a square cavity but in an infinitely long channel formed by two parallel plates i.e. $\Omega = \{(x, y) : 0 \leq x \leq L, 0 \leq y \leq 1\}$ where L is a constant as shown in Figure 4.14. The corresponding boundary conditions of ψ on all the walls and of w for only three walls are given in Figure 4.14. The unknown boundary conditions for w along the upper wall are also obtained by using the coordinate matrix as given in Equation (4.28).

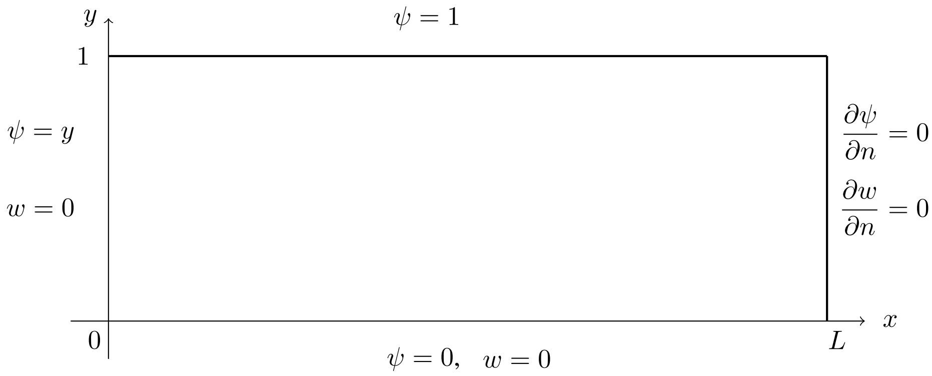

Figure 4.14: Geometry and the boundary conditions for the channel flow.

The numerical results for the channel flow are obtained at steady-state by using DBEM with the fundamental solution of CD equation. The variations of ψ and w along the horizontal lines $y = 0.9$ and $y = 1$, are displayed, respectively, in Figure 4.15 for $Re = 10$ and in Figure 4.16 for Re $(= 10, 50)$. The value of stream function starts from along 0.8, and then it increases slowly up to 1 for both $Re = 10$ and $Re = 50$. On the other hand, the vorticity shows a rapid decrease in magnitude up to 5 for $Re = 10$ and up to 10 for $Re = 50$. These are the well known characteristics of ψ and w [75], and they could be captured by DBEM with the fundamental solution of CD equation. It is also observed that the channel length can be taken longer, i.e. $L = 10$, for the small values of $Re = 10$ while one needs to take a channel with shorter length, i.e. $L = 5$ for $Re = 50$, to obtain reasonable results for the DBEM solution of the channel flow. Thus, to be able to see the variation of the solution with respect to Reynolds number, the streamlines and isotherms are further drawn in the channel with $L = 5$ for $Re = 10, 50$ in Figure 4.16. It is observed that no significant change occurs in streamlines as Re increases, whereas the drop observed in the value of vorticity at $Re = 10$ is reduced with an increase in Re to 50.

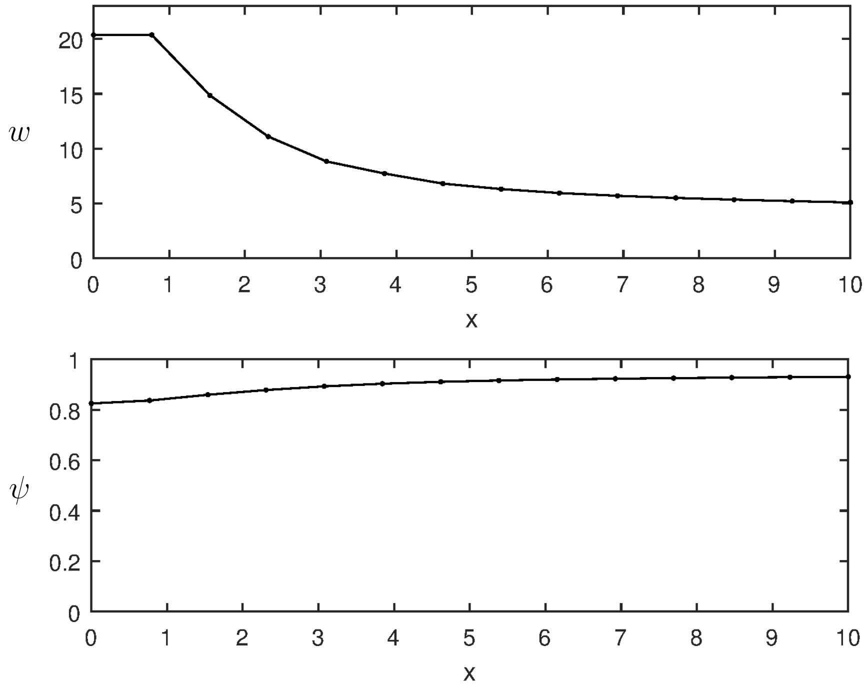

Figure 4.15: Vorticity (at $y = 1$) and stream function (at $y = 0.9$) by DBEM: $Re = 10$.

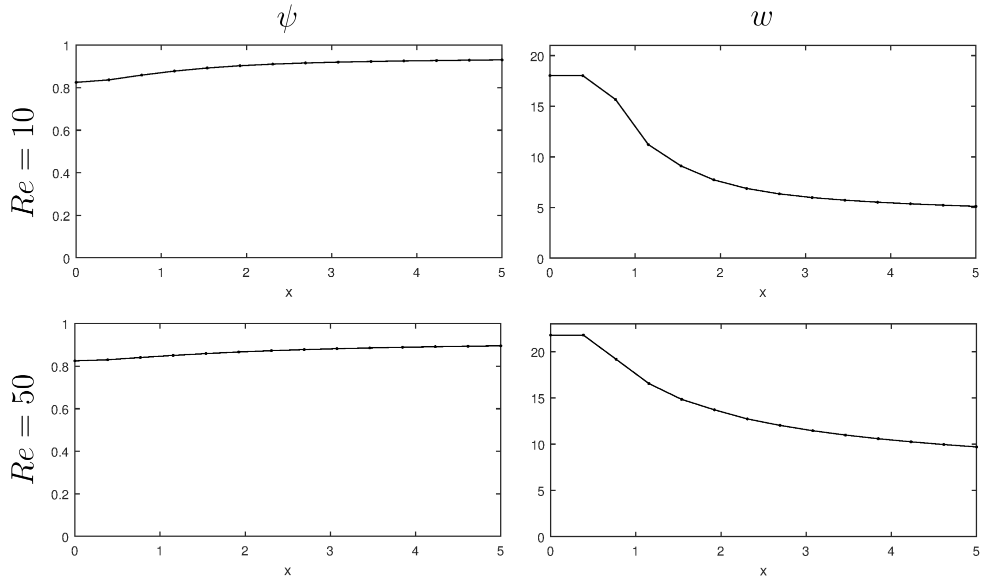

Figure 4.16: Stream function (at $y = 0.9$) and vorticity (at $y = 1$) by DBEM: $Re = 10, 50$.

4.2.2.5 MHD Natural Convection in a Square Cavity Filled with a Porous Medium

Finally, we consider the MHD natural convection flow in a square enclosure filled with a saturated porous medium. The geometry of the problem under consideration is illustrated in Figure 4.17. The left vertical wall of the cavity is heated while the right vertical wall is cooled, and the top and bottom horizontal walls are taken as to be adiabatic (i.e. thermally insulated). The external, uniform magnetic field is applied vertically with an intensity B_0.

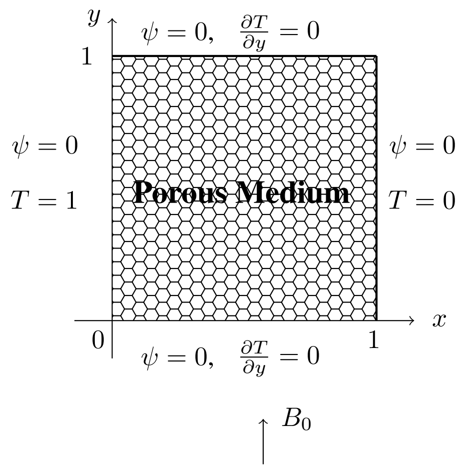

Figure 4.17: Geometry and the boundary conditions for the problem.

In this problem,

- the flow is incompressible and laminar which is assumed to obey Darcy law[1].
- the porous medium and fluid have a thermal equilibrium and also has isotropic and homogenous permeability.
- all of the physical properties of the fluid are assumed to be constant except the density variation in the body force term in the momentum equation which employs the Boussinesq approximation.

Under these assumptions, the dimensional conservation equations for the MHD natural convection flow can be written as [77, 78]:

[1] Darcy law is an equation that defines the ability of a fluid to flow through a porous media [76].

$$\text{Continuity Equation} \quad : \quad \frac{\partial u}{\partial X} + \frac{\partial v}{\partial Y} = 0 \tag{4.44}$$

$$\text{Momentum Equations} \quad : \quad u = -\frac{K}{\mu}\frac{\partial p}{\partial X} + \frac{B_0^2 K\sigma}{\mu}u, \tag{4.45}$$

$$v = -\frac{K}{\mu}\frac{\partial p}{\partial Y} + \frac{\bar{T} - T_c}{\nu}Kg\bar{\beta} \tag{4.46}$$

$$\text{Energy Equation} \quad : \quad u\frac{\partial \bar{T}}{\partial Y} + v\frac{\partial \bar{T}}{\partial X} = \alpha(\frac{\partial^2 \bar{T}}{\partial X^2} + \frac{\partial^2 \bar{T}}{\partial Y^2}) \tag{4.47}$$

where μ, B_0, σ, α, ρ, c_p and T_c represent the dynamic viscosity, intensity of the uniform magnetic field, electrical conductivity, thermal diffusivity, density, specific heat at constant pressure and cold wall temperature, respectively. When the pressure terms in the momentum equations (4.45) and (4.46) are eliminated, we obtain

$$\frac{\partial u}{\partial Y} - \frac{\partial v}{\partial X} = \frac{B_0^2 K\sigma}{\mu}\frac{\partial u}{\partial Y} - \frac{Kg\bar{\beta}}{\nu}\frac{\partial \bar{T}}{\partial X} \tag{4.48}$$

in which the K, g, $\bar{\beta}$ and ν are permeability of porous media, gravity, coefficient of thermal expansion, kinematic viscosity, respectively. The boundary conditions are taken as:

$$\text{at } X = 0,\ u = 0,\ v = 0\ \bar{T} = T_h \text{ at } X = L,\ u = 0,\ v = 0,\ \bar{T} = T_c \tag{4.49}$$

$$\text{at } Y = 0,\ u = 0,\ v = 0,\ \frac{\partial \bar{T}}{\partial y} = 0 \text{ at } Y = L,\ u = 0,\ v = 0,\ \frac{\partial \bar{T}}{\partial Y} = 0. \tag{4.50}$$

By defining $u = \frac{\partial \psi}{\partial Y}$ and $v = -\frac{\partial \psi}{\partial X}$ the continuity equation (4.44) is automatically satisfied. By the use of non-dimensional parameters

$$x = \frac{X}{L}, \quad y = \frac{Y}{L}, \quad \psi = \frac{\psi^*}{\alpha}, \quad T = \frac{\bar{T} - T_c}{T_h - T_c} \tag{4.51}$$

the dimensionless governing equations of the MHD natural convection flow under the effect of a vertically applied magnetic field can be obtained as [79]

$$\nabla^2\psi = -Ra\frac{\partial T}{\partial x} - M^2\frac{\partial^2\psi}{\partial y^2} \tag{4.52}$$

$$\nabla^2 T = u\frac{\partial T}{\partial x} + v\frac{\partial T}{\partial y} \tag{4.53}$$

where

$$\text{Darcy-modified Rayleigh number:} \quad Ra = \frac{g\bar{\beta}\Delta TKL}{\nu\alpha}, \tag{4.54}$$

$$\text{Hartmann number for porous medium:} \quad M^2 = \frac{B_0^2 K\sigma}{\mu}. \tag{4.55}$$

To obtain the solution, Equation (4.53) is solved by DBEM with the fundamental solution of CD equation while stream function equation (4.52) is solved by DRBEM with the fundamental solution of Laplace equation. The stream function equation (4.52) involves the x derivative of the temperature $\frac{\partial T}{\partial x}$ and is computed by forward difference approximation (see Equation (4.43)).

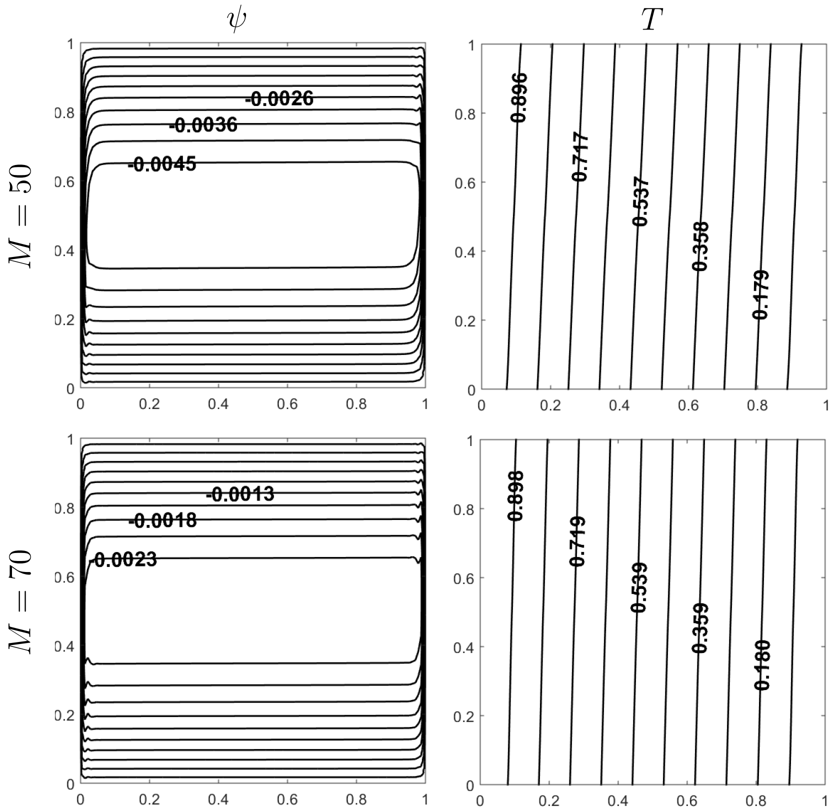

Figure 4.18: Effect of M on the stream function and temperature by DBEM: $M = 50, 70$, $Ra = 100$.

To be able to observe the temperature distribution and flow patterns, the isotherms and streamlines are drawn in Figure 4.18, respectively for $M = 50$ and $M = 70$, when $Ra = 100$. Following the temperature difference between the hot left and cold right walls, a negative vortex is formed in the fluid motion by the effect of buoyancy forces. As M increases the streamlines decrease in magnitude which is the well-known flattening tendency of the flow in the presence of external magnetic field. On the other hand, there is no significant change on the isotherm profiles as M increases, that is, isotherms are almost vertical line showing the dominance of conduction in the heat transfer.

4.3 Summary of the Obtained Results in Chapter 4

In this chapter, numerical solutions of CD type equations with variable coefficients are obtained by using DBEM and DRBEM with the fundamental solution of CD equation. As mentioned before, the main difference between Chapter 3 and present chapter is that the former investigates the CD type equations with constant coefficients while in the latter the CD type equations with variable coefficients are considered. The obtained results are illustrated for two kinds of test problems, namely heat conduction and fluid flow problems, for which some notes can be written down as follows:

- For the heat conduction problems involving variable coefficients of space variable, the use of both DBEM and DRBEM with the fundamental solution of CD equation results in reasonably well compatible results with the exact solutions.
- It can also be said that for the fluid dynamics problems governed by either NS equations or NS and energy equations, the DBEM with the fundamental solution of CD equation can be performed as an alternative numerical technique which gives quite well results for small and moderate values of problem physical parameters, namely Reynolds, Rayleigh and Hartmann numbers for each test problems.

CHAPTER 5

CONCLUSION

In this thesis, the time-dependent CDR type equations with constant and variable convective coefficients are solved numerically. The spatial derivatives are discretized by two BEM techniques, namely DRBEM and DBEM, while the implicit backward finite difference is employed for the time integration. The application of DRBEM and DBEM with the fundamental solution of CDR and mH equations are presented for several fluid flow problems.

First, we provide numerical solutions of time-dependent CDR equations with constant convective coefficients. DRBEM and DBEM are used to obtain the numerical solution with the fundamental solutions of CDR and mH equations. We validate the accuracy of our numerical simulations by comparing them with the exact solution of the CDR equation (commonly known as the concentration problem). The results indicate the followings: (i) the fundamental solution of CDR equation provides a good agreement with the exact solution offering an acceptable degree of accuracy for both DBEM and DRBEM; and (ii) the fundamental solution of mH equation yields good accuracy for only DBEM in the sense of decreasing diffusion parameter which causes convection-dominated system.

Moreover, as a CD type equation with constant coefficients, transient magnetohydrodynamic flow problems in ducts are solved by using DRBEM and DBEM with the aforementioned fundamental solutions. The MHD duct flow problems are studied either with insulated or conducting walls with variable conductivity, under the inclined or vertically applied magnetic field with no-slip walls, and in ducts with flat or perturbed walls. Numerical solutions are illustrated for several values of Hartmann number M, inclination angle β and conductivity parameter λ, and well-known behaviors are observed. The results indicate that DBEM with fundamental solutions of both CD and mH equations performs quite well even for higher values of Hartmann number M. Yet, DRBEM with the fundamental solution of CD equation gives compatible results for rather small values of M. Lastly, for some cases, DRBEM with the fundamental solution of mH equation may fail to yield reasonable results even for small values of M.

Moreover, when the effect of a perturbed boundary on the numerical results is examined by using DBEM and DRBEM with the fundamental solution of CD equation, both techniques provide similar results. That is, additional vortices occur at small values of Hartmann number (e.g. $M = 5, 10$) and these vortices move upward with an increase in the perturbation parameter ξ. For higher values of M, the side layer formations are observed, and the fluid becomes stagnant at the center of the cavity. Therefore, the effect of the perturbation can be well observed for smaller values of $M(\leq 30)$. On the other hand, current lines (equal induced magnetic field lines) occupy all the region with a good harmony with the perturbed boundary.

In the second part of the thesis, the nonlinear CD type equations with variable convective coefficients are solved by the proposed numerical techniques with the fundamental solution of CD equation. These variable coefficients can contain either only the space variables or the unknowns as well. When they include the unknowns, the CD equation become nonlinear. Thus, as applications of the time-dependent fluid dynamics problems governed by NS equation or NS and energy equations, such as lid-driven cavity flow, natural convection flow, MHD natural convection flow and channel flow, are solved by DBEM with fundamental solution of CD equation. It is observed that the well-known behaviors of the fluid flow and temperature distribution are well-captured for moderate values of Reynolds, Rayleigh and Hartmann numbers.

To conclude, it can be said that both DBEM and DRBEM, the techniques within the scope of the thesis, especially with the fundamental solution of CD equation, and in some cases with the fundamental solution of mH equation, are effective numerical techniques for the solution of time-dependent CD type equations governing some fluid dynamics problems in the presence/absence of magnetic field. Reasonably well results which capture the physical behavior of the fluid flow are obtained for moderate/high values of problem parameters.

As a continuation of the thesis, the problem of nanofluid/ferrofluid flows and heat transfer problems, which are also governed by nonlinear CD type equations, can be considered and solved by using the DBEM with the fundamental solution of CD equation. Moreover, the study can be extended by using DBEM with time-dependent fundamental solution which is called time-domain boundary element method (TDBEM) for the solution of the problems considered in the thesis.

REFERENCES

[1] P. Partridge, C. Brebbia, and L. Wrobel, *The Dual Reciprocity Boundary Element Method*. Computational Mechanics Publications, Southampton Boston, 1992.

[2] B. R. Munson, D. F. Young, and T. H. Okiishi, *Fundamentals of Fluid Mechanics*. John Wiley & Sons, 2006.

[3] J. Blazek, *Computational Fluid Dynamics: Principles and Applications*. Butterworth-Heinemann, 2015.

[4] T. J. Chung, *Computational Fluid Dynamics*. Cambridge University Press, 2010.

[5] J. Reddy, *An Introduction to the Finite Element Method*. McGraw-Hill Education, 2005.

[6] M. Efendiev and H. Eberl, "On positivity of solutions of semi-linear convection-diffusion-reaction systems, with applications in ecology and environmental engineering," *Departmental Bulletin Paper Kyoto University*, vol. 1542, pp. 92–101, 2007.

[7] W. Hundsdorfer and J. Verwer, *Numerical Solution of Time-Dependent Advection-Diffusion-Reaction Equations*. Springer-Verlag, Berlin, Heidelberg, New York, 2003.

[8] J. A. Shercliff, *A Textbook of Magnetohydrodynamics*. Pergamon Press, Oxford-New York-Paris, 1965.

[9] P. Davidson, *An Introduction to Magnetohydrodynamics*. Cambridge University Press, New York, 2001.

[10] L. Dragos, *Magneto-Fluid Dynamics*. Abacus Press, England, 1975.

[11] D. J. Tritton, *Physical Fluid Dynamics*. Clarendon press, Oxford, 1998.

[12] J. R. Welty, C. E. Wicks, R. E. Wilson, and G. L. Rorrer, *Fundamentals of Momentum, Heat, and Mass Transfer*. John Wiley & Sons, 2008.

[13] T. Bergman, F. Incropera, D. DeWitt, and A. Lavine, *Fundamentals of Heat and Mass Transfer*. Wiley, 2011.

[14] M. Griebel, T. Dornseifer, and T. Neunhoeffer, *Numerical Simulation in Fluid Dynamics*. Siam, 1998.

[15] C. Shu and H. Xue, "Comparison of two approaches for implementing stream function boundary conditions in DQ simulation of natural convection in a square cavity," *Int. J. of Heat Fluid Fl.*, vol. 19, pp. 59 – 68, 1998.

[16] X.-T. Yan and Y. Xu, *Chemical Vapour Deposition: An Integrated Engineering Design for Advanced Materials*. Springer, 2010.

[17] C. Clavero and J. Gracia, "A uniformly convergent alternating direction HODIE finite difference scheme for 2D time-dependent convection-diffusion problems," *IMA J. Numer. Anal.*, vol. 26, pp. 155–172, 2006.

[18] J. Douglas and T. F. Russell, "Numerical methods for convection-dominated diffusion problems based on combining the method of characteristics with finite element or finite difference procedures," *SIAM J. Numer. Anal.*, vol. 19, no. 5, pp. 871–885, 1982.

[19] T. Tezduyar, Y. Park, and H. Deans, "Finite element procedures for time-dependent convection-diffusion-reaction systems," *Int. J. Numer. Meth. Fl.*, vol. 7, pp. 1013–1033, 1987.

[20] V. John and E. Schmeyer, "Finite element methods for time-dependent convection-diffusion-reaction equations with small diffusion," *Comput. Method Appl. M.*, vol. 198, pp. 475–494, 2008.

[21] E. Burman and M. Fernández, "Finite element methods with symmetric stabilization for the transient convection-diffusion-reaction equation," *Comput. Method Appl. M.*, vol. 198, pp. 2508–2519, 2009.

[22] R. Codina and J. Blasco, "Analysis of a stabilized finite element approximation

of the transient convection-diffusion-reaction equation using orthogonal subscales," *Comput. Visual. Sci.*, vol. 4, pp. 167–174, 2002.

[23] M. Feistauer, J. Hájek, and K. Švadlenka, "Space-time discontinuos Galerkin method for solving nonstationary convection-diffusion-reaction problems," *Appl. Math-Czech*, vol. 3, pp. 197–233, 2007.

[24] R. Codina, "Comparison of some finite element methods for solving the diffusion-convection-reaction equation," *Comput. Method Appl. M.*, vol. 156, pp. 185–210, 1998.

[25] M. M. Grigoriev and G. F. Dargush, "Efficiency of boundary element methods for time-dependent convective heat diffusion at high Peclet numbers," *Commun. Numer. Meth. En.*, vol. 21, no. 4, pp. 149–161, 2005.

[26] M. M. Grigoriev and G. F. Dargush, "Boundary element methods for transient convective diffusion. part ii: 2D implementation," *Comput. Method Appl. M.*, vol. 192, no. 39, pp. 4299 – 4312, 2003.

[27] M. M. Grigoriev and G. F. Dargush, "Boundary element methods for transient convective diffusion. part iii: Numerical examples," *Comput. Method Appl. M.*, vol. 192, no. 39, pp. 4313 – 4335, 2003.

[28] C. Cunha, J. Carrer, M. Oliveira, and V. Costa, "A study concerning the solution of advection-diffusion problems by the boundary element method," *Eng. Anal. Bound. Elem.*, vol. 65, pp. 79–94, 2016.

[29] K. Singh and M. Tanaka, "Dual reciprocity boundary element analysis of transient advection-diffusion," *Int. J. Numer. Method H.*, vol. 13, pp. 633–646, 2003.

[30] S. A. AL-Bayati and L. C. Wrobel, "A novel dual reciprocity boundary element formulation for two-dimensional transient convection–diffusion–reaction problems with variable velocity," *Eng. Anal. Bound. Elem.*, vol. 94, pp. 60 – 68, 2018.

[31] D. Young, Y. Wang, and T. Eldho, "Solution of the advection-diffusion equation using the Eulerian-Lagrangian boundary element method," *Eng. Anal. Bound. Elem.*, vol. 24, pp. 449–457, 2000.

[32] B. Singh and J. Lal, "MHD axial flow in a triangular pipe under transverse magnetic field parallel to a side of the triangle," *Indian J. Technol.*, vol. 17, pp. 184 – 189, 1979.

[33] B. Singh and J. Lal, "Finite element method of MHD channel flow with arbitrary wall conductivity," *Journal of Mathematical and Physical Sciences*, vol. 18, pp. 501 – 516, 1984.

[34] M. Tezer-Sezgin and S. Köksal, "Finite element method for solving MHD flow in a rectangular duct," *Int. J. Numer. Meth. Eng.*, vol. 28, pp. 445–459, 1989.

[35] C. Bozkaya and M. Tezer-Sezgin, "Magnetohydrodynamic pipe flow in annular-like domains," *European Journal of Computational Mechanics*, vol. 26, pp. 394 – 410, 2017.

[36] B. Singh and J. Lal, "Finite element method for unsteady MHD flow through pipes with arbitrary wall conductivity," *Int. J. Numer. Meth. Fl.*, vol. 4, pp. 291–302, 1984.

[37] N. B. Salah, A. Soulaimani, and W. G. Habashi, "A finite element method for magnetohydrodynamics," *Comput. Method Appl. M.*, vol. 190, pp. 5867 – 5892, 2001.

[38] L. Seungsoo and G. Dulikravich, "Magnetohydrodynamic steady flow computation in three dimensions," *Int. J. Numer. Meth. Fl.*, vol. 13, pp. 917–936, 1991.

[39] T. Sheu and R. Lin, "Development of a convection-diffusion-reaction magnetohydrodynamic solver on nonstaggered grids.," *Int. J. Numer. Meth. Fl.*, vol. 45, pp. 1209–1233, 2004.

[40] M. Dehghan and D. Mirzaei, "Meshless local boundary integral equation (LBIE) method for the unsteady magnetohydrodynamic (MHD) flow in rectangular and circular pipes," *Comput. Phys. Commun.*, vol. 180, pp. 1458 – 1466, 2009.

[41] M. Dehghan and D. Mirzaei, "Meshless local Petrov-Galerkin (MLPG) method for the unsteady magnetohydrodynamic (MHD) flow through pipe with arbitrary wall conductivity," *Appl. Numer. Math.*, vol. 59, pp. 1043 – 1058, 2009.

[42] V. Loukopoulos, G. Bourantas, E. Skouras, and G. Nikiforidis, “Localized meshless point collocation method for time-dependent magnetohydrodynamics flow through pipes under a variety of wall conductivity conditions,” *Comput. Mech.*, vol. 47, pp. 137–159, 2011.

[43] C. Bozkaya and M. Tezer-Sezgin, “Boundary element solution of unsteady magnetohydrodynamic duct flow with differential quadrature time integration scheme,” *Int. J. Numer. Meth. Fl.*, vol. 51, pp. 567–584, 2006.

[44] N. Bozkaya and M. Tezer-Sezgin, “Time-domain BEM solution of convection-diffusion type MHD equations,” *Int. J. Numer. Meth. Fl.*, vol. 56, pp. 1969–1991, 2008.

[45] U. S. Mahabaleshwar, I. Pažanin, M. Radulović, and F. J. Suárez-Grau, “Effects of small boundary perturbation on the MHD duct flow,” *Theor. Appl.*, vol. 44, pp. 83–101, 2017.

[46] E. Marušić-Paloka and I. Pažanin, “On the Darcy-Brinkman flow through channel with slightly perturbed boundary,” *Transport Porous Med.*, vol. 117, pp. 27 – 44, 2017.

[47] W. Jäger and A. Mikelić, “On the roughness-induced effective boundary conditions for an incompressible viscous flow,” *J. Differ. Equations*, vol. 170, pp. 96 – 122, 2001.

[48] C. Aydın and M. Tezer-Sezgin, “DRBEM solution of the cauchy MHD duct flow with a slipping perturbed boundary,” *Eng. Anal. Bound. Elem.*, vol. 93, pp. 94 – 104, 2018.

[49] U. Ghia, K. Ghia, and C. Shin, “High-Re solutions for incompressible flow using the Navier-Stokes equations and a multigrid method,” *J. Comput. Phys.*, vol. 48, pp. 387 – 411, 1982.

[50] K. Onishi, T. Kuroki, and M. Tanaka, “An application of boundary element method to incompressible laminar viscous flows,” *Engineering Analysis*, vol. 1, pp. 122 – 127, 1984.

[51] F. Ghadi, V. Ruas, and M. Wakrim, “Numerical solution of the time-dependent incompressible Navier-Stokes equations in the stream function and vorticity formulation,” *Proc. Appl. Math. Mech*, vol. 7, 2007.

[52] F. Ghadi, V. Ruas, and M. Wakrim, “Numerical solution of the time-dependent incompressible Navier–Stokes equations by piecewise linear finite elements,” *J. Comput. Appl. Math.*, vol. 215, pp. 429 – 437, 2008.

[53] E. Sousa and I. J. Sobey, “Effect of boundary vorticity discretization on explicit stream-function vorticity calculations,” *Int. J. Numer. Meth. Fl.*, vol. 49, pp. 371–393, 2005.

[54] Z. Luo and W. Jiang, “A reduced-order extrapolated Crank–Nicolson finite spectral element method for the 2D non-stationary Navier-Stokes equations about vorticity-stream functions,” *Appl. Numer. Math.*, vol. 147, pp. 161 – 173, 2020.

[55] M. Lashckarbolok and E. Jabbari, “Collocated discrete least squares (CDLS) meshless method for the stream function-vorticity formulation of 2D incompressible Navier–Stokes equations,” *Sci. Iran.*, vol. 19, no. 6, pp. 1422 – 1430, 2012.

[56] Y. Kim, D. W. Kim, S. Jun, and J. H. Lee, “Meshfree point collocation method for the stream-vorticity formulation of 2D incompressible Navier–Stokes equations,” *Computer Methods in Applied Mechanics and Engineering*, vol. 196, no. 33, pp. 3095 – 3109, 2007.

[57] M. Ramšak, L. Škerget, M. Hriberšek, and Z. Žunič, “A multidomain boundary element method for unsteady laminar flow using stream function–vorticity equations,” *Eng. Anal. Bound. Elem.*, vol. 29, pp. 1 – 14, 2005.

[58] P. Ghadimi and A. Dashtimanesh, “Solution of 2D Navier–Stokes equation by coupled finite difference-dual reciprocity boundary element method,” *Appl. Math. Model.*, vol. 35, no. 5, pp. 2110 – 2121, 2011.

[59] N. Sheikhi, M. Najafi, and V. Enjilela, “Solving natural convection heat transfer in turbulent flow by extending the meshless local Petrov–Galerkin method,” *Eng. Anal. Bound. Elem.*, vol. 93, pp. 29 – 43, 2018.

[60] A. Arefmanesh, M. Najafi, and S. Musavi, "Buoyancy-driven fluid flow and heat transfer in a square cavity with a wavy baffle-Meshless numerical analysis," *Eng. Anal. Bound. Elem.*, vol. 37, no. 2, pp. 366 – 382, 2013.

[61] H. Liang and T. Zhang, "Parallel two-grid finite element method for the time-dependent natural convection problem with non-smooth initial data," *Comput. Math. Appl.*, vol. 77, no. 8, pp. 2221 – 2241, 2019.

[62] B. Šarler, J. Perko, D. Gobin, B. Goyeau, and H. Power, "Dual reciprocity boundary element method solution of natural convection in Darcy–Brinkman porous media," *Eng. Anal. Bound. Elem.*, vol. 28, no. 1, pp. 23 – 41, 2004.

[63] N. Alsoy-Akgun, "The dual reciprocity boundary element solution of Helmholtz-type equations in fluid dynamics," *Ph.D. Thesis, Middle East Technical University*, 2013.

[64] M. Abramovitz and I. A. Stegun, *Handbook of mathematical functions: with formulas, graphs and mathematical tables*. Dover Publications, Ing, New York, 1972.

[65] C. Chen and Y. Rashed, "Evaluation of thin plate spline based particular solutions for Helmholtz-type operators for DRM," *Mech. Res. Commun.*, vol. 25, pp. 195–201, 1998.

[66] A. Muleshkov, M. Golberg, and C. Chen, "Particular solution of Helmholtz-type operators using higher order polyharmonic splines," *Comput. Mech.*, vol. 23, pp. 411–419, 1999.

[67] L. W. Johnson and R. D. Riess, *Numerical Analysis*. Addison-Wesley Publishing Company, 1977.

[68] U. Müller and L. Bühler, *Magnetofluiddynamics in Channels and Containers*. Springer, 2001.

[69] M. AL-Jawary, J. Ravnik, L. Wrobel, and L. Škerget, "Boundary element formulations for the numerical solution of two-dimensional diffusion problems with variable coefficients," *Computers and Mathematics with Applications*, vol. 64, no. 8, pp. 2695 – 2711, 2012.

[70] Z. Yun-Xin and T. Yong-Ji, “Meshless schemes for unsteady Navier–Stokes equations in vorticity formulation using radial basis functions,” *J. Comput. Appl. Math.*, vol. 192, no. 2, pp. 328 – 338, 2006.

[71] M. Şahin and R. Owens, “A novel fully implicit finite volume method applied to lid-driven cavity problem - part i: High Reynolds number flow calculations,” *Int. J. Numer. Meth. Fl.*, vol. 42, pp. 57–77, 2003.

[72] J. S. Wu and Y. L. Shao, “Simulation of lid-driven cavity flows by parallel lattice Boltzmann method using multi-relaxation-time scheme,” *Int. J. Numer. Meth. Fl.*, vol. 46, pp. 921–937, 2004.

[73] D. Lo, D. Young, and C. Tsai, “High resolution of 2D natural convection in a cavity by the DQ method,” *J. of Comput. and Appl. Math.*, vol. 203, pp. 219 – 236, 2007.

[74] H. Ding, C. Shu, K. Yeo, and D. Xu, “Development of least-square-based two-dimensional finite-difference schemes and their application to simulate natural convection in a cavity,” *Computers and Fluids*, vol. 33, pp. 137 – 154, 2004.

[75] M. Sezgin, “Finite element formulation and programming aspects of Navier Stokes equations,” *Master of Science Thesis, Middle East Technical University*, 1976.

[76] J. Cai and X. Hu, *Petrophysical Characterization and Fluids Transport in Unconventional Reservoirs*. Elsevier, 2019.

[77] I. A. Badruddin, Z. A. Zainal, P. A. Narayana, and K. N. Seetharamu, “Heat transfer in porous cavity under the influence radiation and viscous dissipation,” *Int. Commun. Heat Mass.*, vol. 33, pp. 491 – 499, 2006.

[78] I. Zahmatkesh, “Influence of thermal radiation on free convection inside a porous enclosure,” *Emirates Journal for Engineering Research*, vol. 12, pp. 47–52, 2007.

[79] S. E. Ahmed, A. K. Hussein, H. Mohammed, I. Adegun, X. Zhang, L. Kolsi, A. Hasanpour, and S. Sivasankaran, “Viscous dissipation and radiation effects on MHD natural convection in a square enclosure filled with a porous medium,” *Nucl. Eng. Des.*, vol. 266, pp. 34 – 42, 2014.

CURRICULUM VITAE

PERSONAL INFORMATION

Surname, Name: FENDOĞLU, Hande
Nationality: Turkish (TC)
Date and Place of Birth: 27.06.1989, Yozgat
Marital Status: Married
Email: handefendoglu@gmail.com

EDUCATION

Degree	Institution	Year of Graduation
Ph.D.	Department of Mathematics, Middle East Technical University	2020
M.S.	Department of Mathematics, TOBB University of Economics and Technology	2013
B.S.	Department of Mathematics, Ankara University	2011

LANGUAGE SKILLS

English (Advanced)

COMPUTER SKILLS

Matlab, Mathematica, Maple, Latex,

PUBLICATIONS

International Journal Publications

1. H. Fendoğlu, C. Bozkaya and M. Tezer-Sezgin, DBEM and DRBEM solutions to 2D transient convection-diffusion-reaction type equations, Eng. Anal. Bound. Elem., vol. 93, pp. 124-134, 2018.
2. H. Fendoğlu, C. Bozkaya and M. Tezer-Sezgin, MHD flow in a rectangular duct with a perturbed boundary, Comput. Math. Appl., vol. 77, no. 2, pp. 374-388, 2019.

International Conference Proceedings

1. H. Fendoğlu, C. Bozkaya and M. Tezer-Sezgin, BEM solution of transient magnetohydrodynamic flows in ducts, Ukrainian Conference on Applied Mathematics-UCAM 2017, Lviv, Ukraine, 28-30 September 2017, pp. 51-52.
2. H. Fendoğlu, C. Bozkaya and M. Tezer-Sezgin, A BEM approach for convection-diffusion type equations with variable coefficients, International Conference on Boundary Element and Meshless Techniques- BETEQ 2019, Palermo, Italy, 22-24 July 2019, pp. 39-45.

International Conference Abstracts

1. H. Yücel (Fendoğlu), H. Merdan, Stability of an option pricing model, International Workshop on Differential Equations and Applications- WDEA 2013, Izmir, Turkey, 11-14 September 2013.
2. H. Fendoğlu, C. Bozkaya and M. Tezer-Sezgin, Boundary integral solutions to the transient convection-diffusion type equations, International Conference on Applied Analysis and Mathematical Modeling-ICAAMM 2017, Istanbul, Turkey, 3-7 July 2017.
3. H. Fendoğlu, C. Bozkaya and M. Tezer-Sezgin, MHD flow in a rectangular duct with a perturbed boundary, Symposium of the International Association

for Boundary Element Methods- IABEM 2018, Paris, France, 26-28 June 2018.

PROJECTS

- H. Fendoğlu, C. Bozkaya and M. Tezer-Sezgin, Department of Mathematics, Middle East Technical University,
  Project Title: Zamana bağlı magnetohidrodinamik akış probleminin pertürbe edilmiş sınıra sahip dikdörtgen kanal kesitinde sınır elemanları metodu ile çözümü,
  Project Type: General Research Projects,
  Project Group: Engineering-Architecture,
  Project Term: 09.05.2018 - 09.05.2019,
  Project No: GAP-101-2018-2768.

AWARDS

- Ankara University, High honor student degree 2010
- TOBB University of Economics and Technology,
  MSc Education Grant, 2011-2013
- The Scientific and Technological Research Council of Turkey (TUBITAK-BIDEB),
  - National scholarship for MSc (2210-A), 2011-2013
  - National scholarship for Ph.D. (2211-E), 2013-2017